Bacias de Margem Passiva

Importância:

- Maior volume de sedimentos no planeta hoje
- Grande potencial de preservação
- Elemento de orógenos colisionais
- Geologia do petróleo

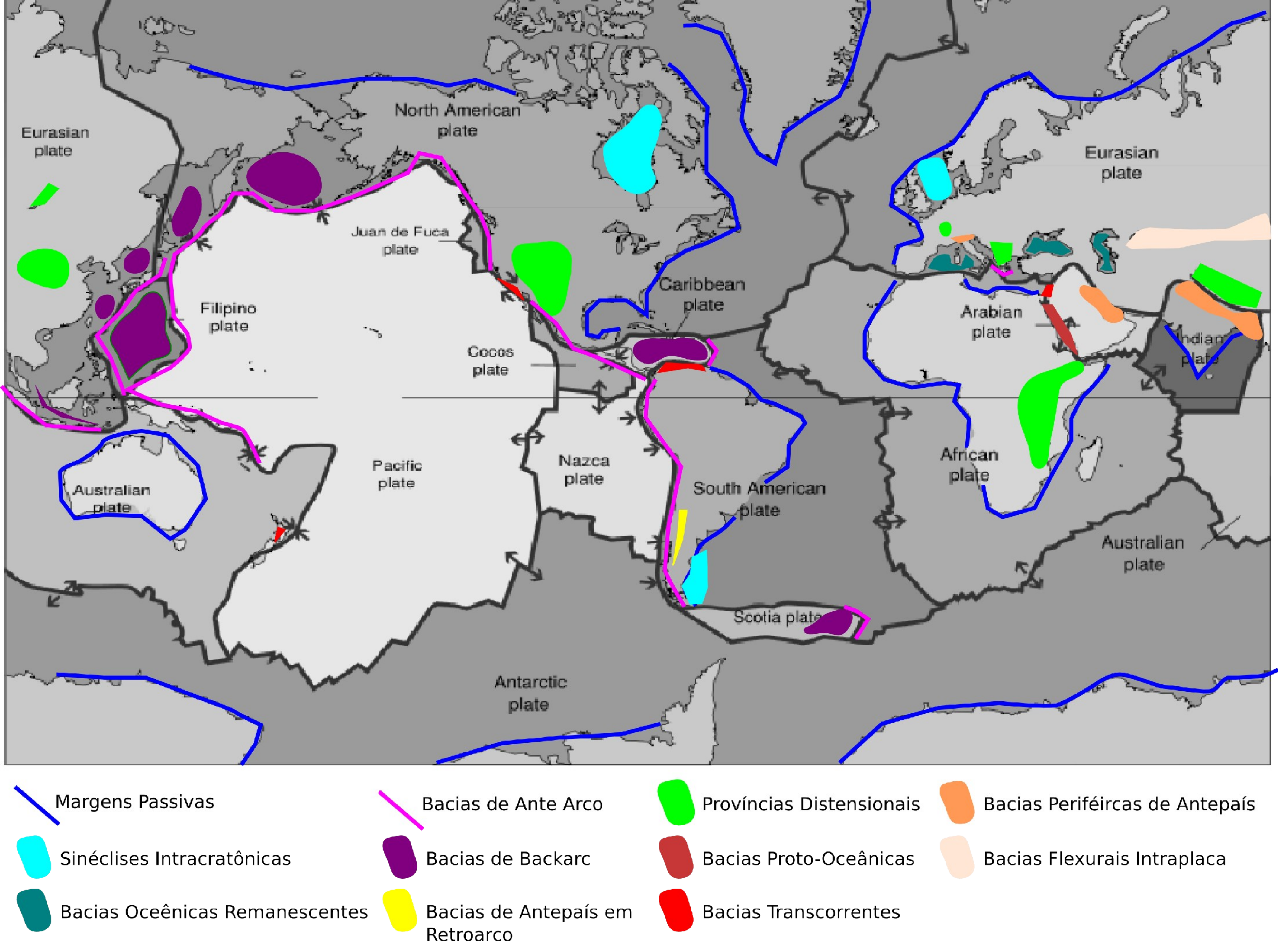
Eurasian plate
North American plate
Juan de Fuca plate
Filipino plate
Caribbean plate
Cocos plate
Eurasian plate
Arabian plate
Indian plate
Pacific plate
Nazca plate
African plate
South American plate
Australian plate
Australian plate
Scotia plate
Antarctic plate
Margens Passivas
Bacias de Ante Arco
Províncias Distensionais
Bacias Periféircas de Antepaís
Sinéclises Intracratônicas
Bacias de Backarc
Bacias Proto-Oceânicas
Bacias Flexurais Intraplaca
Bacias Oceênicas Remanescentes
Bacias de Antepaís em Retroarco
Bacias Transcorrentes

Transferência de calor

Condução
Depende da propriedade condutividade térmica, o calor se propaga do ponto de maior temperatura para menor temperatura. A Terra desde sua formação está esfriando através da perda de calor por condução. Calor radiogênico pode contribuir para aumentar o valor do fluxo térmico medido, especialmente em litosfera continental.

Convecção
Redistribuição de calor através da circulação de massa, exemplo, variação de temperatura em uma bacia sedimentar em função do deslocamento de fluídos.

Radiação
Transferência de calor em função da emissão de ondas eletromagnéticas devido à altas temperaturas. Exemplos, sol ou núcleo terrestre.

Lei de Fourier Condução 1-D

Estado estacionário e variação Linear T

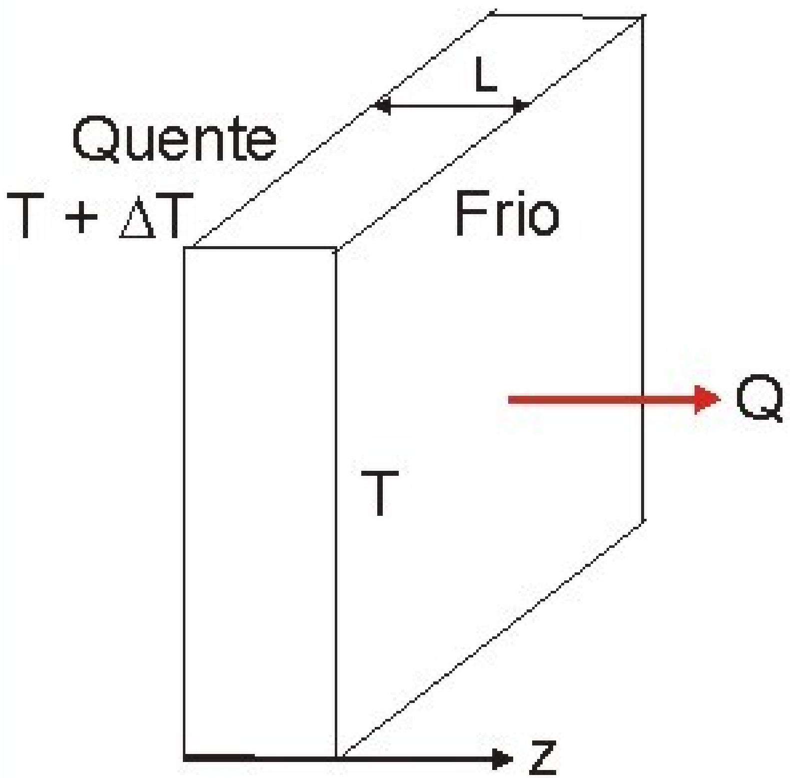

$$Q = -k \frac{dT}{dz}$$

k = condutividade térmica

$$\frac{dT}{dz} = -\frac{\Delta T}{L}$$

k medido em laboratório para diferentes litologias

Q é dado em W/m^2

Lembrando que:

$$W = J/s = N\ m\ /s = kg\ m^2\ /\ s^3$$

Qual a origem do calor da Terra?

Produção de Calor Radiogênico

Table 2.3 Typical concentrations of radioactive elements and heat generation from typical rock types comprising the continental and oceanic crust and undepleted mantle (from Fowler 1990).

	Granite	Tholeiitic basalt	Alkali basalt	Peridotite	Average continental upper crust	Average oceanic crust	Undepleted mantle
Concentration by weight							
U (ppm)	4	0.1	0.8	0.006	1.6	0.9	0.02
Th (ppm)	15	0.4	2.5	0.04	5.8	2.7	0.10
K (%)	3.5	0.2	1.2	0.01	2.0	0.4	0.02
Heat generation (10^{-10} W kg^{-1})							
U	3.9	0.1	0.8	0.006	1.6	0.9	0.02
Th	4.1	0.1	0.7	0.010	1.6	0.7	0.03
K	1.3	0.1	0.4	0.004	0.7	0.1	0.007
Total	9.3	0.3	1.9	0.020	3.9	1.7	0.057
Density (10^3 kg m^{-3})	2.7	2.8	2.7	3.2	2.7	2.9	3.2
Heat generation (10^{-6} W m^{-3})	2.5	0.08	0.5	0.006	1.0	0.5	0.02

Portanto, a contribuição do calor radiogênico é mais importante em litosfera continental, especialmente na sua parte mais rasa (crosta).

GEOCIÊNCIAS USP

Geotermas

$$k\frac{d^2T}{dz^2}+\rho H(z)=0$$

k = condutividade térmica W / (m . K)

- ρ = densidade volumétrica

H(z) = distribuição de calor radiogênico

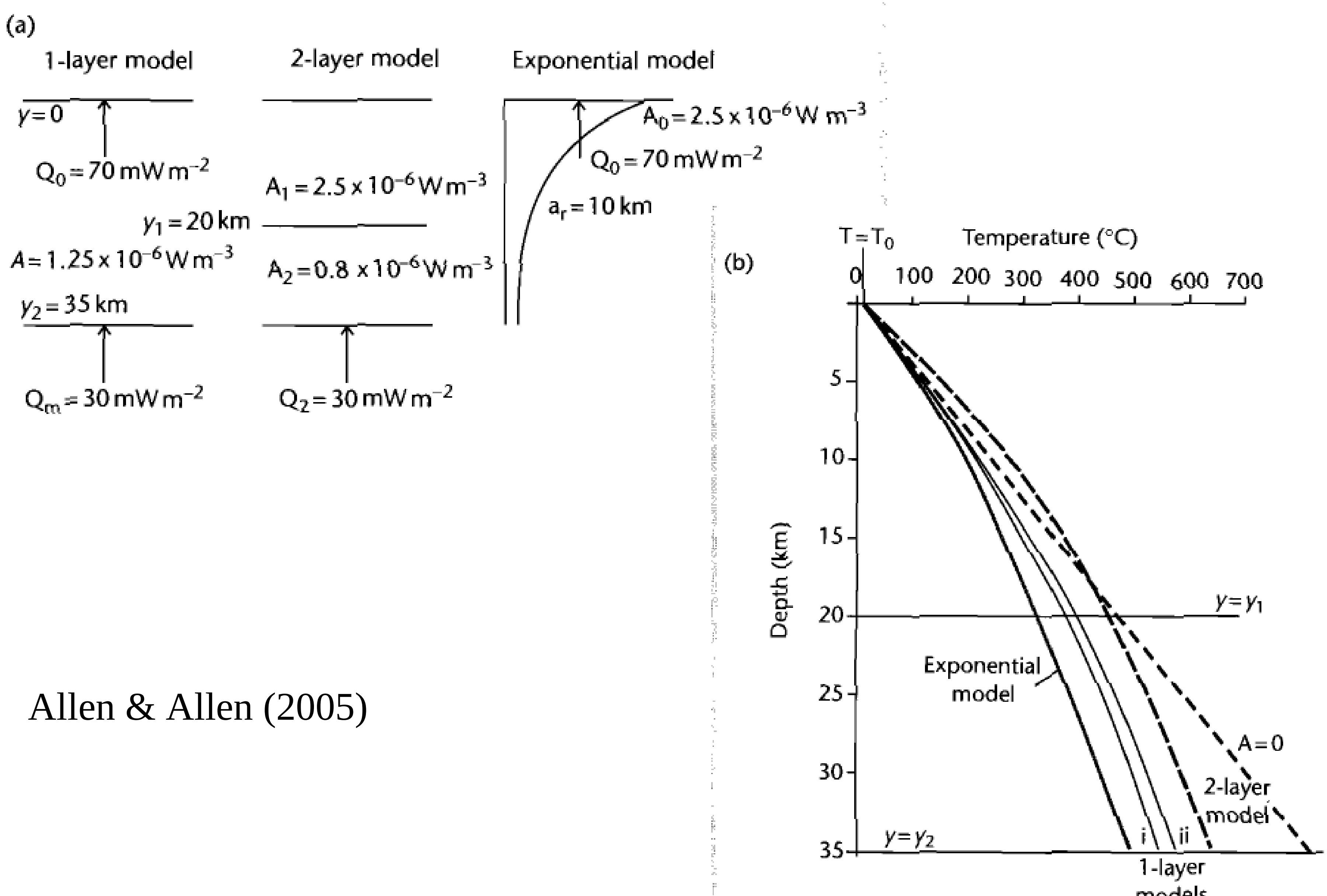

Allen & Allen (2005)

Fig. 2.14 Geotherms for the continental crust. (a) Model set-up; one-layer model with a constant internal heat generation for a 35 km-thick crust, with (i) a surface heat flow of $70\,mW\,m^{-2}$, and (ii) a basal heat flow of $30\,mW\,m^{-2}$; a two-layer model with a highly radiogenic 20 km-thick upper crust and a weakly radiogenic 15 km-thick lower crust; and a model with an exponentially decreasing radiogenic heat production with depth; (b) Resultant geotherms, with a linear geotherm for zero radiogenic heat production ($A = 0$) and surface heat flow of $70\,mW\,m^{-2}$ shown for comparison.

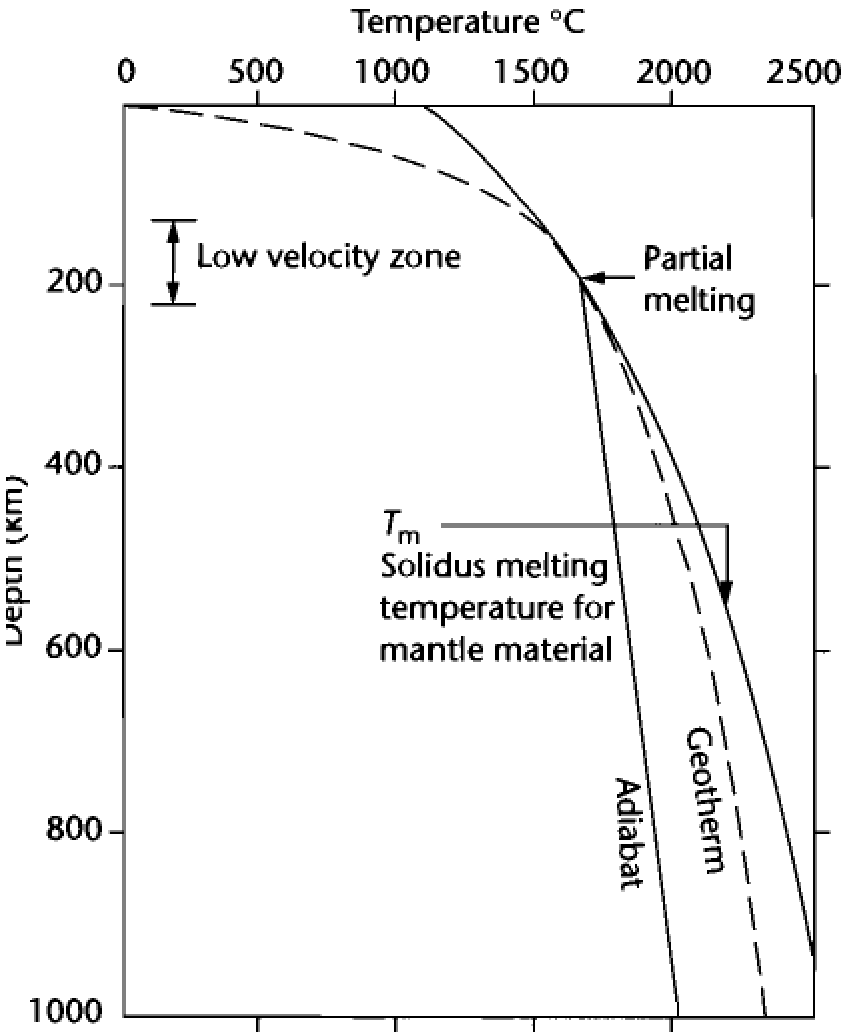

Fig. 1.4 Variation of temperature with depth, or geotherm, and the solidus temperature for mantle material (peridotite). Where the solidus curve (T_m) and the geotherm become tangential, partial melting in the mantle is likely to take place, resulting in a zone of low seismic wave velocities (low velocity zone).

Allen & Allen (2005)

Introdução

Origem

Depósitos

Seqüências Deposicionais

Inversão

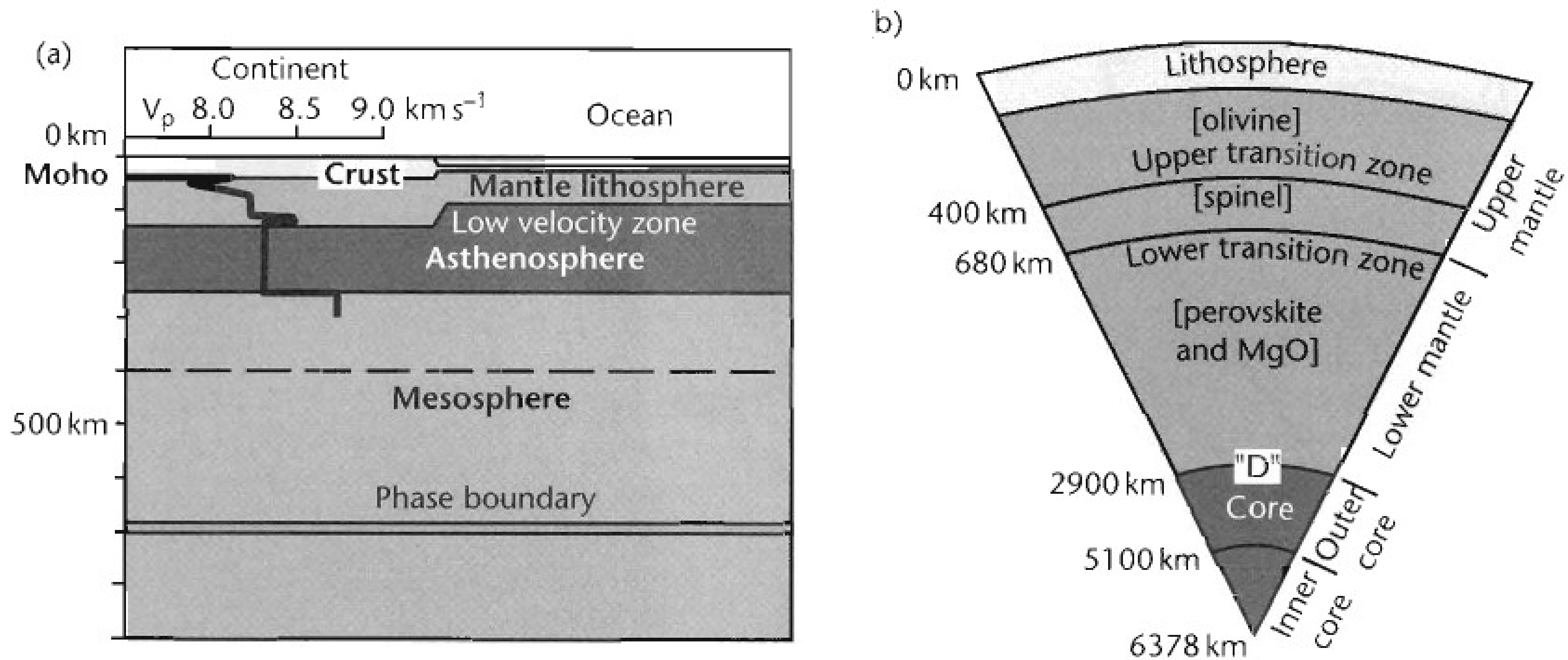

Fig. 1.1 The main compositional (a) and rheological (b) boundaries of the Earth. The most important compositional boundary is between crust, mantle, and core. There are strong compositional variations within the continental crust and compositional variations caused by phase changes in the mantle. V_p is velocity of **P** wave. The main rheological boundary is between the lithosphere and the asthenosphere. **P** wave velocities increase markedly beneath the Moho, but decrease in a low velocity zone representing the weak asthenosphere. The lithosphere is rigid enough to act as a coherent plate. **P** wave velocity in (a) from western Europe after Hirn (1976).

Allen & Allen (2005)

Condução de Calor Dependente do Tempo, 1-D

Aplica-se a muitos problemas geológicos como resfriamento de corpos ígneos, litosfera, efeito térmico devido erosão e sedimentação.

$$\frac{\partial T}{\partial t} = \kappa \frac{\partial^2 T}{\partial z^2}$$

$$\kappa = \frac{k}{\rho c}$$

Onde κ é a difusividade térmica, k a condutividade térmica, ρ é densidade e c a capacidade térmica.

Capacidade térmica é a quantidade de calor necessária para alterar a temperatura de uma dada substância em 1 K.

É expressa em J / K

A abertura de um oceano

- Distensão por cisalhamento simples

- Conseqüências na geometria da plataforma

- Variação lateral do fator Beta e da taxa de subsidência mecânica

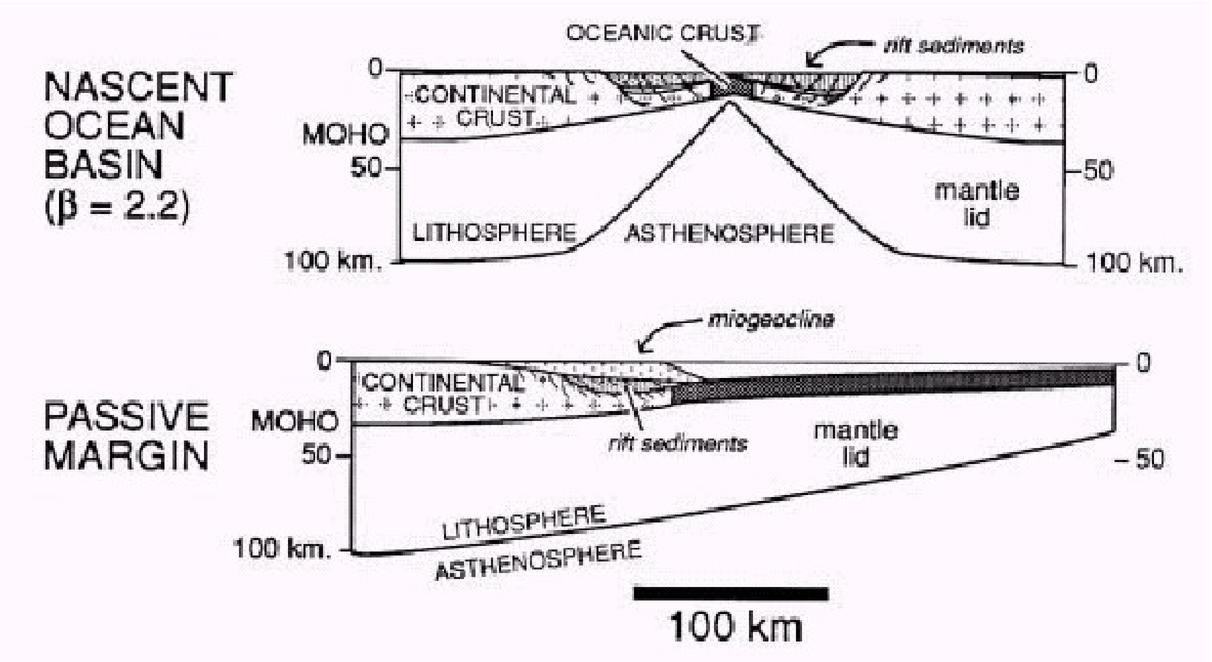
NASCENT OCEAN BASIN (β = 2.2)
OCEANIC CRUST
rift sediments
CONTINENTAL CRUST
MOHO
0
50
100 km.
LITHOSPHERE
ASTHENOSPHERE
mantle lid
PASSIVE MARGIN
miogeocline
rift sediments
100 km

GEOCIÊNCIAS USP

Isotermas da Litosfera Oceânica

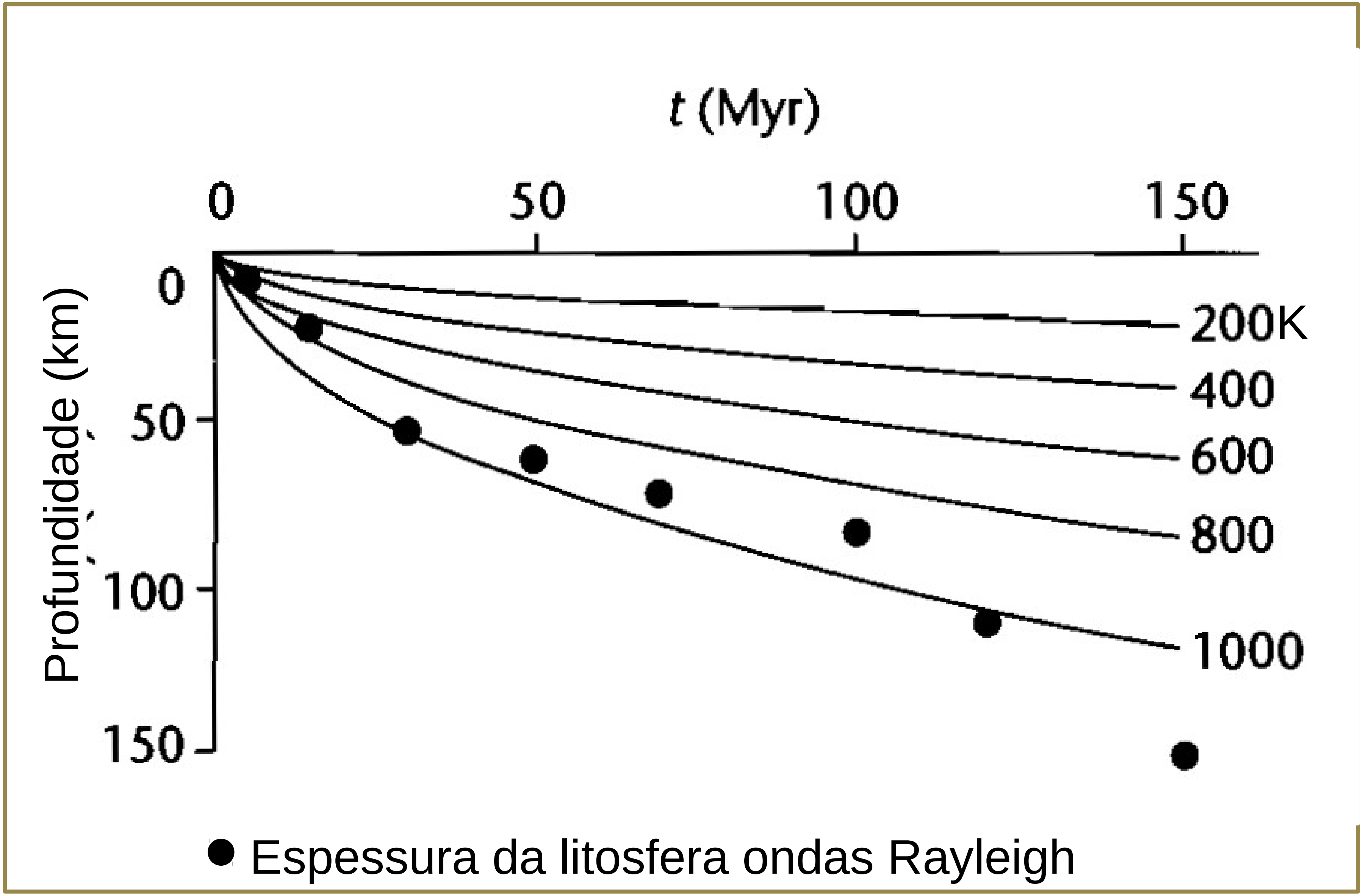

Batimetria Calculada x Observada

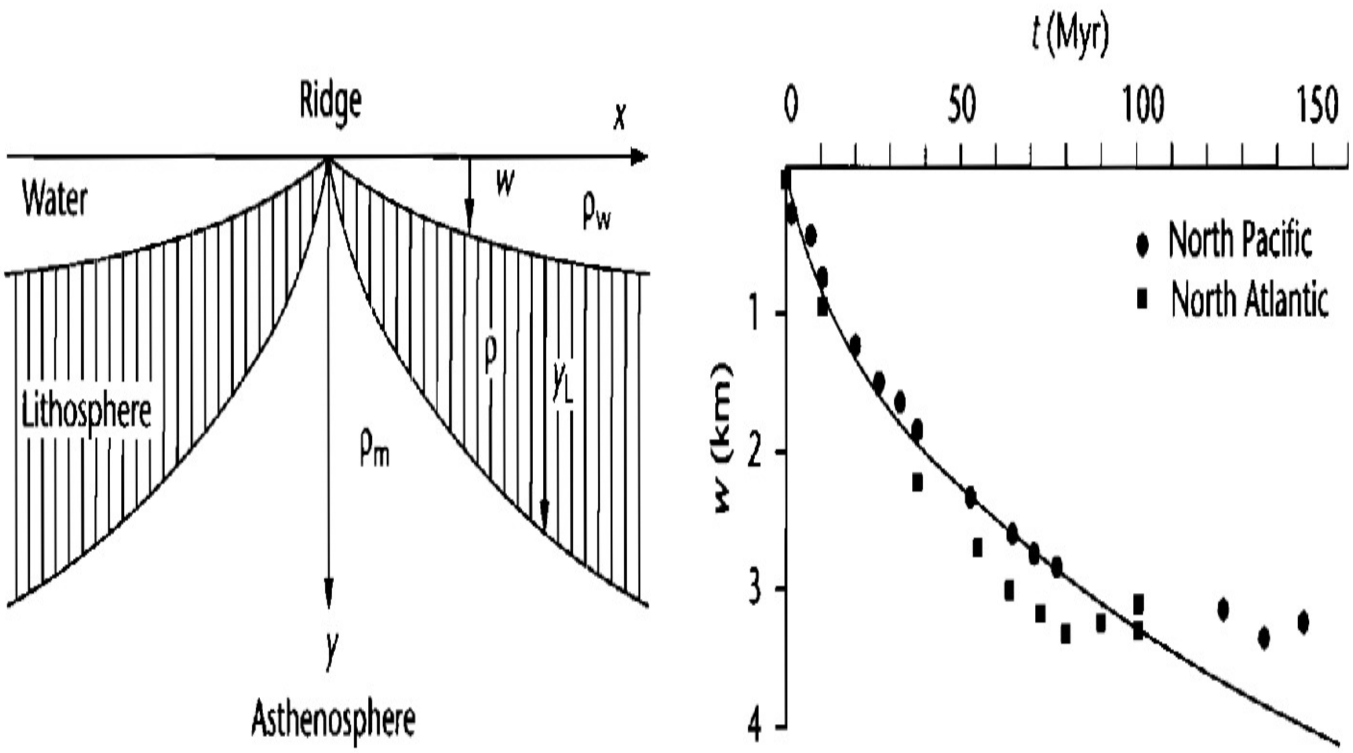

Modelo Resfriamento de Placa

1. Aquecimento ou resfriamento instantâneo do topo de uma placa de espessura finita.
3. **A litosfera continental não se espessa continuamente com a idade mas atinge um estado de equilíbrio térmico**
5. Solução da equação:

$$\frac{\partial T}{\partial t} = \kappa \frac{\partial^2 T}{\partial z^2}$$

$$\kappa = \frac{k}{\rho c}$$

requer outras condições iniciais com espessura da placa zlo

$T = T1$ em $t=0$, $0 \leq z \leq zlo$

$T = To$ em $z=0$ $t > 0$

$T = T1$ em $z=zlo$ $t > 0$

Fluxo Térmico x Modelos Térmicos Semi-Espaço e Placa

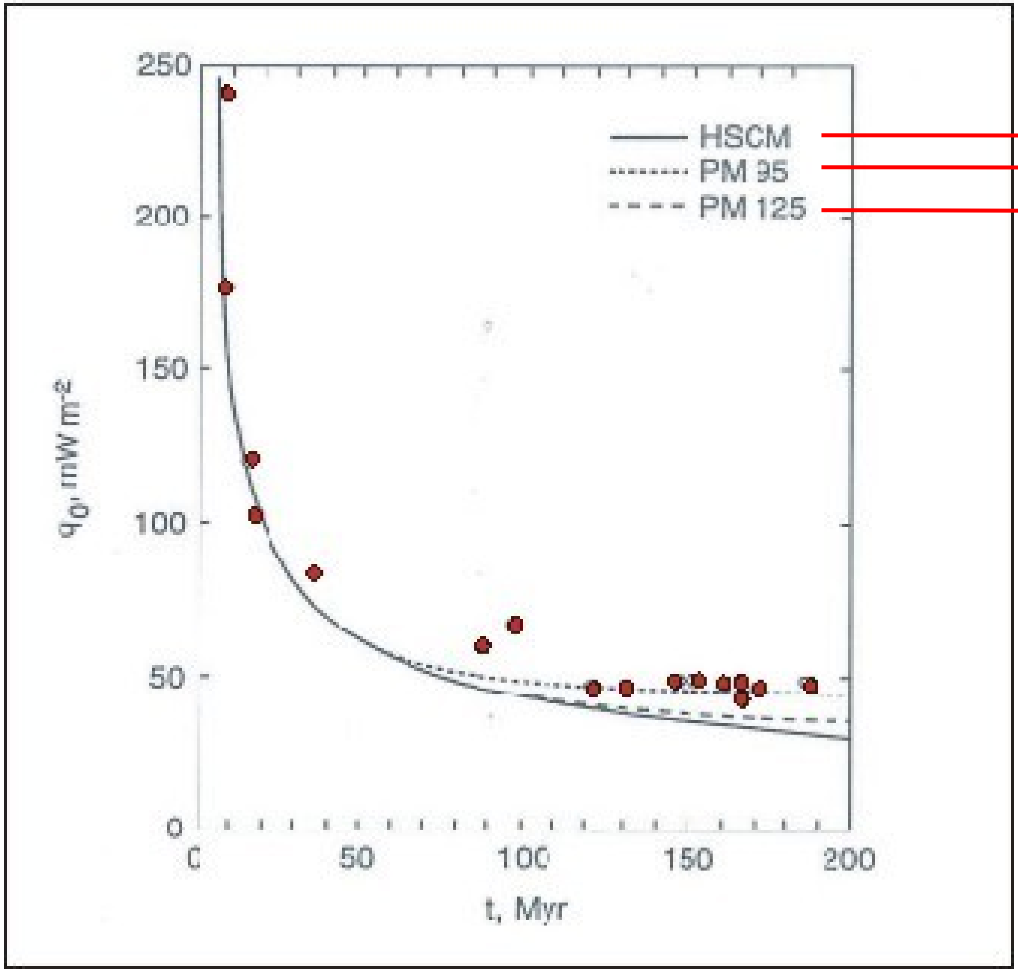

semi-espaço
placa z=95 km
placa z=125 km

Turcotte & Schubert, 2002

Como ocorre a subsidência?

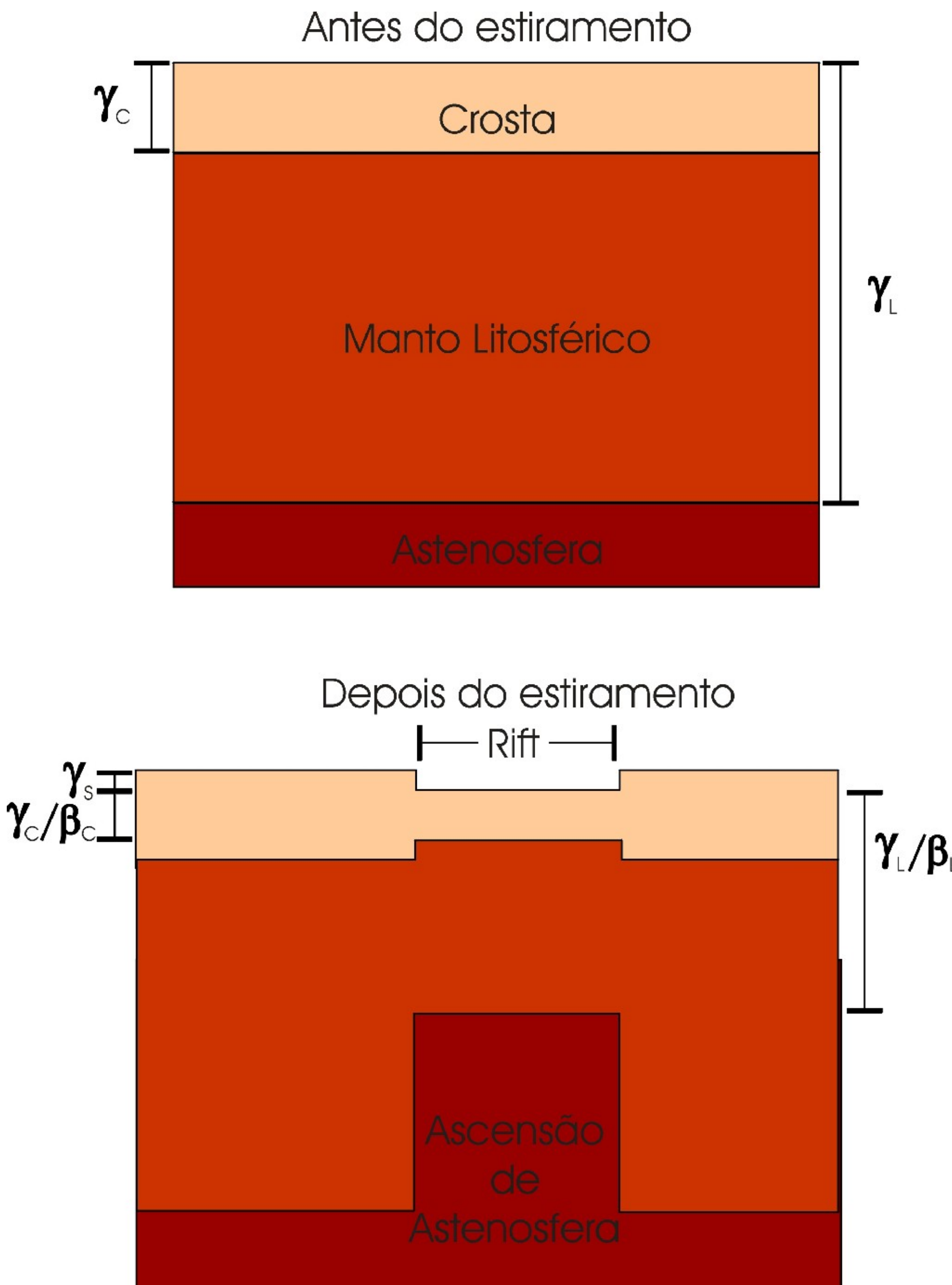

A espessura inicial da crosta ou litosfera sobre a espessura após a distensão determina o fator **β**.

Como distensão da litosfera implica em ascensão de astenosfera, o gradiente térmico aumenta.

O aquecimento da litosfera pode ser rápido se houver adição de magma, e com isso a densidade diminui e a subsidência é reduzida.

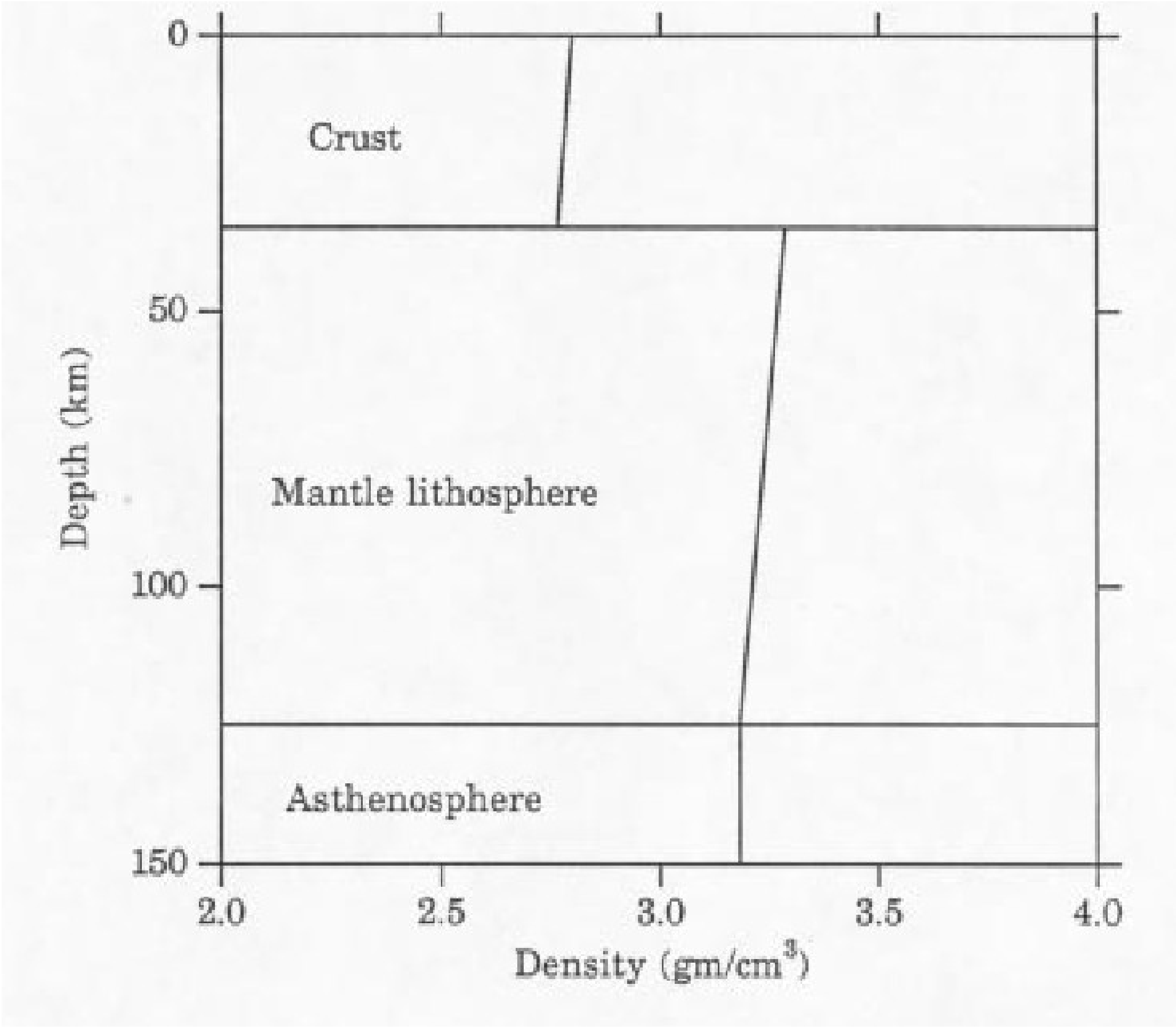
0
50
100
150
Depth (km)
Crust
Mantle lithosphere
Asthenosphere
2.0
2.5
3.0
3.5
4.0
Density (gm/cm³)

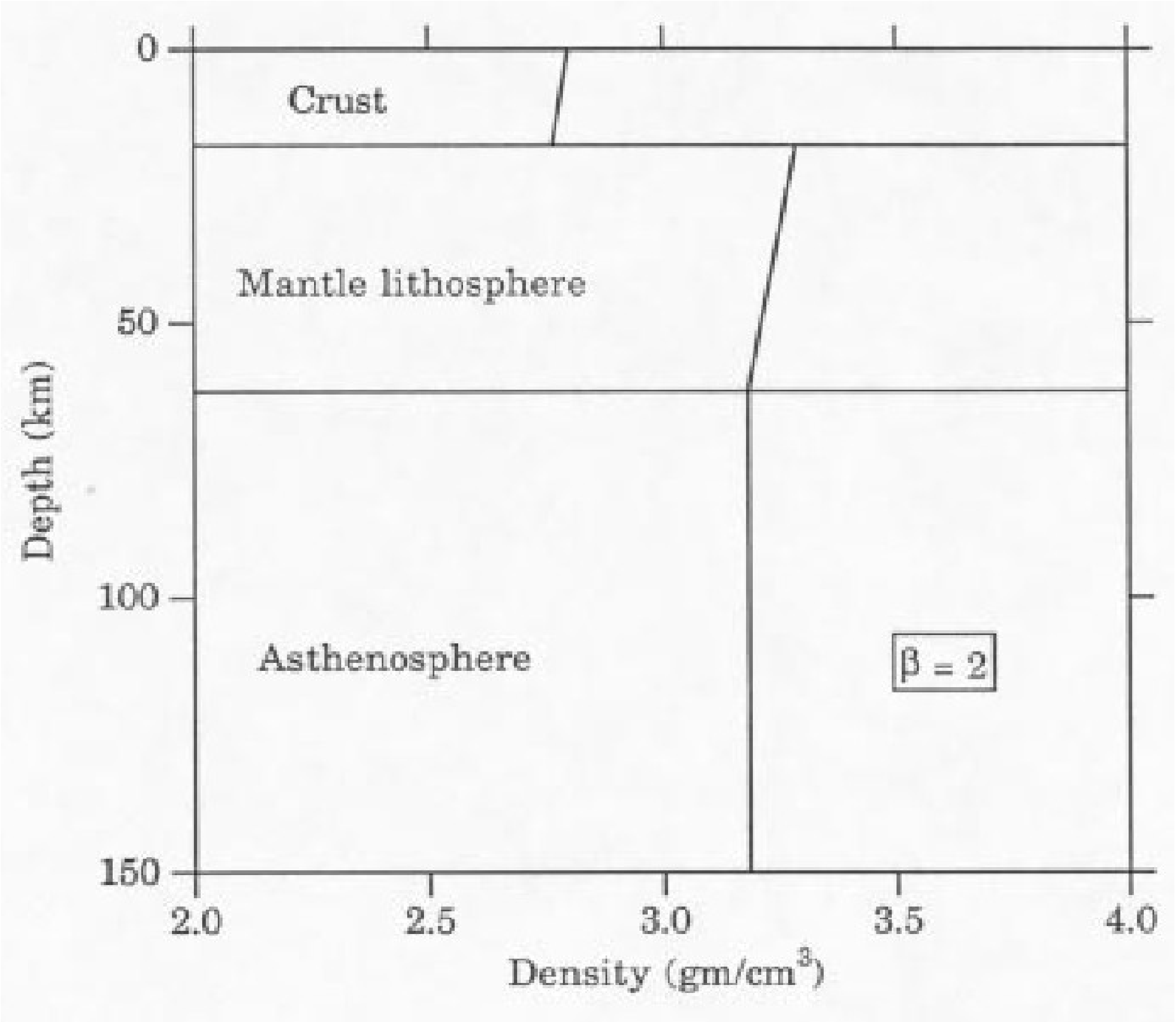
Crust
Mantle lithosphere
Asthenosphere
β = 2
Depth (km)
0
50
100
150
2.0
2.5
3.0
3.5
4.0
Density (gm/cm³)

Introdução

Origem

Depósitos

Seqüências Deposicionais

Inversão

GEOCIÊNCIAS USP

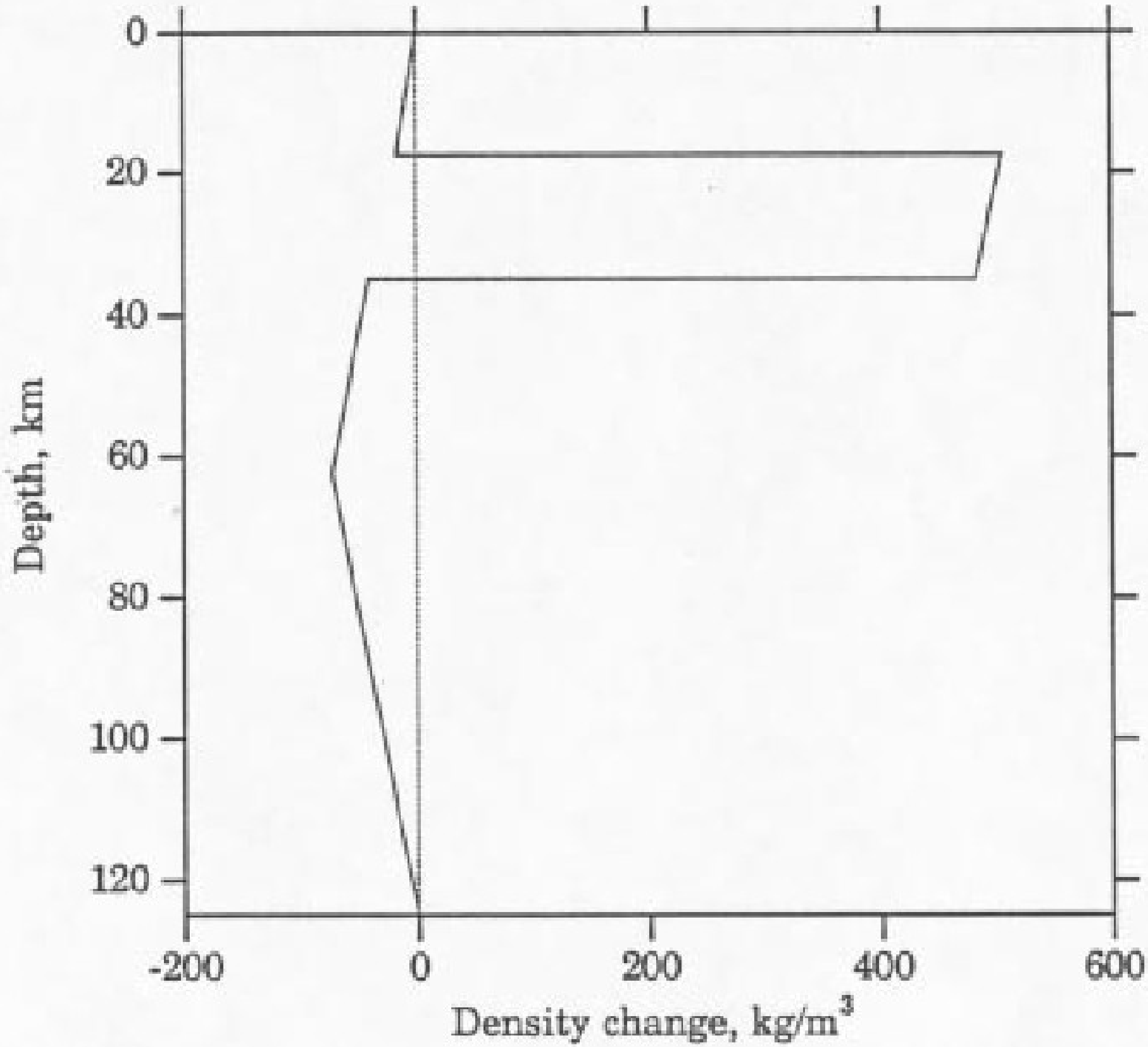

Figure 4.1 Density changes occur when lithosphere is stretched by $\beta = 2$. Original thickness of crust and lithosphere is 35 km and 125 km, respectively. Shallow zone of increased density is due to mantle lithosphere replacing crust. Zones of decreased density are due to heating of the crust and mantle lithosphere, and replacement of mantle lithosphere by asthenosphere.

Quando a distensão termina, a litosfera esfria lentamente e ganha volume com a transformação de astenosfera quente em litosfera mais fria.

Esse resfriamento é acompanhado por aumento de densidade e, portanto **subsidência termal ou térmica**.

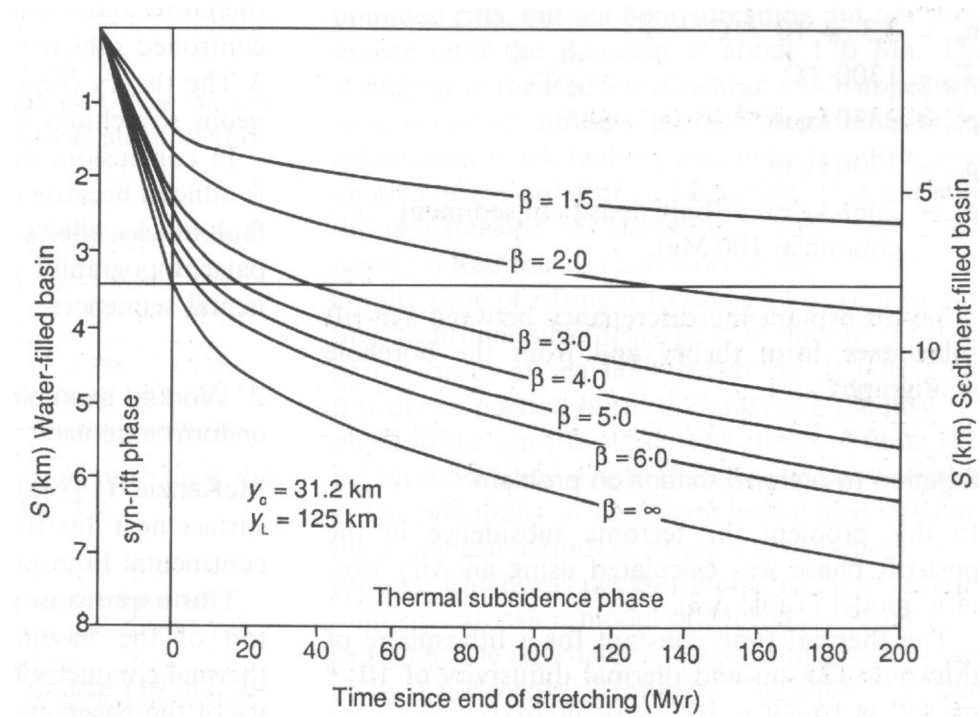

Para cada fator beta há uma curva exponencial de subsidência termal.

Em um modelo unidimensional, a subsidência total é mesma calculada para a compensação isostática sem os efeitos termais, apenas a curva é modificada.

Introdução

Origem

Depósitos

Seqüências Deposicionais

Inversão

GEOCIÊNCIAS USP

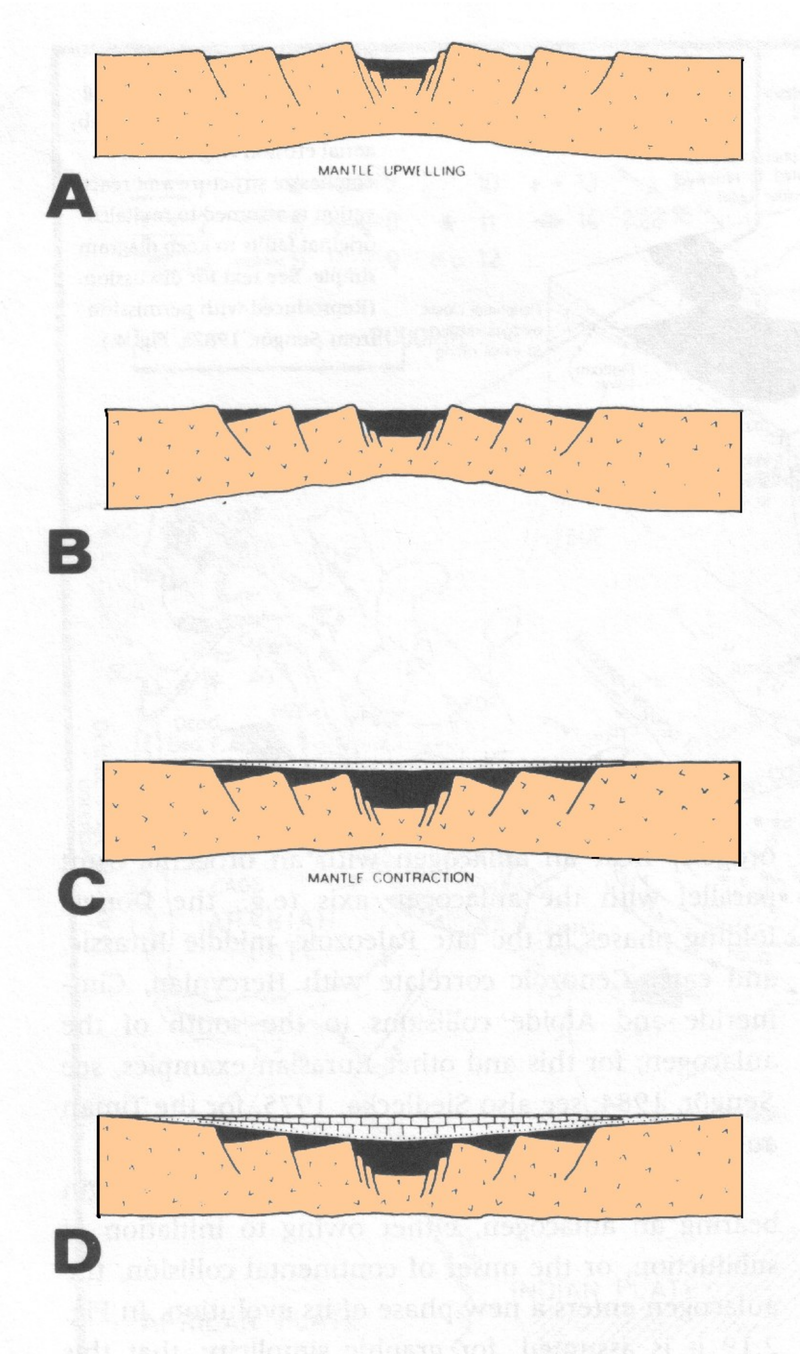

Como a crosta inferior e a litosfera apresentam comportamento dúctil com a deformação, a área de ascensão astenosférica é maior que a de distensão crustal.

Assim, a subsidência termal afeta uma área maior que a subsidência mecânica por ela responsável.

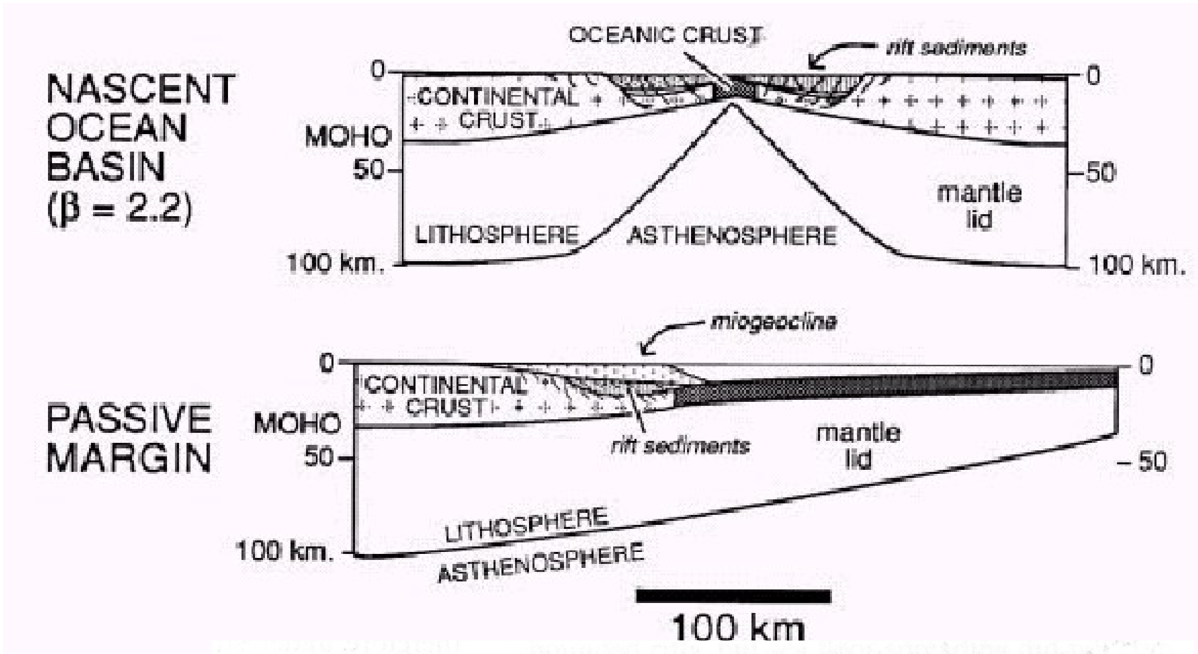

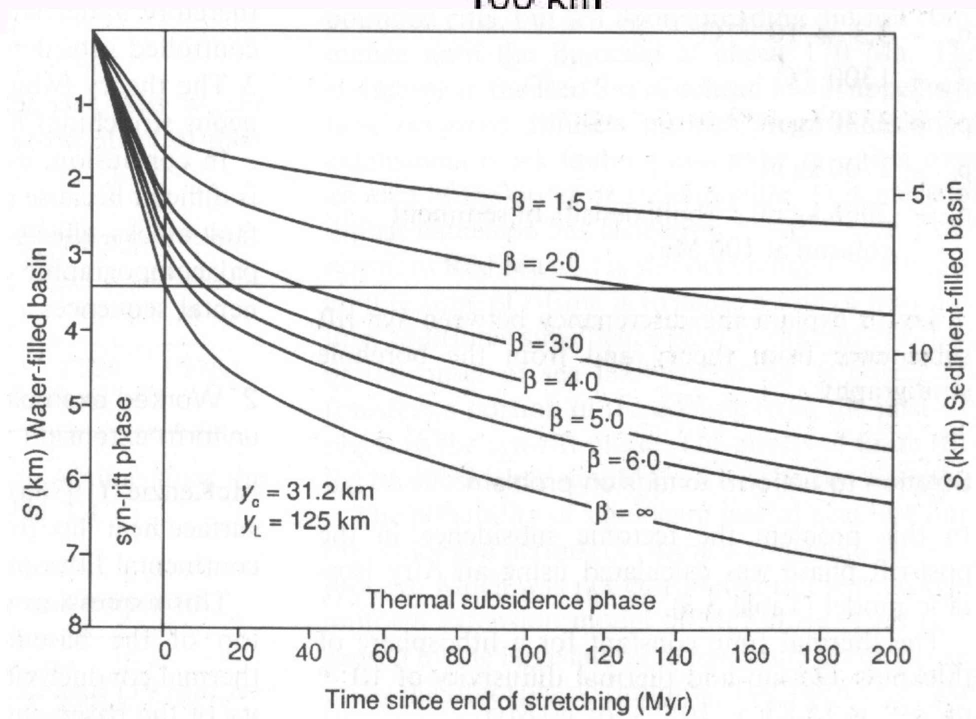

Diferentes taxas de distensão em diferentes posições da margem = Diferentes curvas de subsidência

A abertura de um oceano

- Distensão por cisalhamento simples

- Consequências na geometria da plataforma

- Variação lateral do fator Beta e da taxa de subsidência mecânica

Distensão por cisalhamento simples

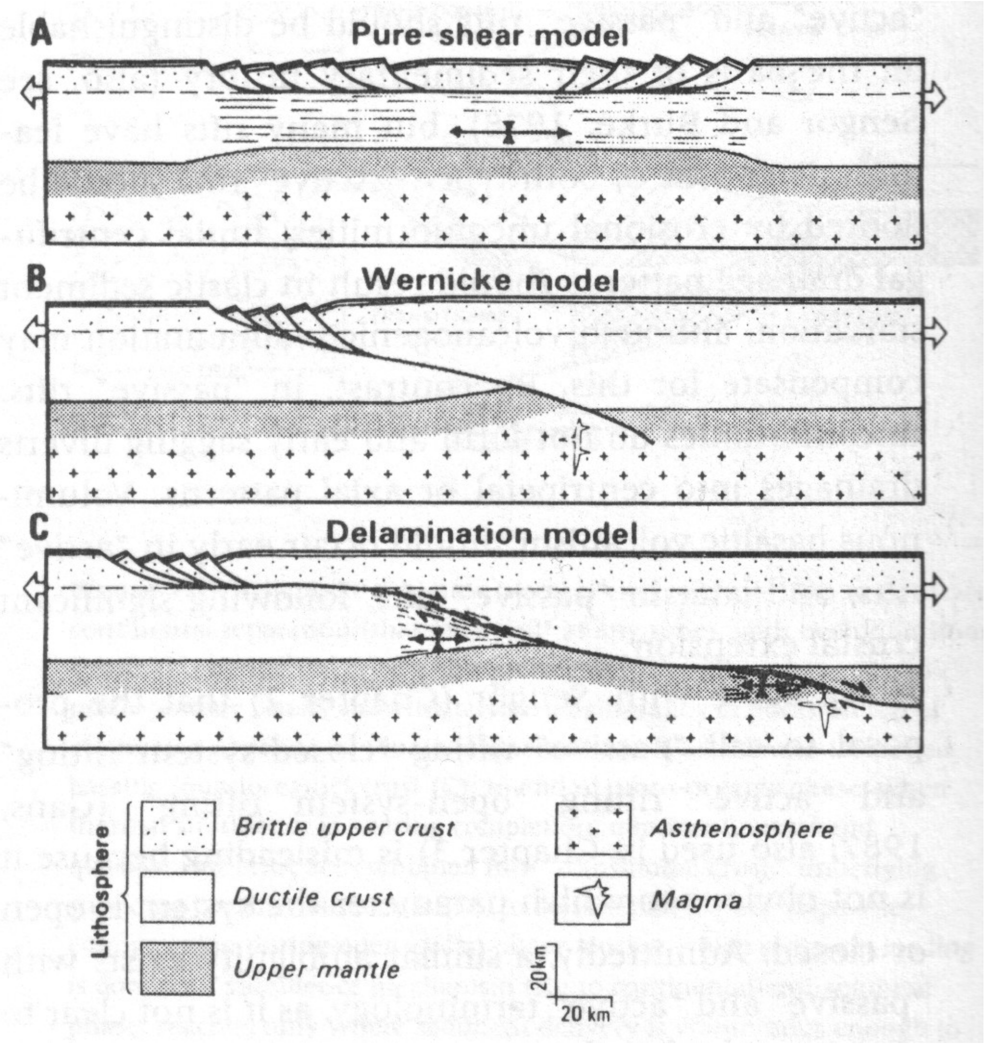

Lister *et al.* (1986)

Geometria resultante na plataforma

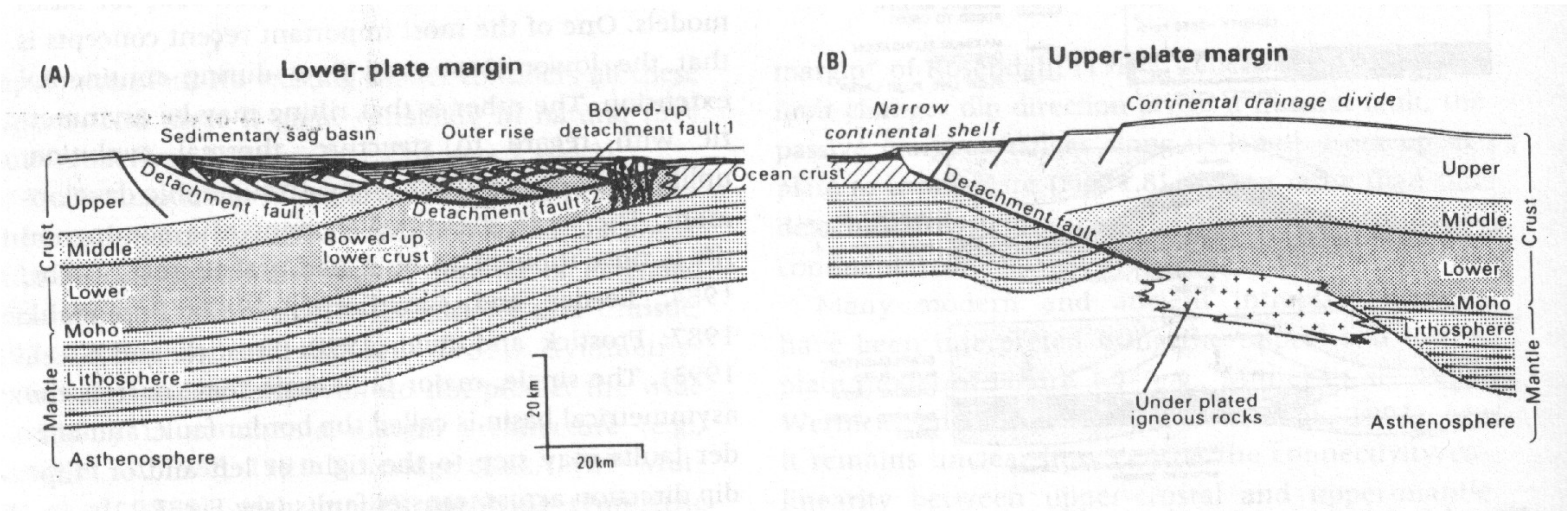

Lister *et al.* (1986)

GEOCIÊNCIAS USP

Introdução

Origem

Depósitos

Seqüências Depositionais

Inversão

Inversão da assimetria

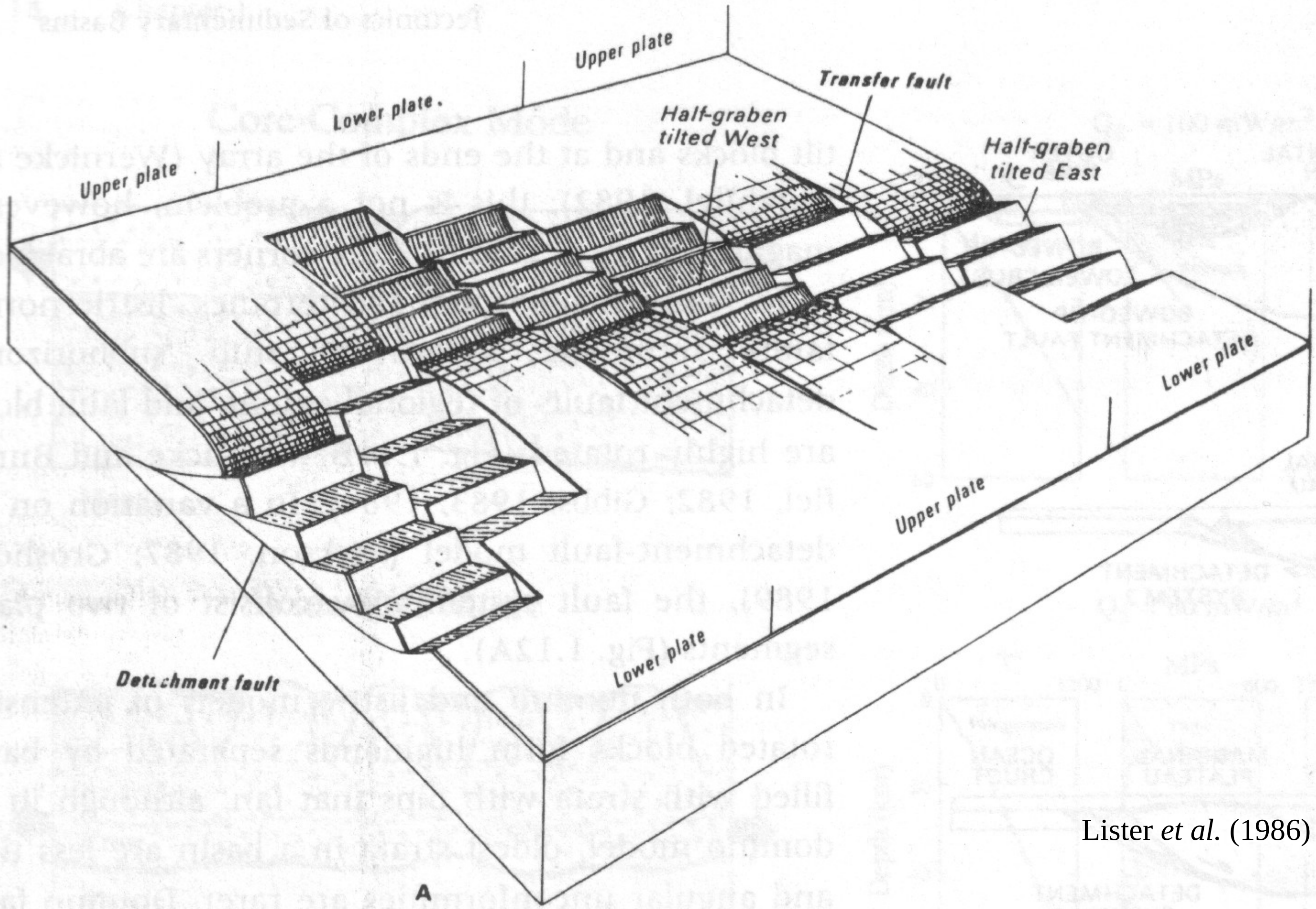

Lister *et al.* (1986)

O "upper plate paradox"

Rosenbaum et al. (2008)

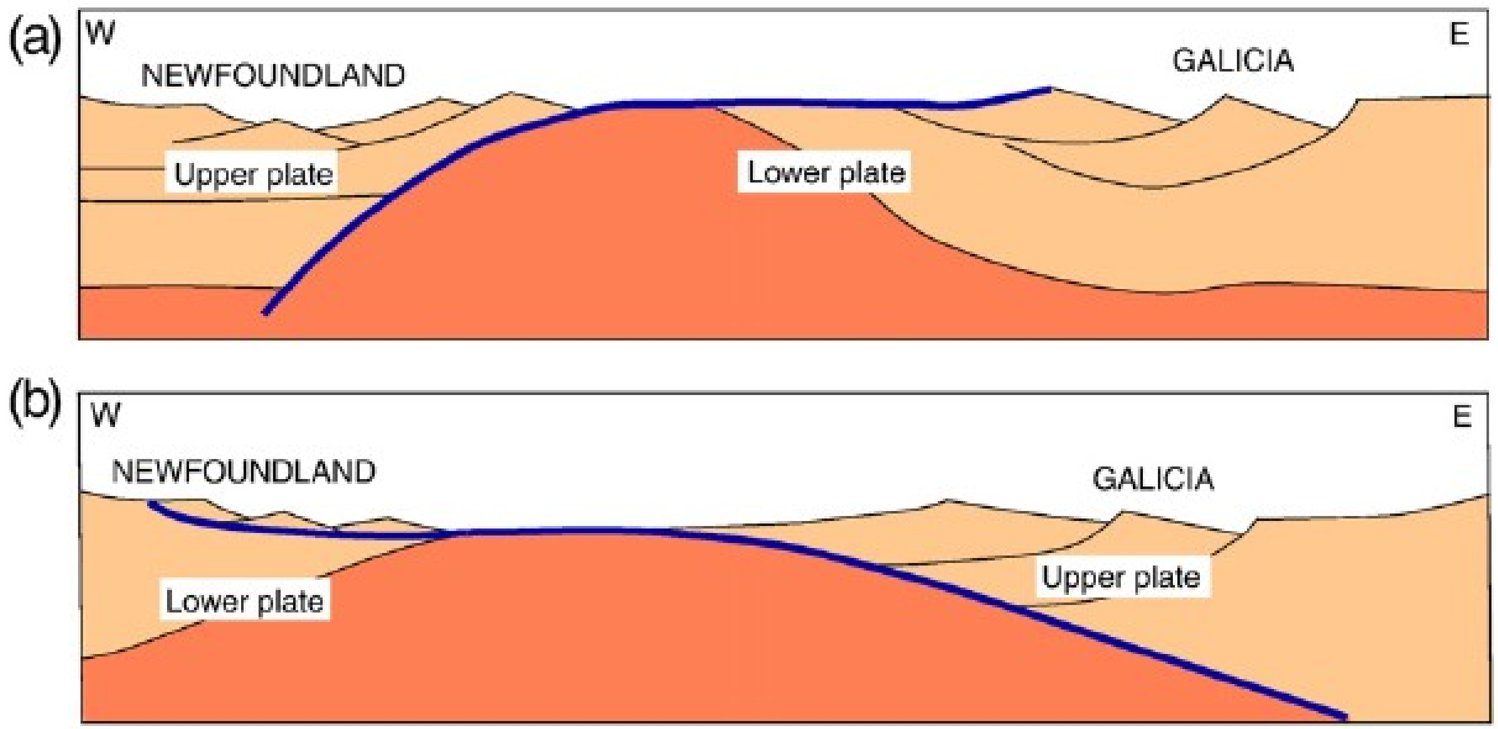

Fig. 3. Contrasting interpretations of the upper-plate and lower-plate in the Galicia–Newfoundland conjugate margins. (a) A west dipping detachment (parallel to the S reflector) implying that the Galicia margin is a lower plate (after Whitmarsh et al., 2001). (b) An east-dipping master detachment parallel to the Moho with the Galicia margin as an upper plate (after Boillot et al., 1987, 1988).

GEOCIÊNCIAS USP

O “upper plate paradox”

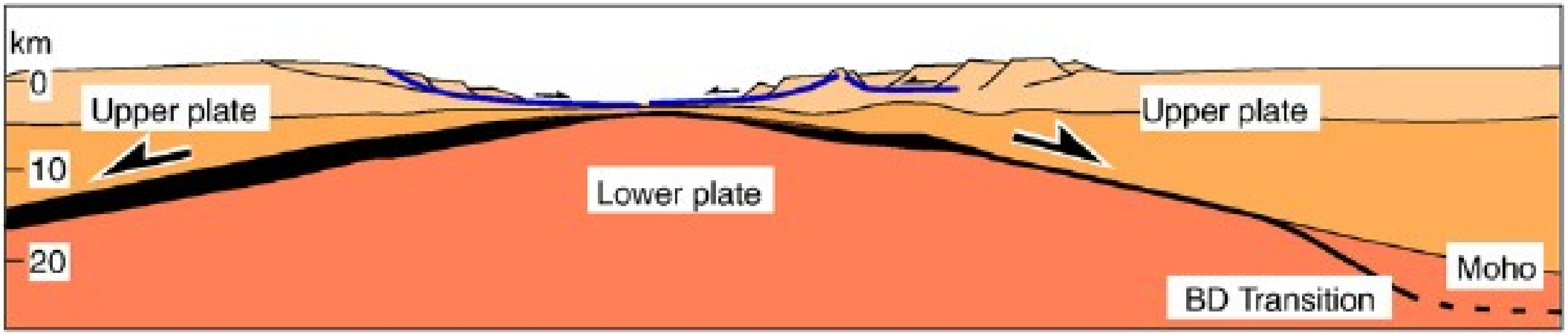

Fig. 4. Mantle dome in rifted passive margins controlled by mantle detachments (black lines) that may nucleate at a sub-Moho brittle–ductile transition (after Weinberg et al., 2007). Activity along both mantle and crustal detachments accounts for depth-dependent stretching and the exposure of the upper plate in both conjugate margins.

Rosenbaum et al. (2008)

A distensão em escala litosférica pode gerar padrões Muito complexos de deformação.

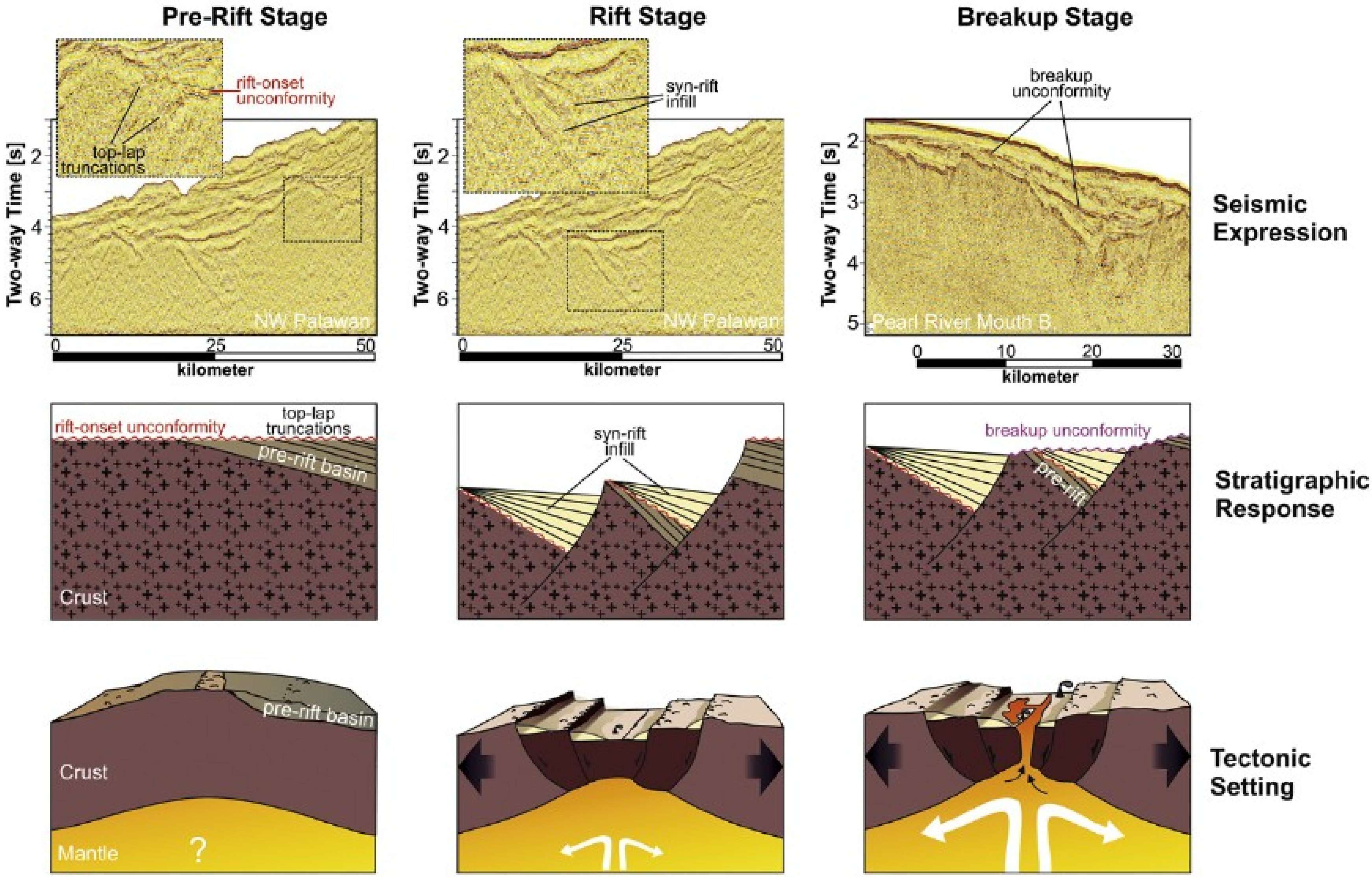

Figure 2. Schematic cross section, a seismic data example and the tectonic setting illustrating the pre-rift erosion, the rift sedimentation, and the breakup stages. During pre- or syn-rift doming erosion a rift-onset unconformity (ROU) forms, which in seismic data often is recognized as angular unconformity with top-lap truncations of seismic reflectors from below. A syn-rift infill typically shows wedge shaped reflector packages with the thin end of the wedge lying on the hangingwall dip-slope. The seismic section shows two subsequent rift deposits before subsidence did outpace sedimentation, resulting in a different relief. This indicates the time of maximum displacement, the rift climax (Prosser, 1993). At continental breakup, a flexural rebound results in uplift of the rift shoulders. This frequently results in the formation of a breakup unconformity (BU), truncating the wedge-shaped syn-rift sediments in the rift basins from the draped post-rift sediments. At the basins outer margins the BU is expected to form an amalgamation with the rift-onset unconformity.

Tipos de marges passivas

Com relação à geodinâmica da abertura:

- Margens vulcânicas

- Margens pobres em magma

Com relação à cinemática da deformação:

- Margens ortogonais

- Margens transformes

GEOCIÊNCIAS USP

Margens Vulcânicas e Pobres em Magma – *End Members*

D. Franke / Marine and Petroleum Geology 43 (2013) 63–87

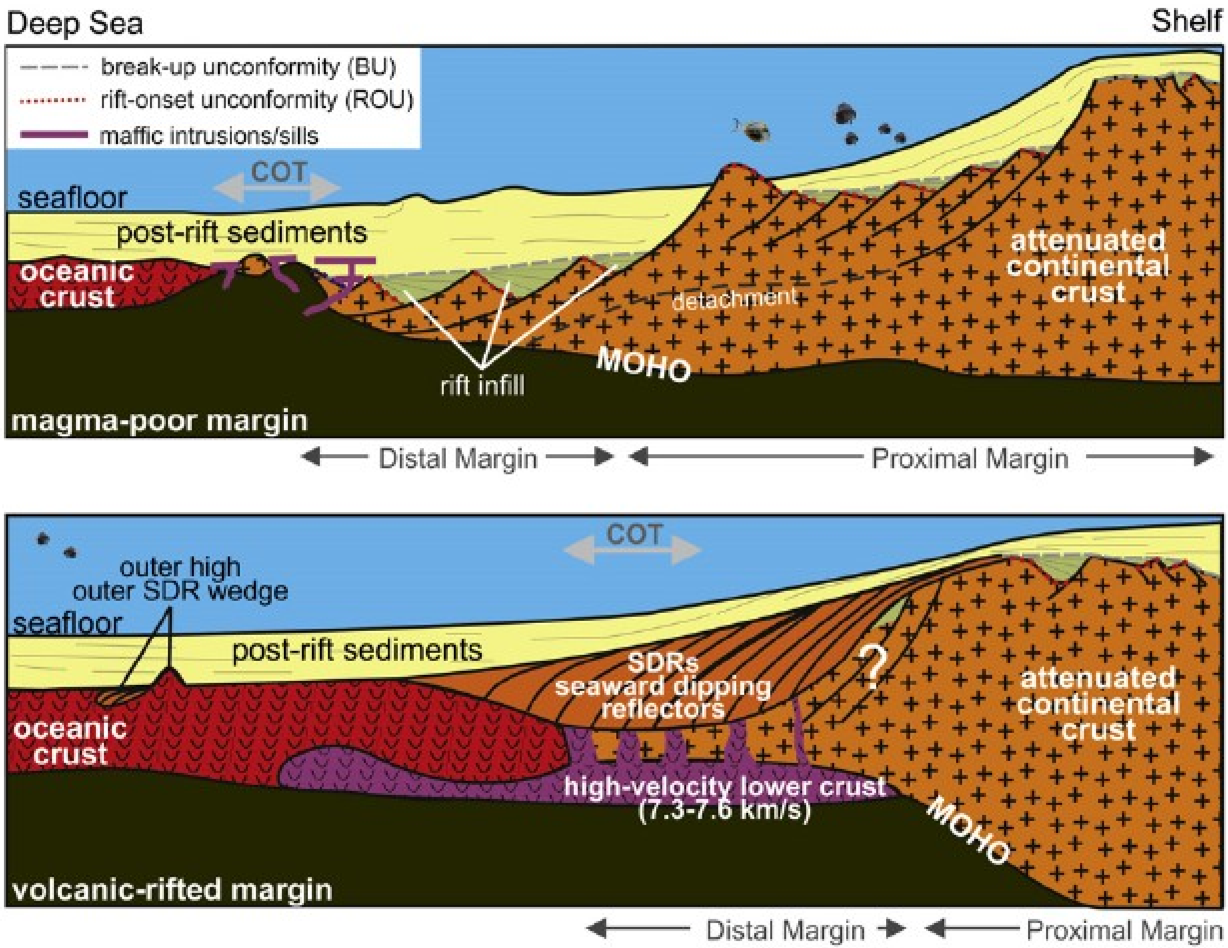

Figure 1. Schematic sketch of the end-member extremes of passive continental margins. Top: The magma-poor margin is defined by a wide area of highly attenuated continental crust where the upper crust is deformed by deep-reaching listric faults that may sole out on a common detachment surface, the proximal margin. In the distal margin the listric faults may cut across the entire crust leading to a detachment at the Mohorovičić (MOHO) discontinuity. Further seaward extensional allochthones may be situated on exhumed mantle before relatively thin oceanic crust is reached. Bottom: Volcanic rifted margins show a comparably narrow proximal margin with considerable crustal thinning over a short distance, thick wedges of syn-rift volcanic flows manifest in seismic reflection data as seaward dipping reflectors (SDRs), and wide high-velocity ($Vp > 7.3$ km/s) lower-crust seaboard of the continental rifted margin. The oceanic crust is comparably thick at those margins, especially close to the continent–ocean transition (COT). ROU is the rift-onset unconformity; BU the breakup unconformity.

Margens vulcânicas

- São mais frequentes que as pobres em magma

- Área de distensão crustal mais estreita que as pobres em magma (50 a 100 km de extensão)

- Espessos derrames na fase rift (até 15 km), compondo refletores de grande amplitude inclinados para o oceano (SDRs)

- Apresentam uma crosta inferior de alta velocidade (>7.3 km/s), geralmente interpretada como *underplating* de magma básico

- Geralmente apresentam COT (transição entre crosta continental e oceânica) abrupta

- O magmatismo implica em grande fusão de manto.
Relação com as LIPs (Large Igneous Provinces)
Plumas ou não (grande debate)

Margens vulcânicas

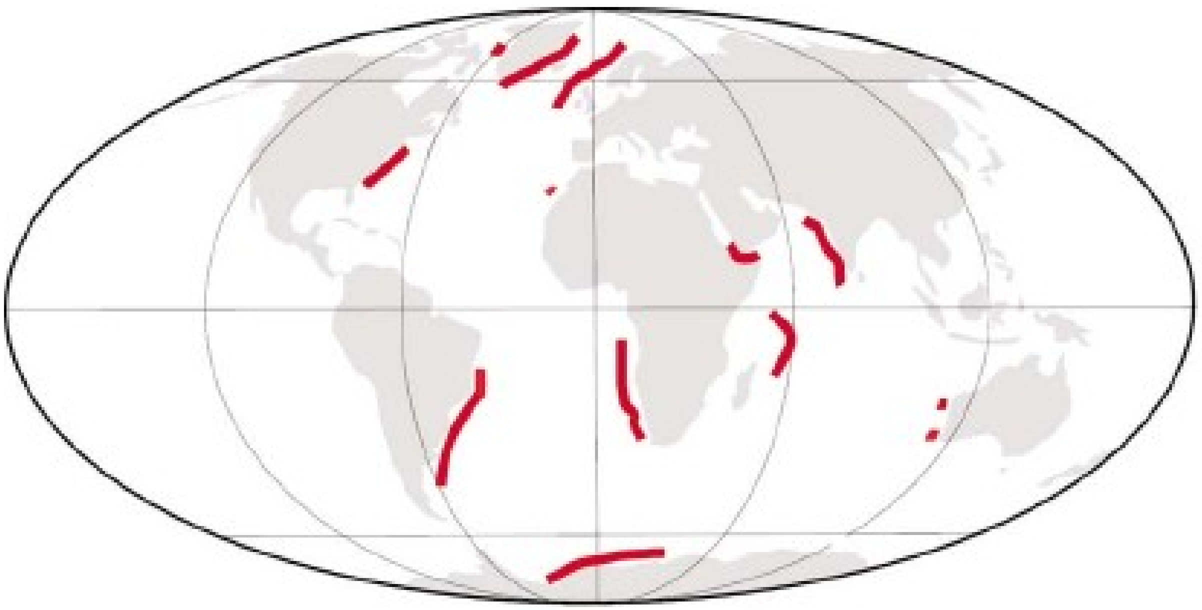

Fig. 2. Worldwide distribution of volcanic passive margins (in [14], after [16]).

L. Geoffroy / C. R. Geoscience 337 (2005) 1395–1408

Introdução

Origem

Depósitos

Seqüências Deposicionais

Inversão

GEOCIÊNCIAS USP

LIPs – Large Igneous Provinces

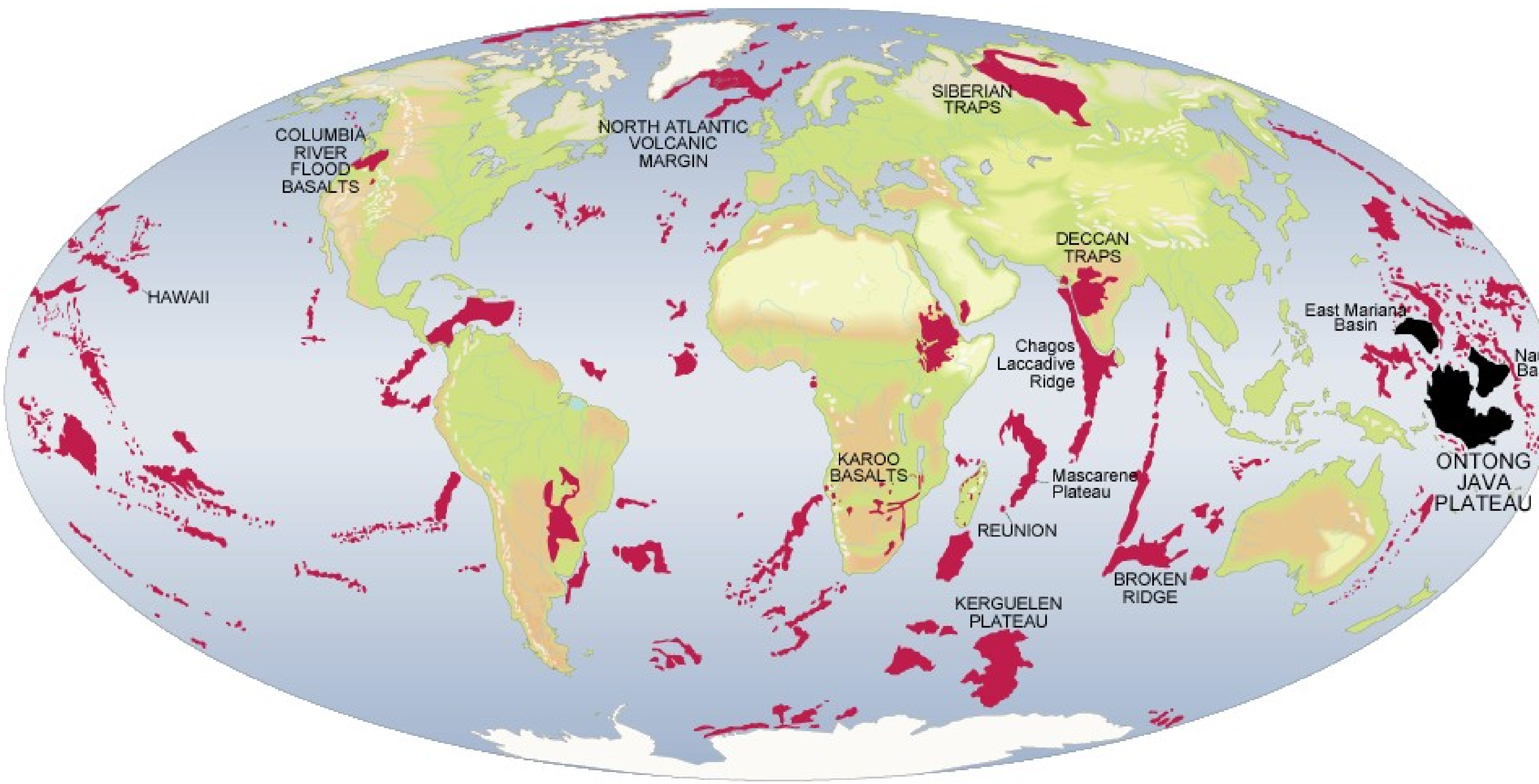

Coffin & Eldholm (1993)

Introdução
Origem
Depósitos
Seqüências Depositionais
Inversão

Plumas?

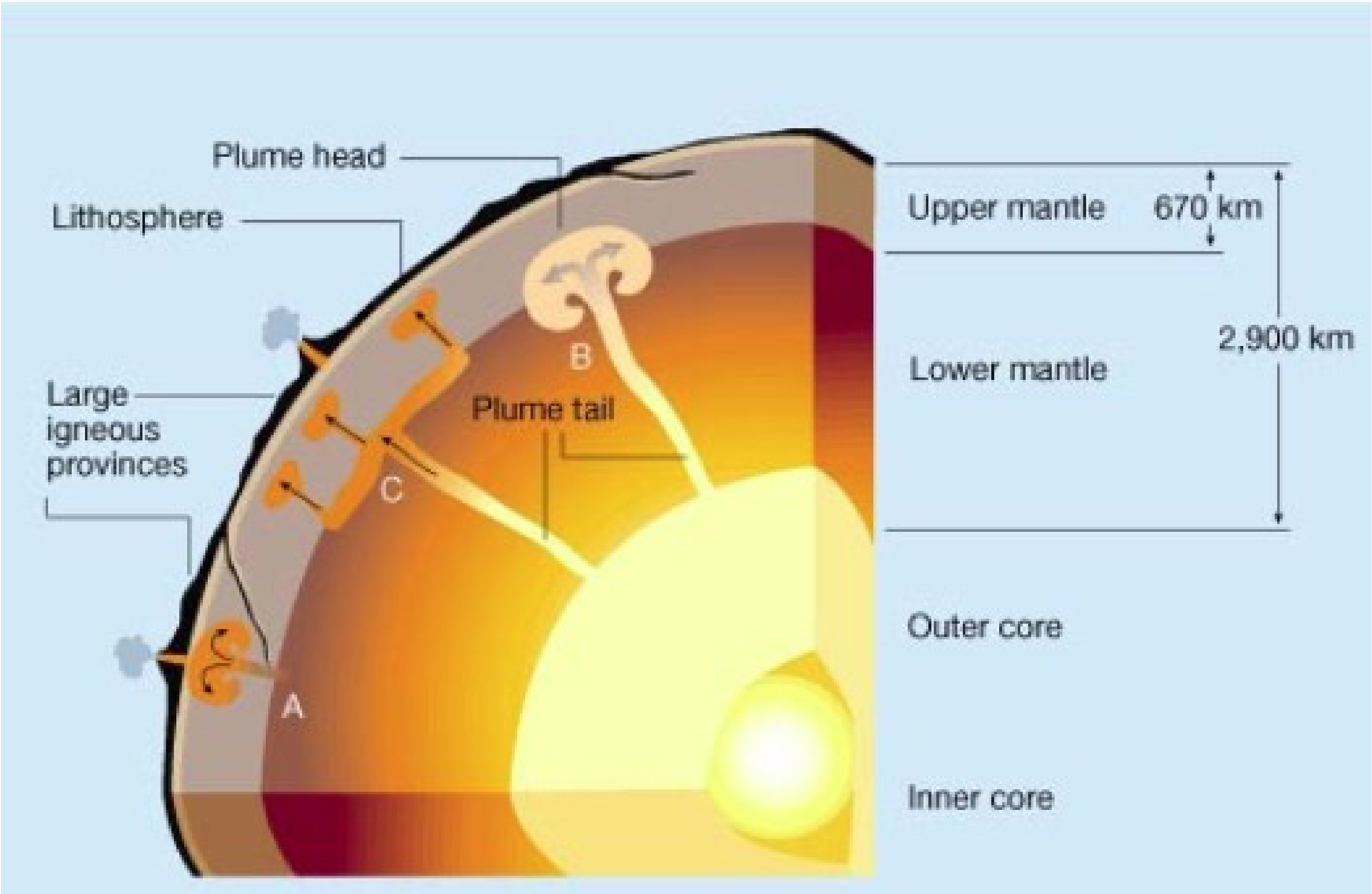

Ou não?

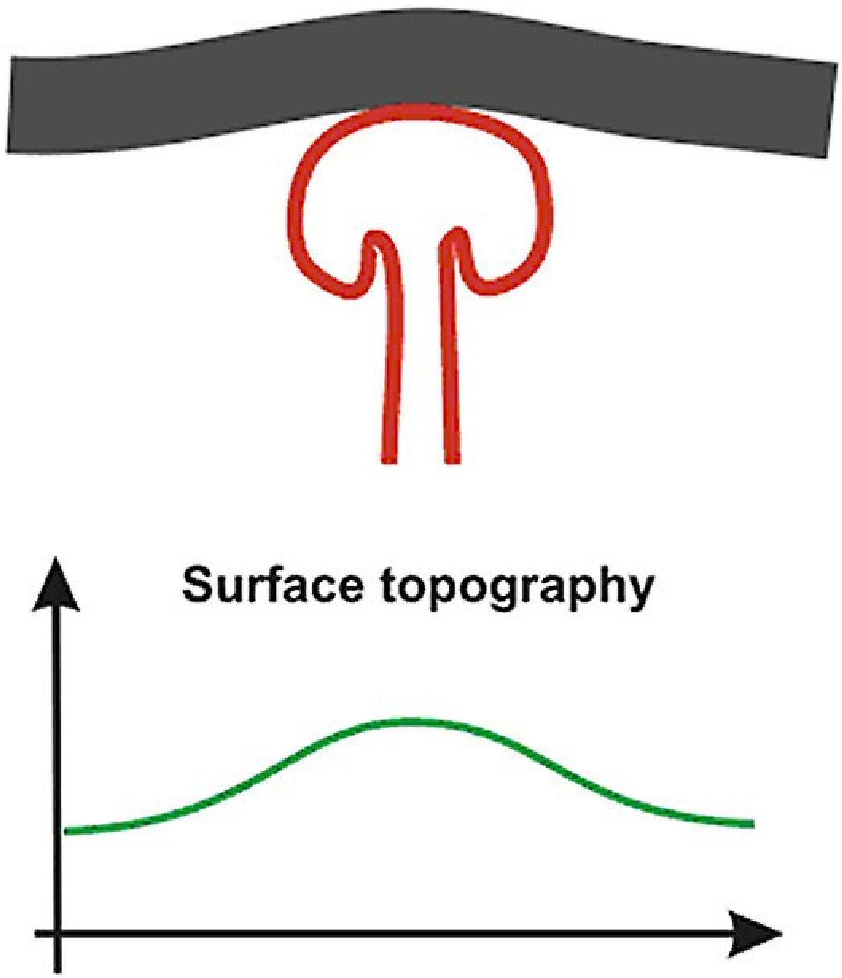

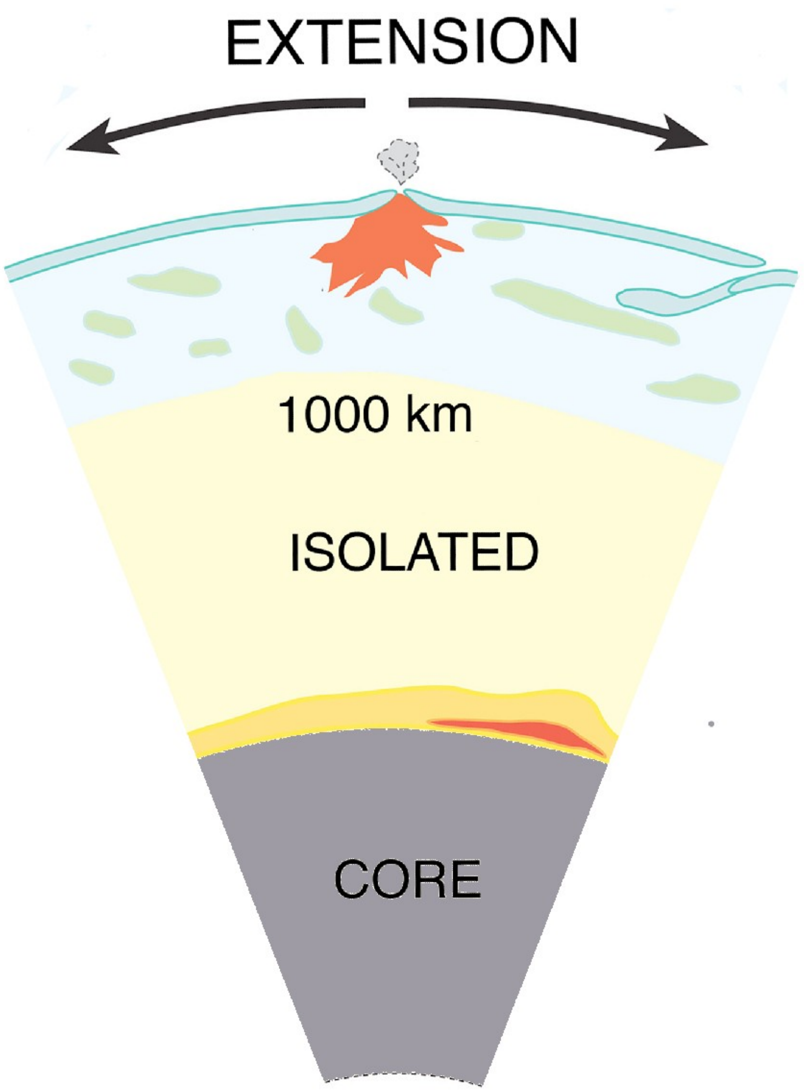

Fertilidade em dorsais meso-oceânicas

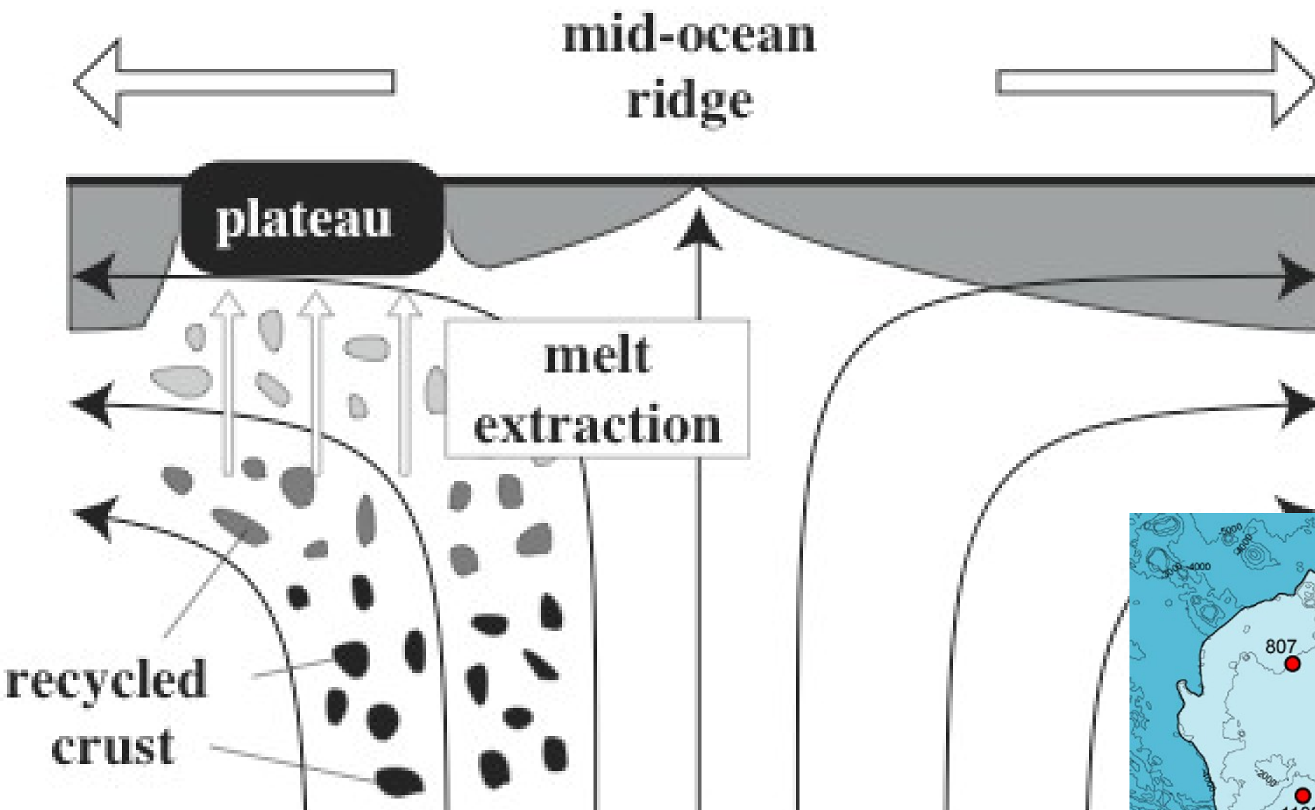

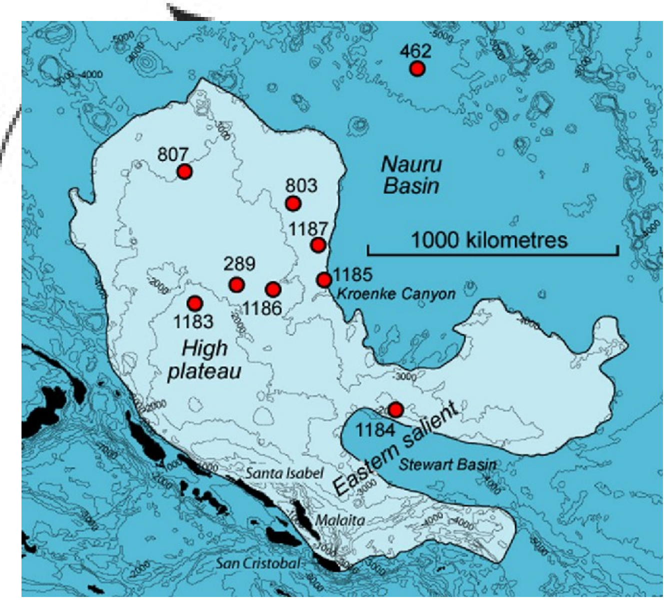

Korenaga (2005)

Introdução

Origem

Depósitos

Seqüências Deposicionais

Inversão

Margens vulcânicas

L. Geoffroy / C. R. Geoscience 337 (2005) 1395–1408 1397

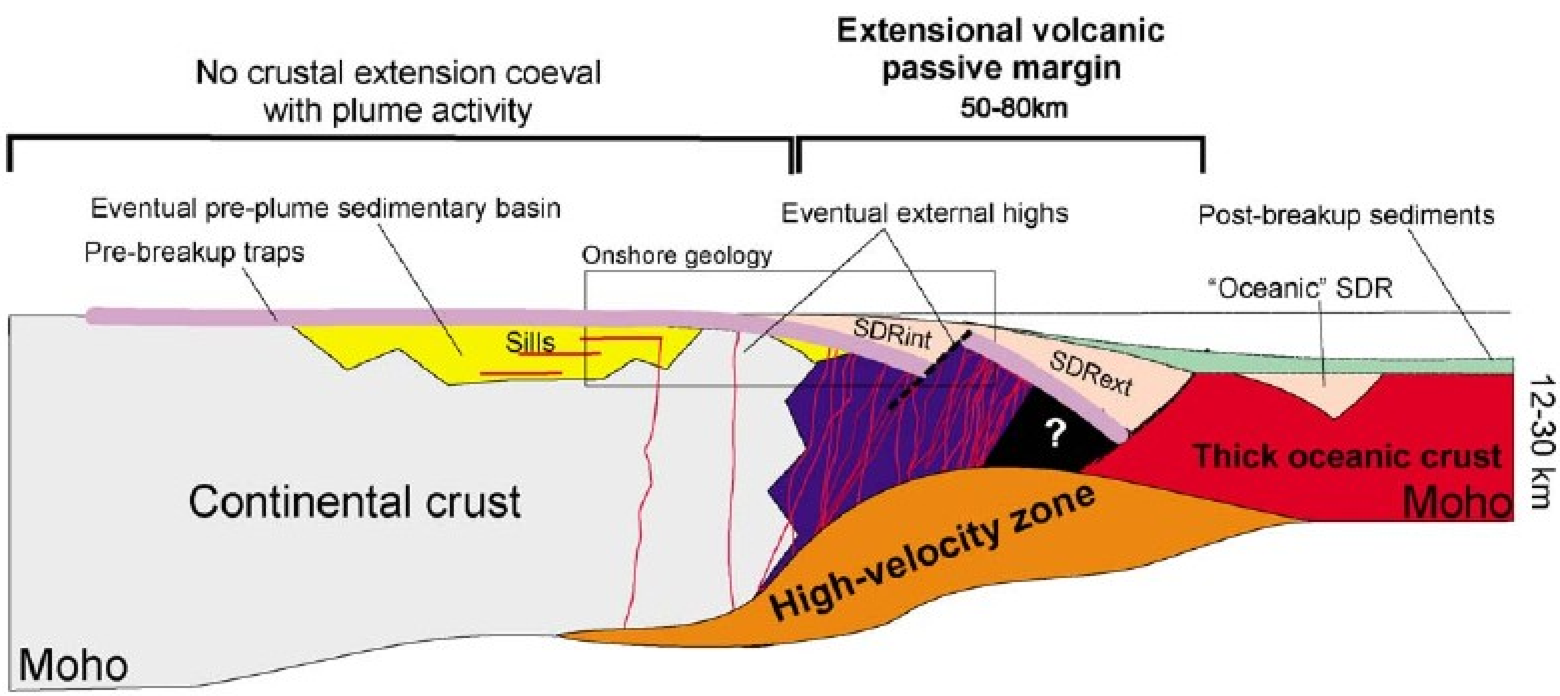

Fig. 1. Across-strike section of a volcanic passive margin. The presence of internal sedimentary basins is not the rule. SDRint and SDRext: respectively, internal and external seaward-dipping lavas and volcanic projections (i.e. 'Seaward-Dipping Reflectors' in offshore studies).

L. Geoffroy / C. R. Geoscience 337 (2005) 1395–1408

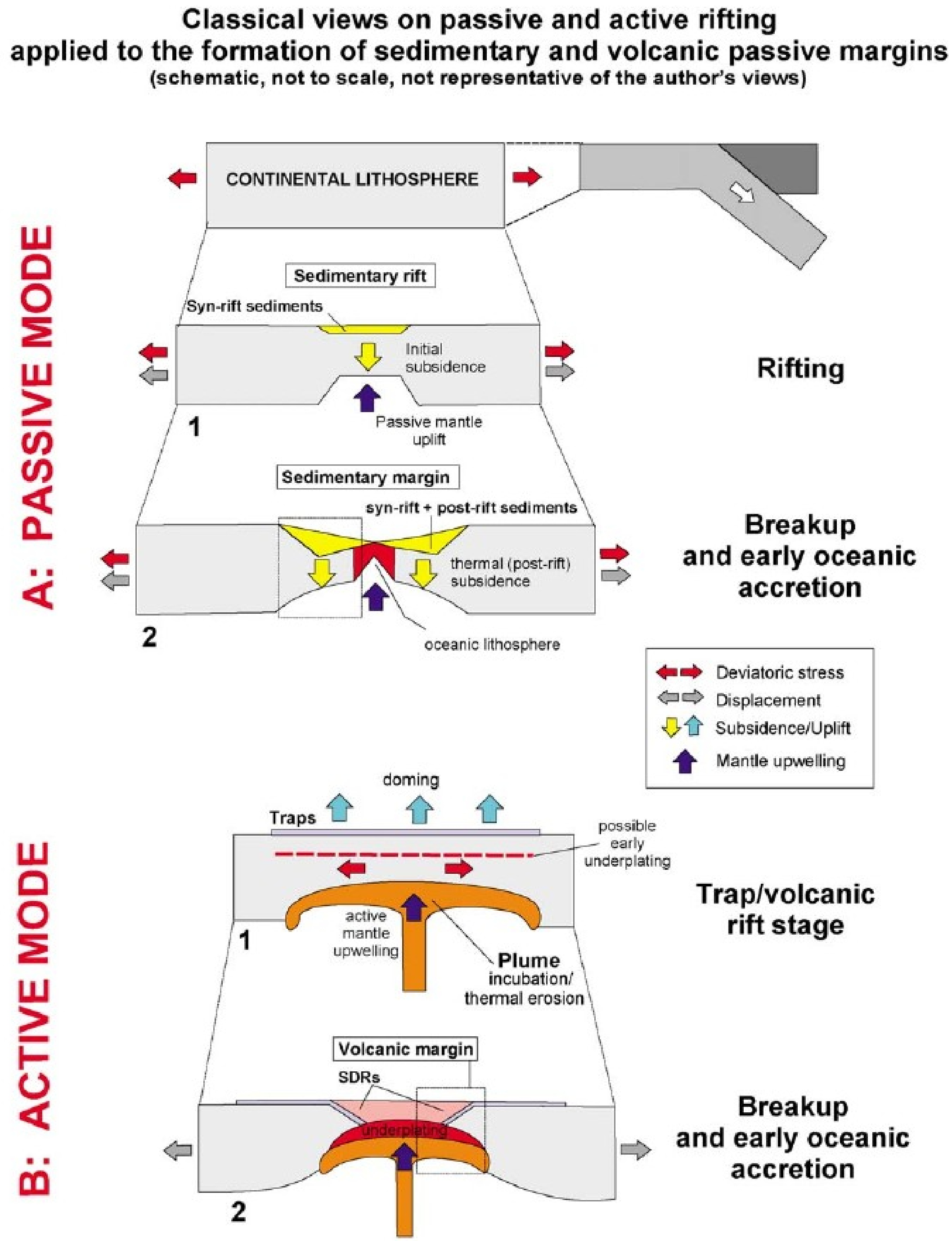

Fig. 3. Passive (**A**) and active (**B**) mechanisms of lithosphere extension. From a synthesis and simplification of numerous studies that followed [76].

Fig. 3. Mécanismes passifs (**A**) et actifs (**B**) d'extension lithosphérique (d'après une synthèse de très nombreux travaux, dont [76]).

Introdução

Origem

Depósitos

Seqüências Deposicionais

Inversão

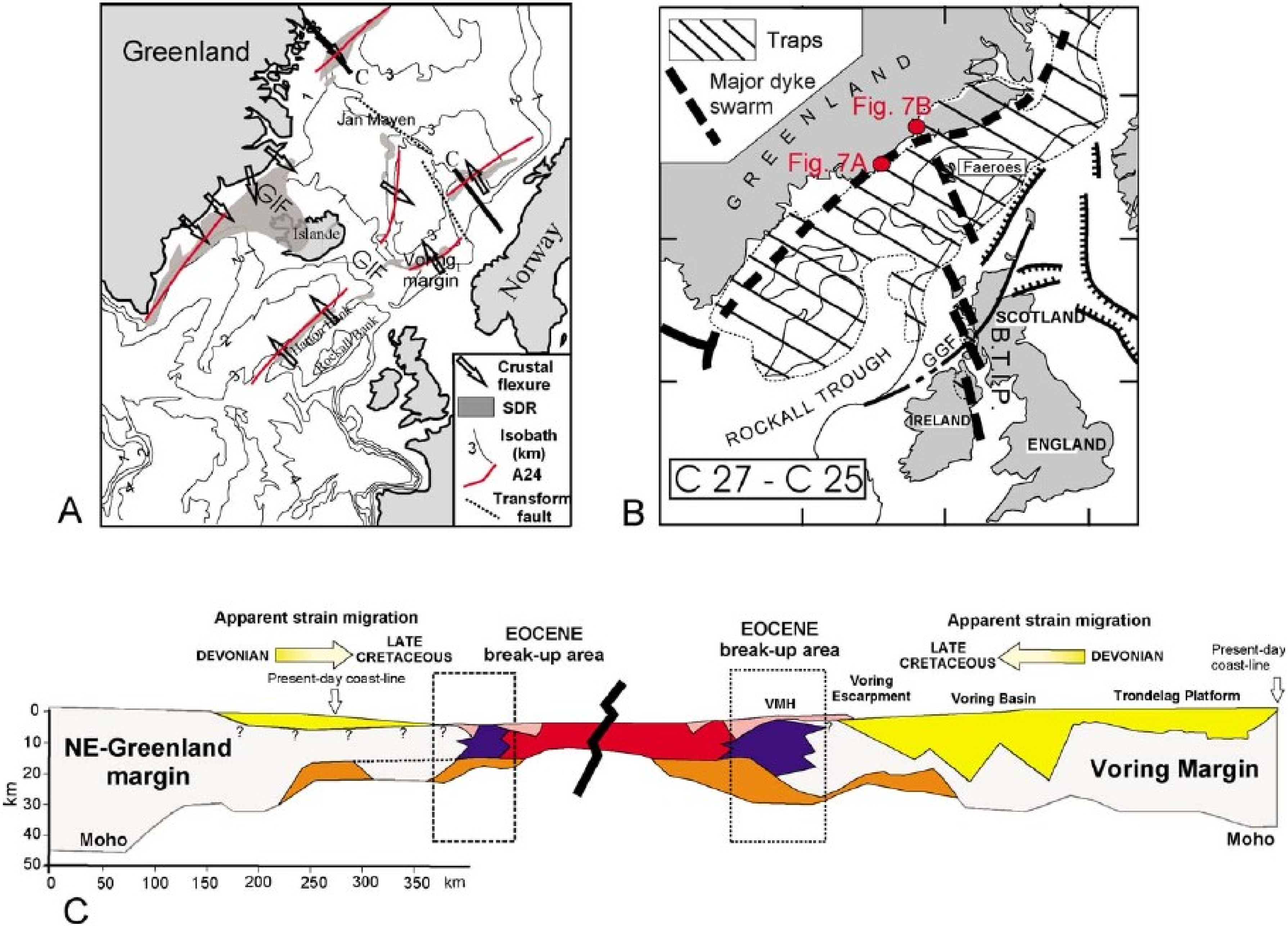

Fig. 4. Conjugated volcanic passive margins in the Northeastern Atlantic. (**A**) Present-day location of VPM (GIF: Greenland-Iceland-Faeroe aseismic ridge). (**B**) North Atlantic Province during the Palaeocene (trap stage, C27–C26). (**C**) Crustal across-strike sections of the conjugated Vıring/NE-Greenland margins). Colours have the same meaning as in Fig. 1. After [29,74] and J.I. Faleide, pers. commun.

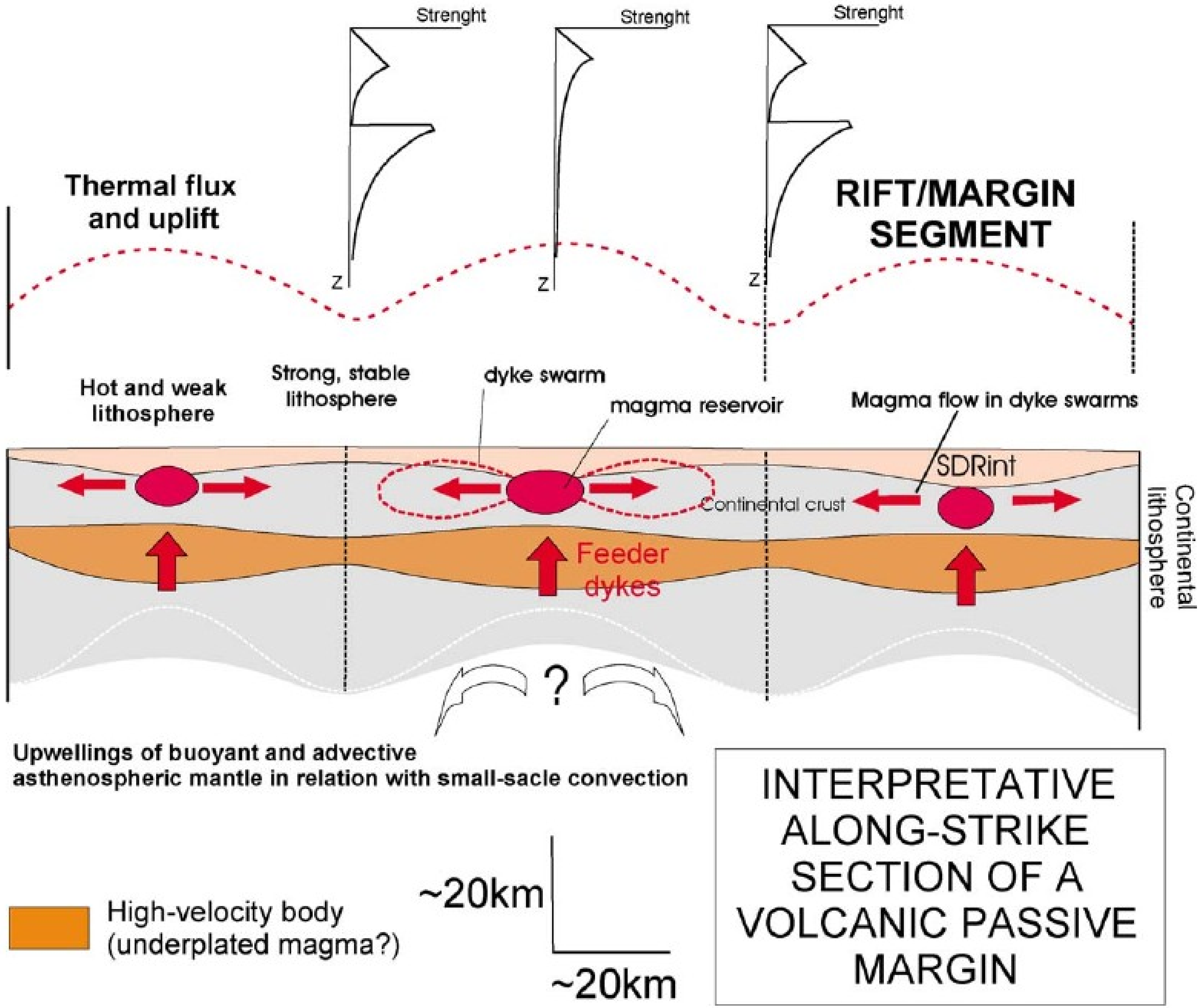

Fig. 5. Along-strike growth model for volcanic passive margins. From [30], modified.

Introdução

Origem

Depósitos

Seqüências Deposicionais

Inversão

Origem dos SDRs

L. Geoffroy / C. R. Geoscience 337 (2005) 1395–1408

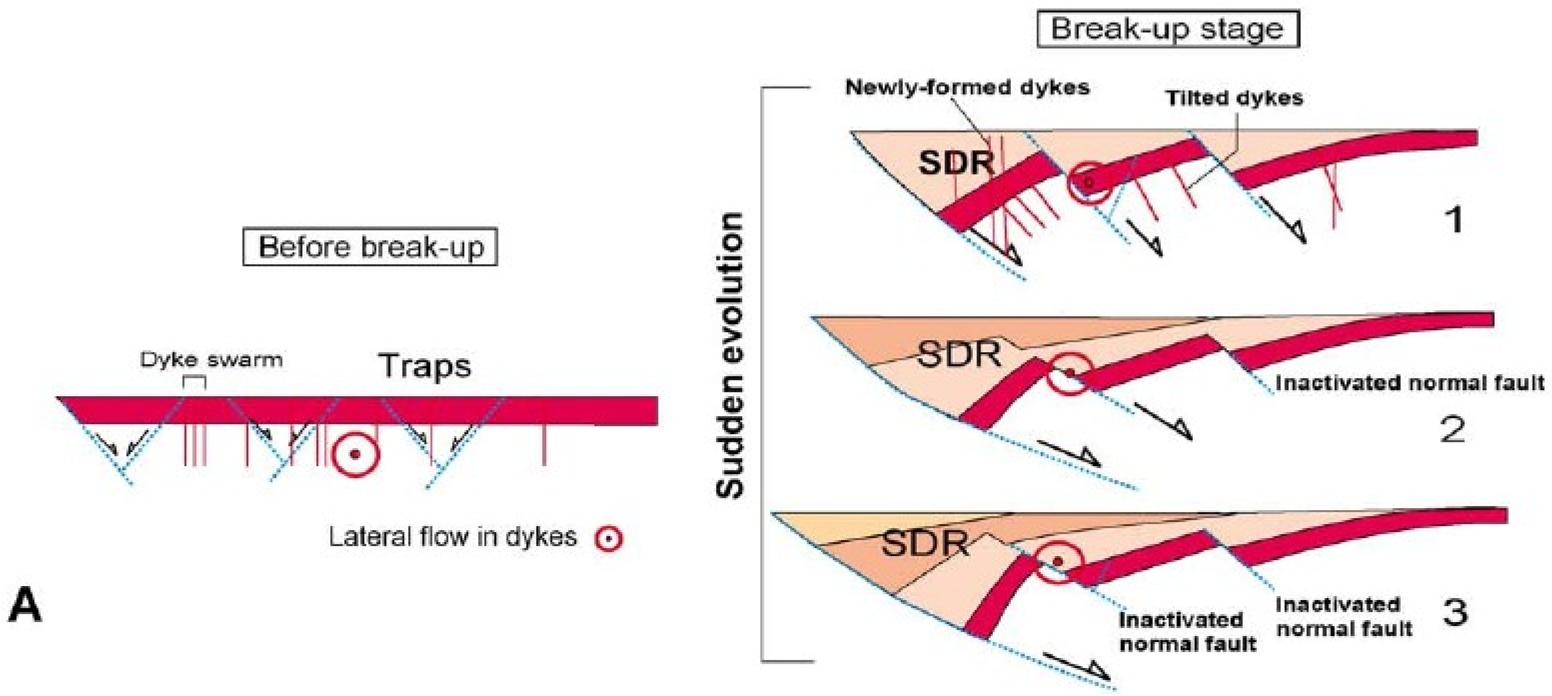

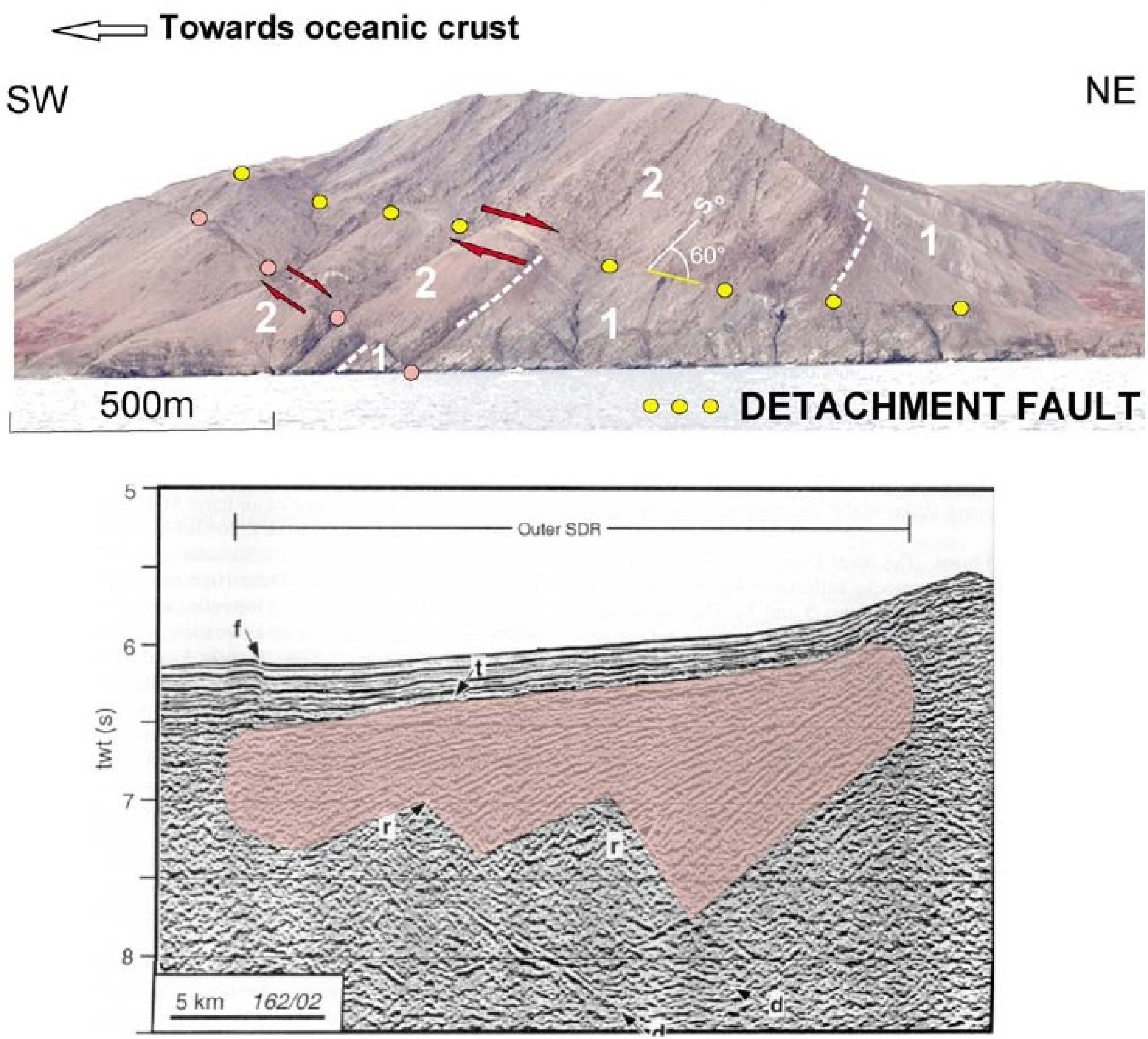

B

C

Fig. 6. (**A**) Formation of SDR at VPM [30]: SDR are syn-magmatic roll-over flexures accommodated by continentward-dipping normal faults. (**B**) Example of tilted continentward-dipping normal fault (yellow dots) in the internal SDR of SE-Baffin Bay (Svartenhuk Peninsula, see [31]). Note also the reactivation of a dyke as a secondary normal fault during the seaward-tilt of the lavas and projections (red dots). (**C**) Outer SDR-prism west of Australia [68]. Note the structure analogue to (**A**) and the existence of continentward-dipping faults (**d**) here interpreted as magma-injected normal faults.

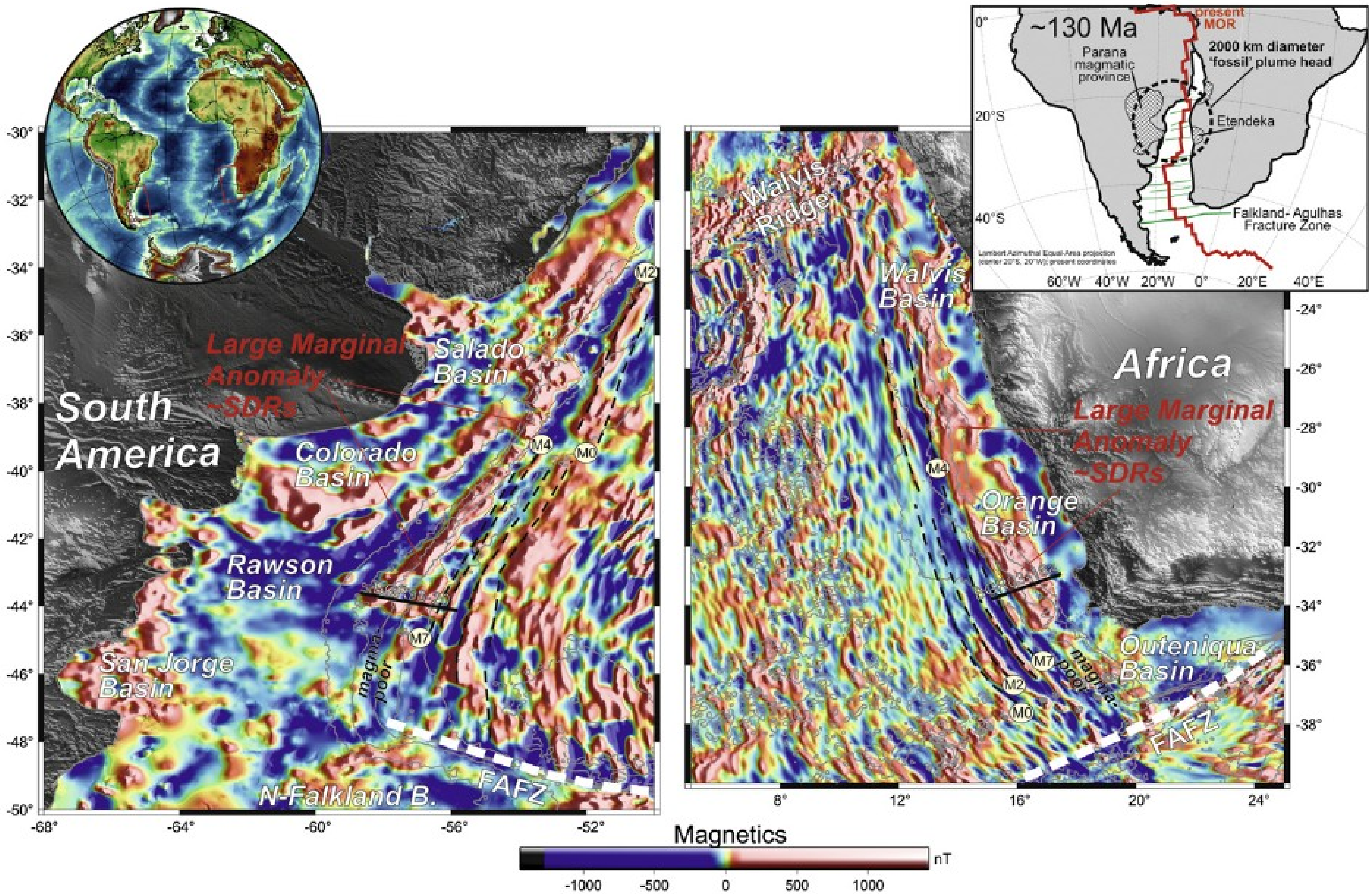

Figure 12. The southern South Atlantic region with the location of the basins discussed. Magnetic map is from Maus et al. (2009). There is a distinct and conjugate southern termination of the Large Marginal Magnetic Anomaly, also named G-anomaly that corresponds to the seaward dipping reflectors (SDRs). The continental margin between this magnetic anomaly and the Falkland-Agulhas Fracture Zone (FAFZ) is magma-poor. Black lines show the location of example seismic sections presented in Figure 14. The 1.000 m isobaths are shown in gray. Magnetic seafloor spreading anomalies M0 through M7 are tentatively interpreted (Schreckenberger et al., 2002). The inlay shows a reconstruction at about 130 Ma with a 2.000 km diameter of the Tristan da Cunha plume head. Abbreviations: SDRs – seaward dipping reflectors, MOR – mid-oceanic ridge.

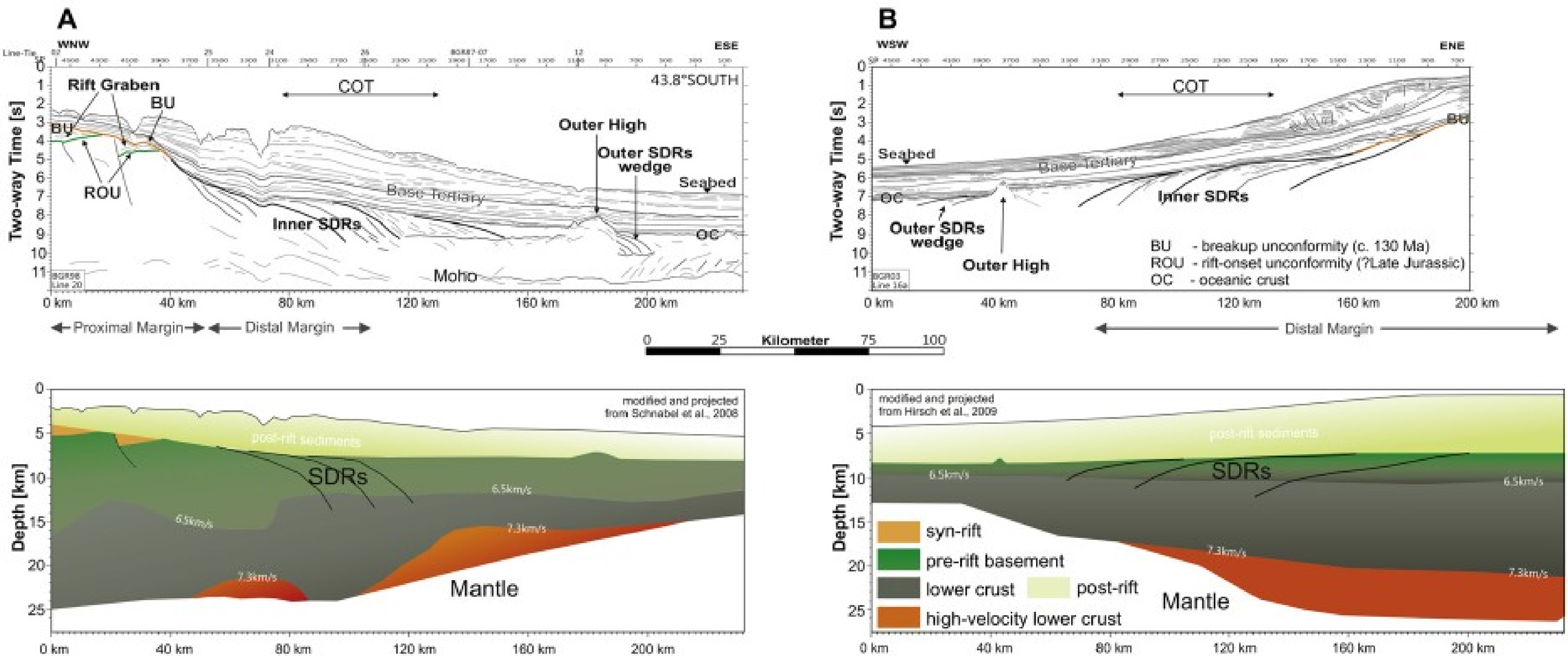

Figure 14. The MCS lines BGR98-20 and BGR03-16a are considered as conjugate because both are crossing the continental margins close to the southern end of the Large Marginal Magnetic Anomaly. The upper panels show line-drawing interpretations of MCS line BGR98-20, running across the Argentine margin and of line BGR03-16a, running across the South African margin. The location of the lines is shown in Figure 12. In the lower panels velocity profiles as derived from refraction seismic modeling were modified and projected onto the lines. The Argentina profile is from Schnabel et al. (2008); the South Africa profile is from Hirsch et al. (2009). While the first line was shot close to the MCS line, the latter profile has an offset of about 200 km. Post-rift sediments are shown in blue, pre-rift sediments in light orange, the upper crust in green and the lower crust (Vp > 6.5 km/s) in gray. High-velocity lower crust (Vp > 7.3 km/s) is shown in orange-red. The seaward dipping reflectors (SDRs) cover an area of about 80 km on the western margin, while they spread over about 100 km on the eastern margin. Also the high-velocity lower crust is much more voluminous on the eastern margin.

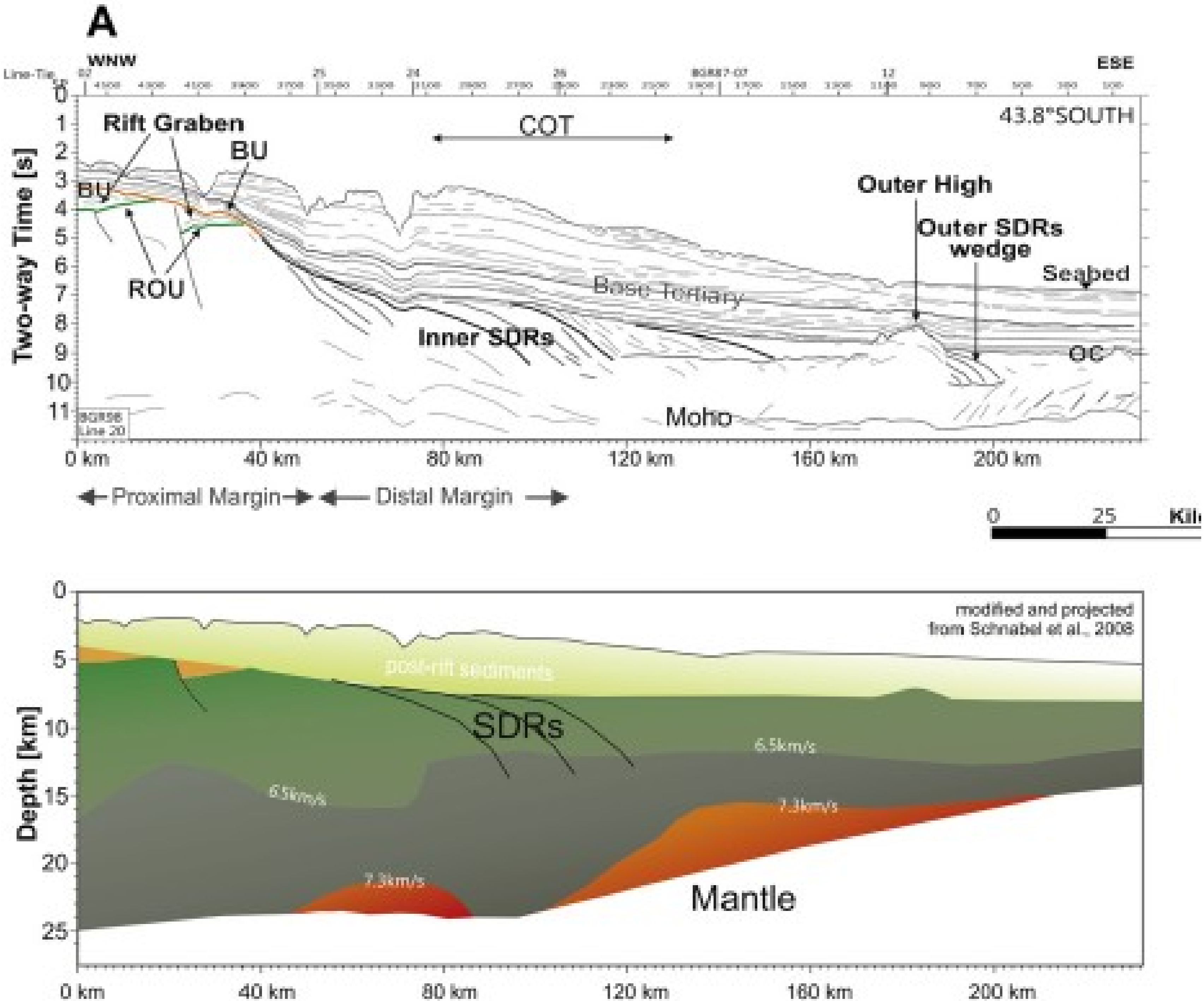

A
WNW
ESE
43.8°SOUTH
COT
Rift Graben
BU
BU
ROU
Outer High
Outer SDRs wedge
Seabed
Base Tertiary
Inner SDRs
OC
Moho
BGR98 Line 20
Two-way Time [s]
0 km
40 km
80 km
120 km
160 km
200 km
Proximal Margin
Distal Margin
0
25
modified and projected from Schnabel et al., 2008
post-rift sediments
SDRs
6.5km/s
6.5km/s
7.3km/s
7.3km/s
Mantle
Depth [km]

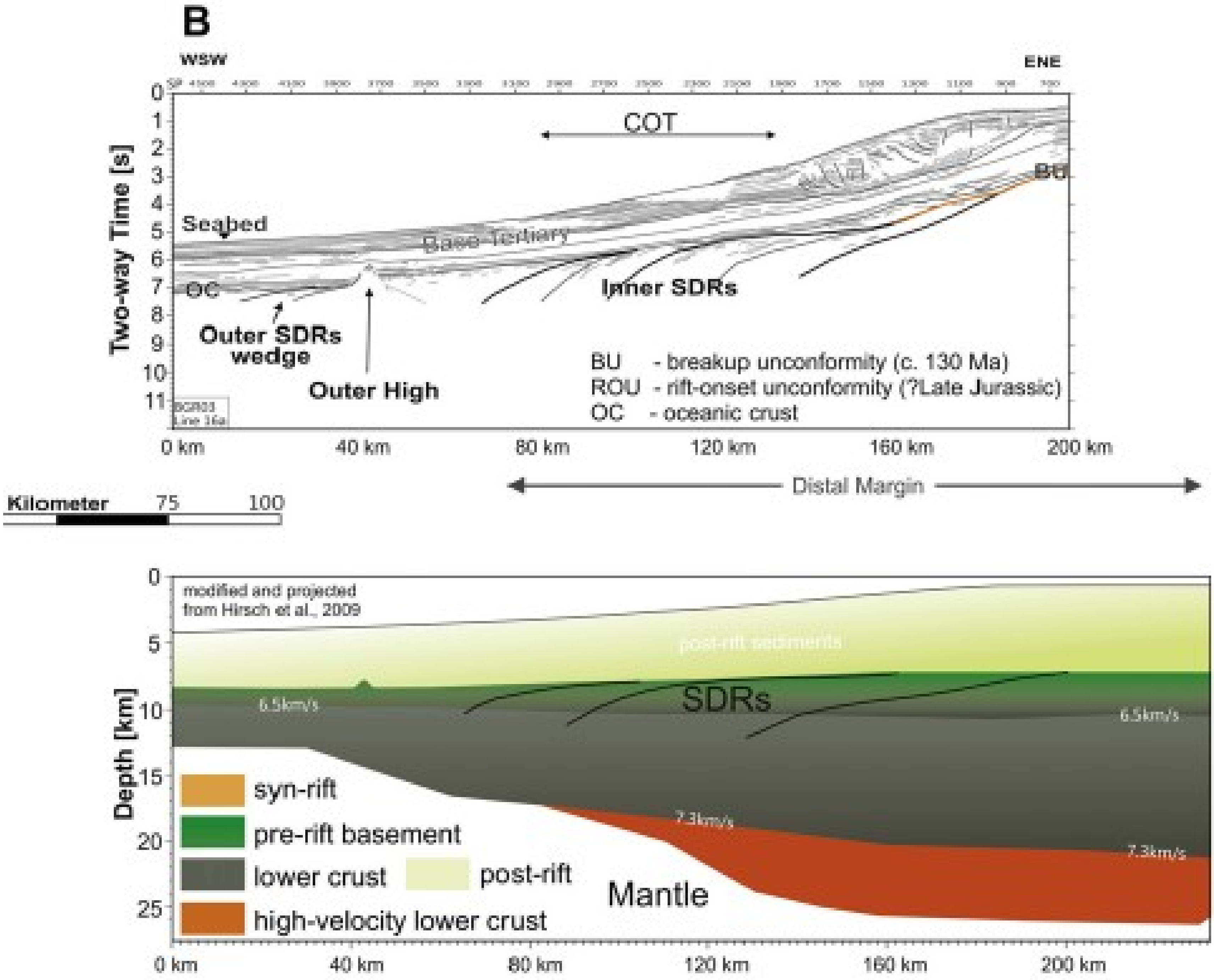
B
WSW
ENE
COT
BU
Seabed
Base Tertiary
OC
Inner SDRs
Outer SDRs wedge
Outer High
Two-way Time [s]
BU - breakup unconformity (c. 130 Ma)
ROU - rift-onset unconformity (?Late Jurassic)
OC - oceanic crust
0 km
40 km
80 km
120 km
160 km
200 km
Distal Margin
Kilometer 75 100
modified and projected from Hirsch et al., 2009
post-rift sediments
SDRs
6.5km/s
7.3km/s
Depth [km]
syn-rift
pre-rift basement
lower crust
post-rift
high-velocity lower crust
Mantle

Margens pobres em magma

- São menos frequentes que as pobres em magma

- Área de distensão crustal de várias centenas de km, com zonas com diferentes estilos e taxas de deformação

- Sucessõe vulcânicas na fase rift apenas restritas

- Geralmente apresentam COT (transição entre crosta continental e oceânica) gradual ou mal definido

- Área mais distal hiperdistendida (fator Beta muito alto, chegando a 10)

- Pode haver exumação de manto

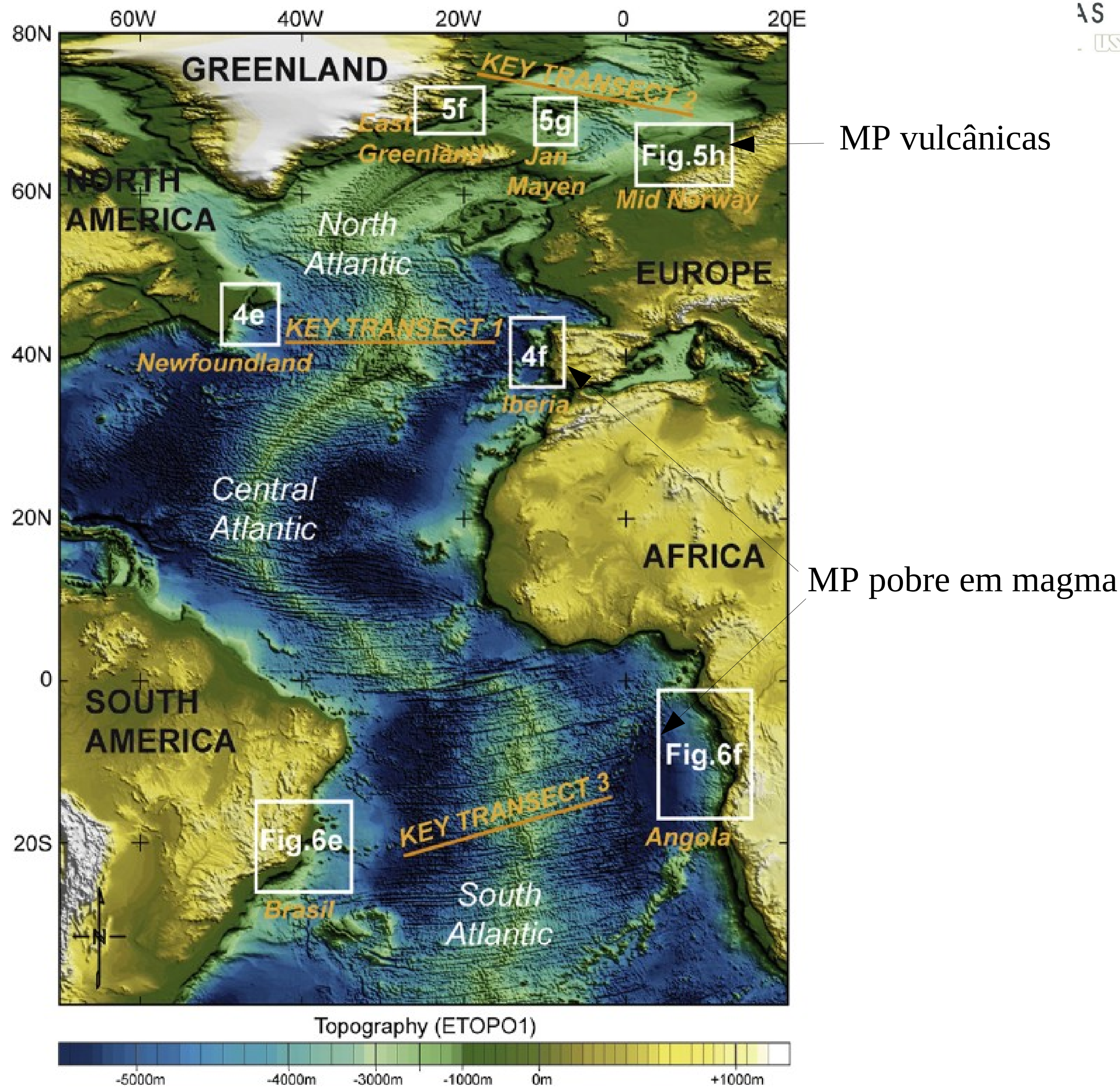

Figure 1. Topographic map of the Atlantic Ocean. The boxes show the location of the rifted areas discussed in the contribution. Topography is ETOPO1 (Amante and Eakins, 2009) presented in geographical latitude–longitude coordinates (datum WGS84).

GEOCIÊNCIAS USP

Margens pobres em magma

MP vulcânicas

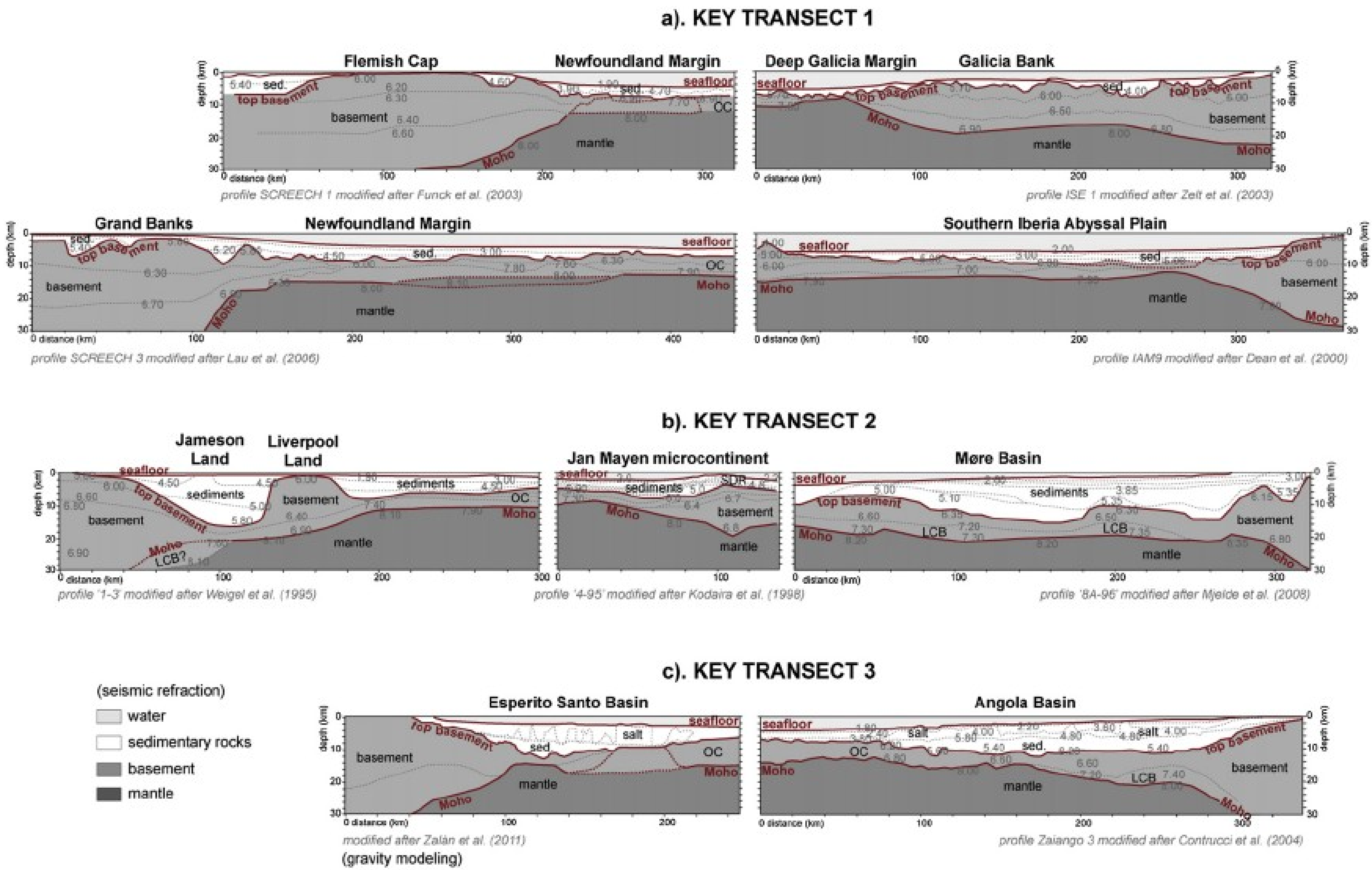

Figure 2. Compilation of published seismic refraction models along the key transects considered in the contribution. Vertical exaggeration ~2. OC: oceanic crust. sed.: Sedimentary rocks. a: Conjugate seismic refraction profiles illustrating the geometries of the northern segment (up) and the central segment (down) of the Iberia–Newfoundland system (data are from Funck et al., 2003; Zelt et al., 2003; Lau et al., 2006a,b; Dean et al., 2000). b: Conjugate seismic refraction profiles illustrating the geometries of the Norwegian–Greenland Sea system (data are from Weigel et al., 1995; Kodaira et al., 1998; Mjelde et al., 2008). c: Conjugate seismic refraction profiles illustrating the geometries of the South Atlantic system (data are from Zalán et al., 2011; Contrucci et al., 2004). The location of the profiles is shown in Figures 4–6. The red segments underline the major refraction horizons: the seafloor, top–basement and Moho.

G. Peron-Pinvidic et al. / Marine and Petroleum Geology 43 (2013) 21–47

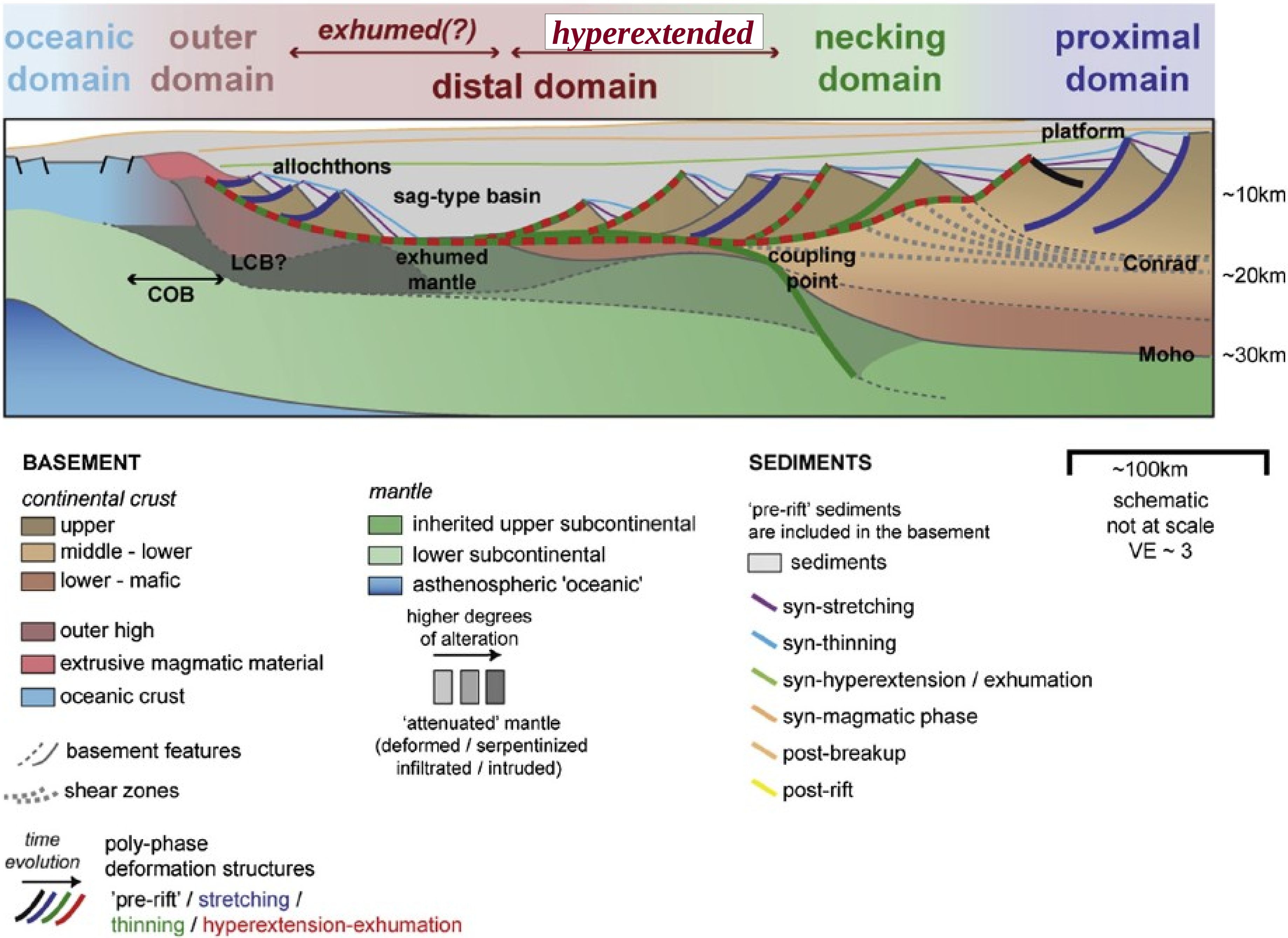

Figure 3. Schematic section of a typical rifted margin illustrating the various terms used in this contribution.

Introdução
Origem
Depósitos
Seqüências Deposicionais
Inversão

The proximal domain - The proximal domain corresponds to the inboard continental crust that has been stretched at low values of extension.

The necking domain - The necking domain corresponds firstly to a specific wedge shape of the crust: this is the zone of the margin where the (seismic) Moho defines an inflection point associated with a drastic crustal thinning from 30 km to less than 10 km.

The distal domain - Depending on the study area and on the terminology, the distal domain corresponds to and/or includes the proximal and distal OCT (oceanecontinent transition), the transitional domain and/or the ZECM (zone of exhumed continental mantle). The distal domain is also regularly referenced as the **hyperextended domain** where seismic refraction shows that basement has been thinned down to <10 km.

G. Peron-Pinvidic et al. / Marine and Petroleum Geology 43 (2013) 21–47

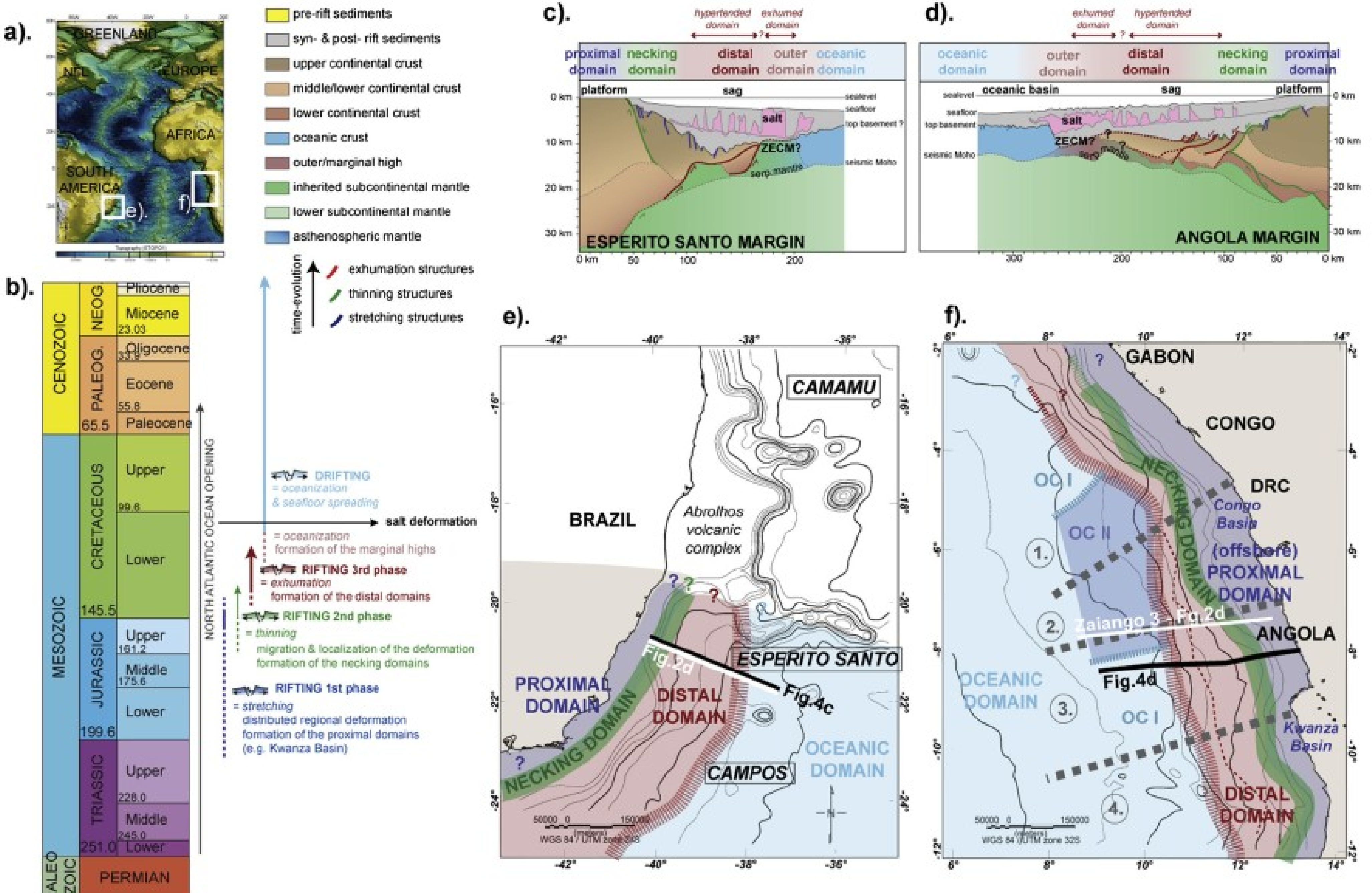

Figure 6. Synthesis figure summarizing the major characteristics of the Angola–Gabon–Campos conjugate system. a: Topography of the Atlantic Ocean with location of the discussed areas. b: Paleozoic–Cenozoic timescale listing the major phases of deformation and tectonic events of the Angola–Brazil rifted margins. c and d: Schematic (composite) sections across the Esperito Santo and Angola margins illustrating the domains and main structural features that characterize the architectures of the margins (after Zalán et al., 2011; Unternehr et al., 2010). e and f: Bathymetric maps (contours every 500 m) of the Angola–Gabon and Campos–Camamu margins with location of the domains, main structural features and illustrated profiles (the white segments refer to profiles displayed in other figures when the black ones locate the sections presented above in c and d).

G. Peron-Pinvidic et al. / Marine and Petroleum Geology 43 (2013) 21–47

a).

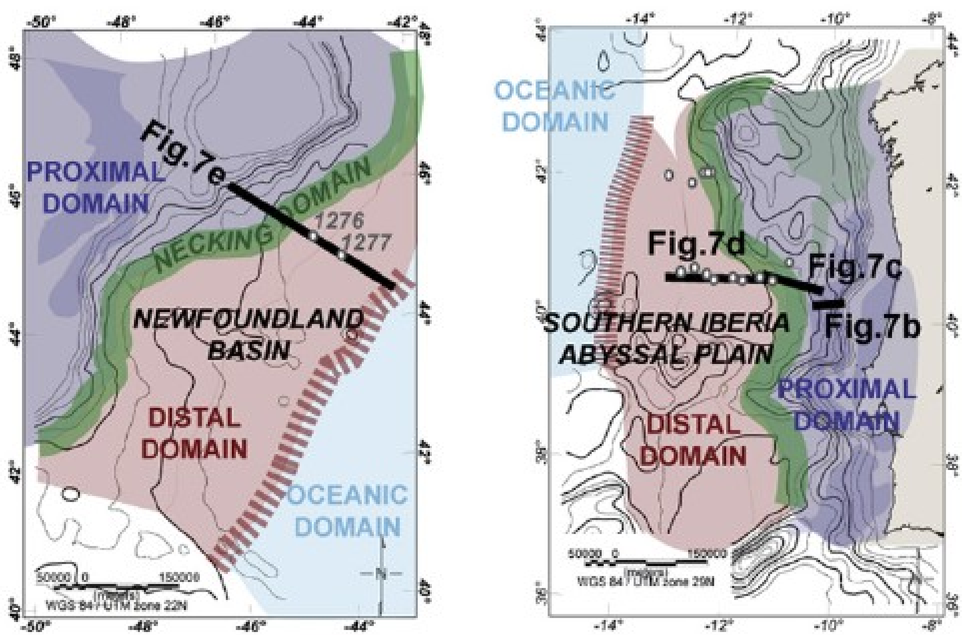

KEY TRANSECT 1

IBERIA NEWFOUNDLAND

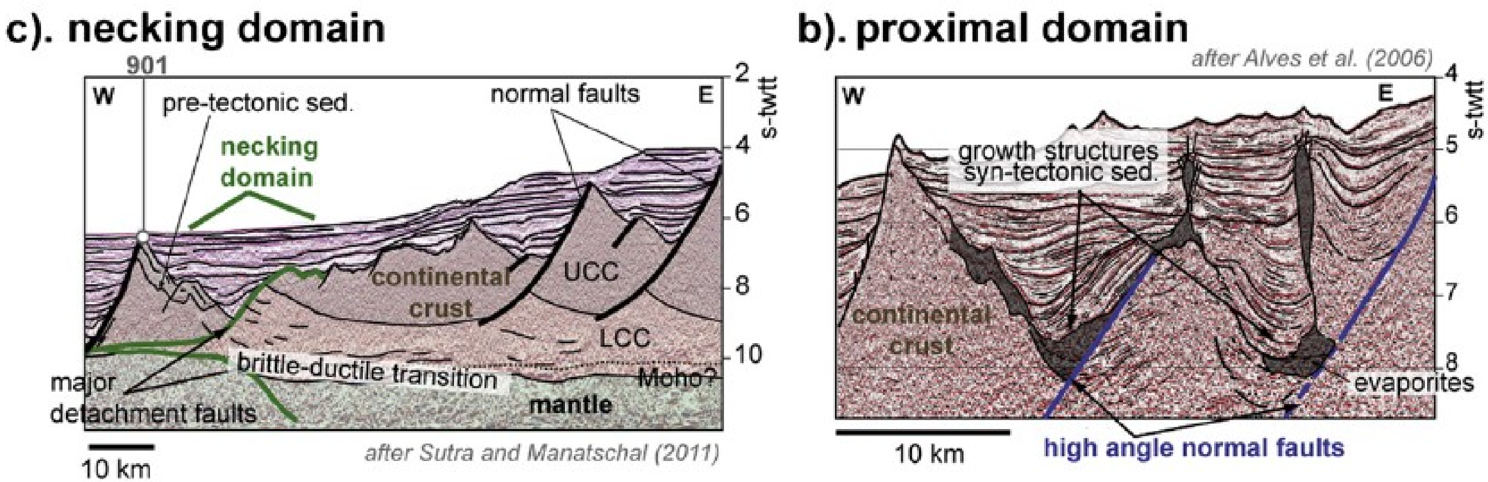

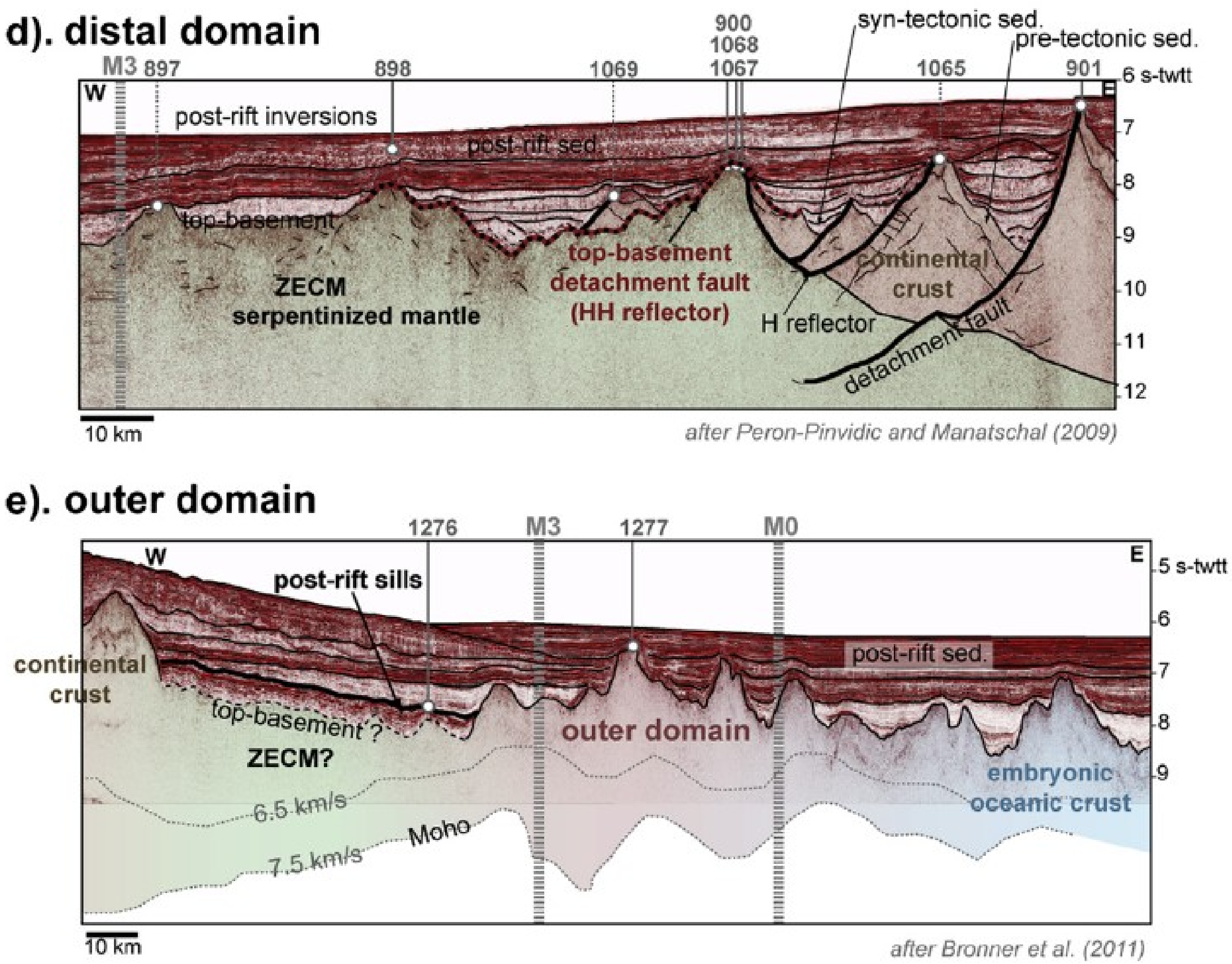

Figure 7. Key data examples of the major domains of the IberiaeNewfoundland conjugate system. a: Bathymetric maps of the Iberia and Newfoundland margins with location of the presented sections. b: Detail of a seismic section illustrating the classical basement (tilted blocks) and sedimentary (wedge shape) geometries observed at the Iberia proximal domain (after Alves et al., 2006). c: Detail of a seismic section illustrating the architecture of the necking domain observed at the Southern Iberia Abyssal Plain (after Sutra and Manatschal, 2012). d: Detail of a seismic section illustrating the basement and sedimentary architecture of the distal domain at the Southern Iberia Abyssal Plain (after Peron-Pinvidic and Manatschal, 2009). e: Detail of a seismic section illustrating the basement and sedimentary architecture of the outer domain observed at the Newfoundland margin (after Bronner et al., 2011).

GEOCIÊNCIAS USP

Bacia de Angola-Gabão

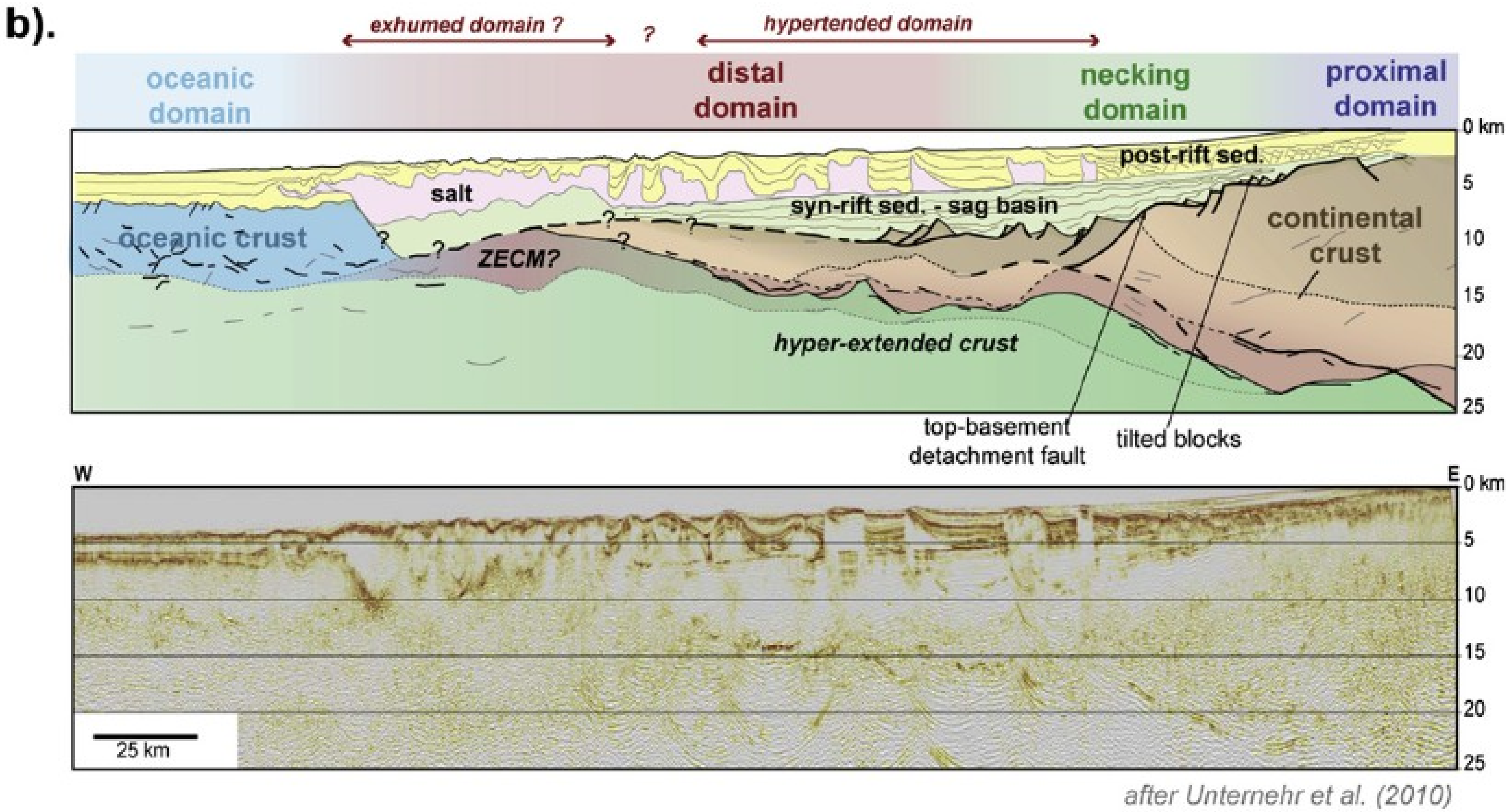

Figure 9. a: Bathymetric map of the Angola–Gabon margin with location of the presented section. b: Seismic reflection profile (courtesy of ion-GXT) and interpretation illustrating the main structural characteristics of the Angola–Gabon margin (segment 3) (after Unternehr et al., 2010).

Exumação de manto

-Distensão de toda a crosta antes da ruptura do manto!

- Serpentinização do manto reduz sua densidade de 3.3 para 2.7 g/cm³

- A reação é fortemente exotérmica – aumento da temperatura das rochas em até 260 C.

Introdução
Origem
Depósitos
Seqüências Deposicionais
Inversão

- Pouca distensão na fase rift e bacias amplas (*sag*) com poucas falhas, sempre em águas rasas no Aptiano – como explicar?

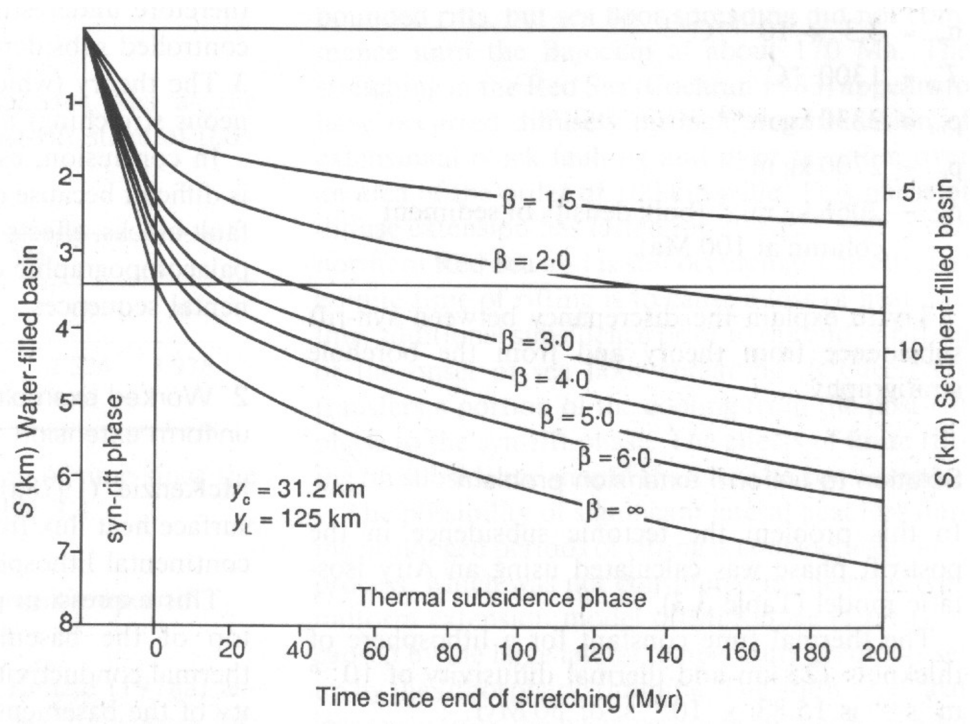

A inadequação do modelo de Mackenzie

- Pouca distensão na fase rift e bacias amplas (*sag*) com poucas falhas, sempre em águas rasas no Aptiano – como explicar?

Unternerh et al.
Petroleum Geoscience, Vol. 16 2010, pp. 207–215
DOI 10.1144/1354-079309-904

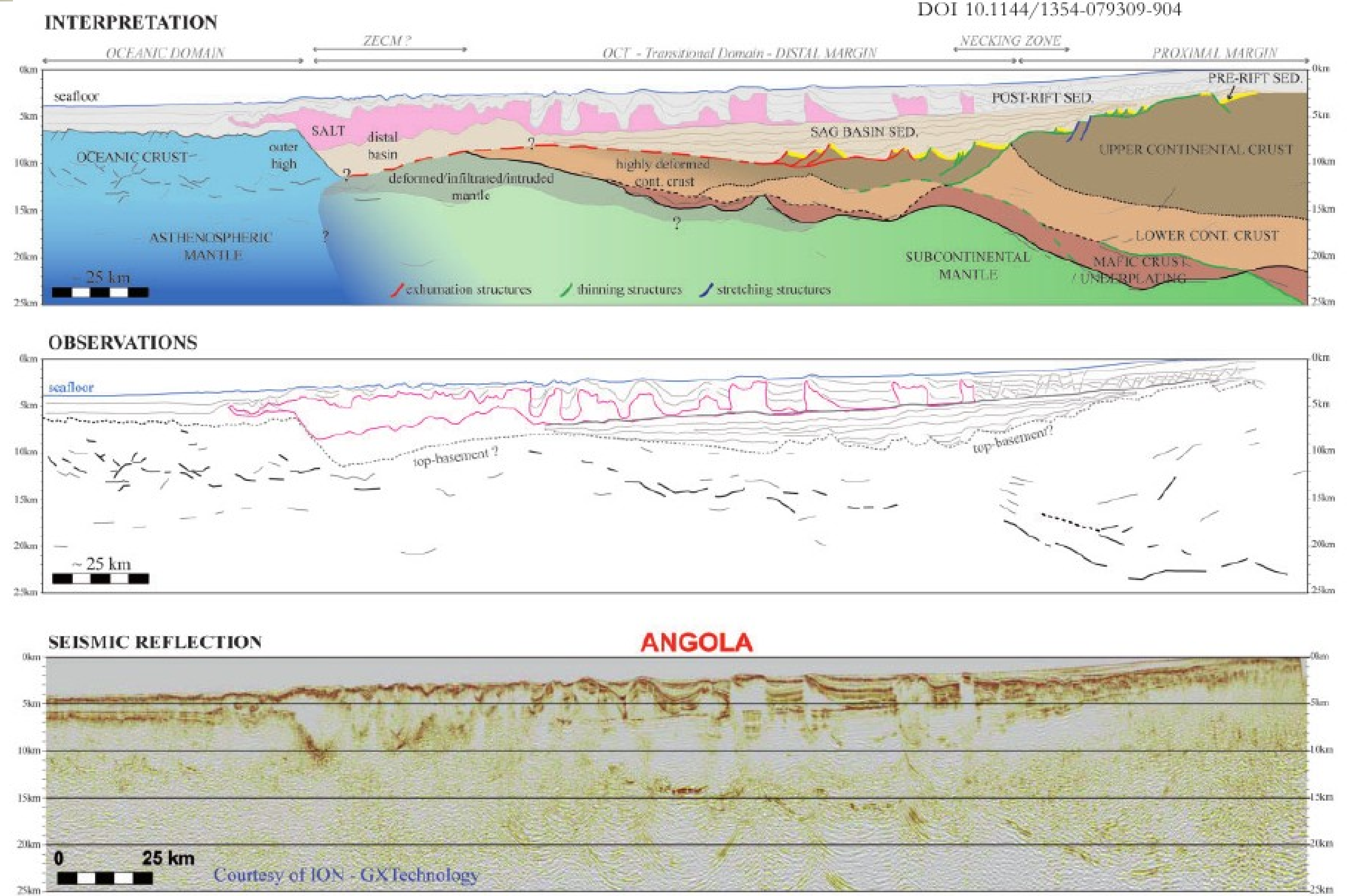

Fig. 2. Angola GXT seismic line. From bottom to top, a depth migrated reflection seismic line, a line drawing and a geological interpretation of one and the same line are shown.

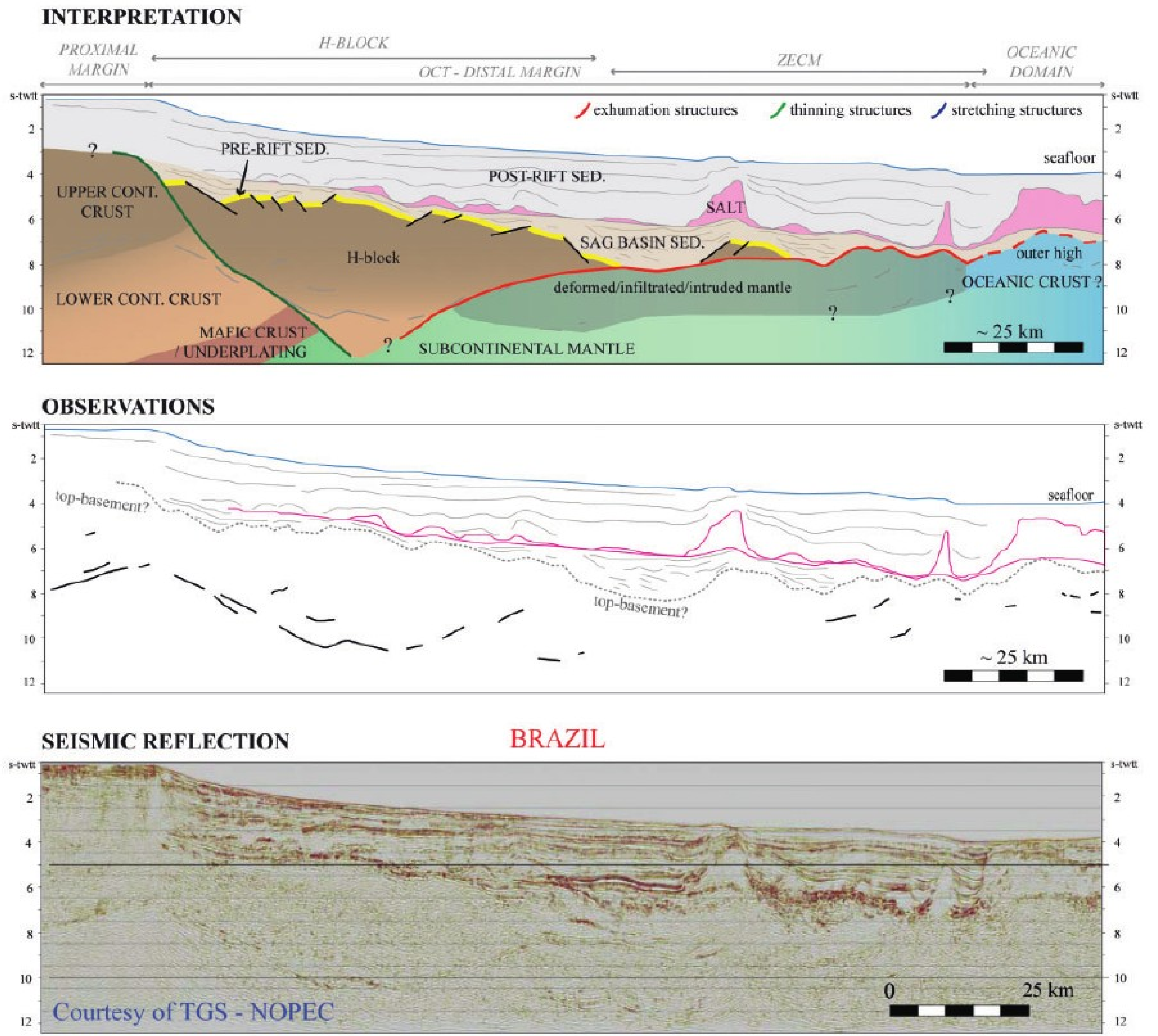

Fig. 4. The TGS line across the Campos Basin offshore Brazil. From bottom to top, a depth migrated reflection seismic line, a line drawing and a geological interpretation of one and the same line are shown.

Introdução

Origem

Depósitos

Seqüências Depositionais

Inversão

GEOCIÊNCIAS USP

Distensão dependente da profundidade e múltiplas fases de deformação

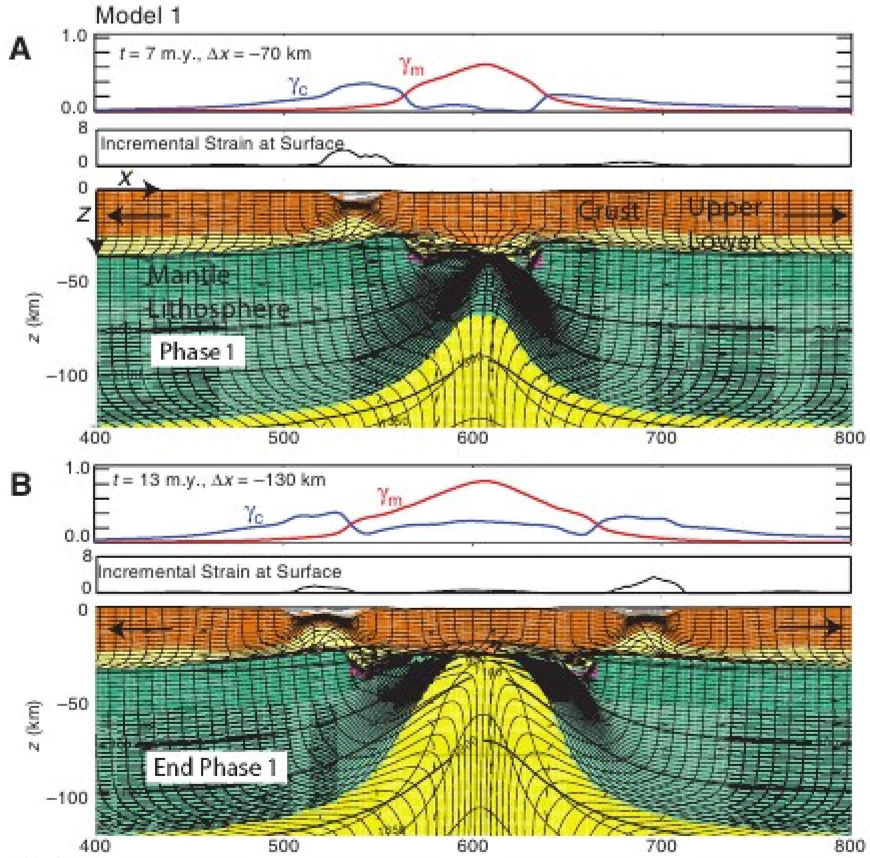

Distensão dúctil de crosta inferior: Subsidência mecânica sem falhas

Complex rifted continental margins explained by dynamical models of depth-dependent lithospheric extension. Ritske S. Huismans and Christopher Beaumont GEOLOGY, February 2008

Distensão dependente da profundidade e múltiplas fases de deformação

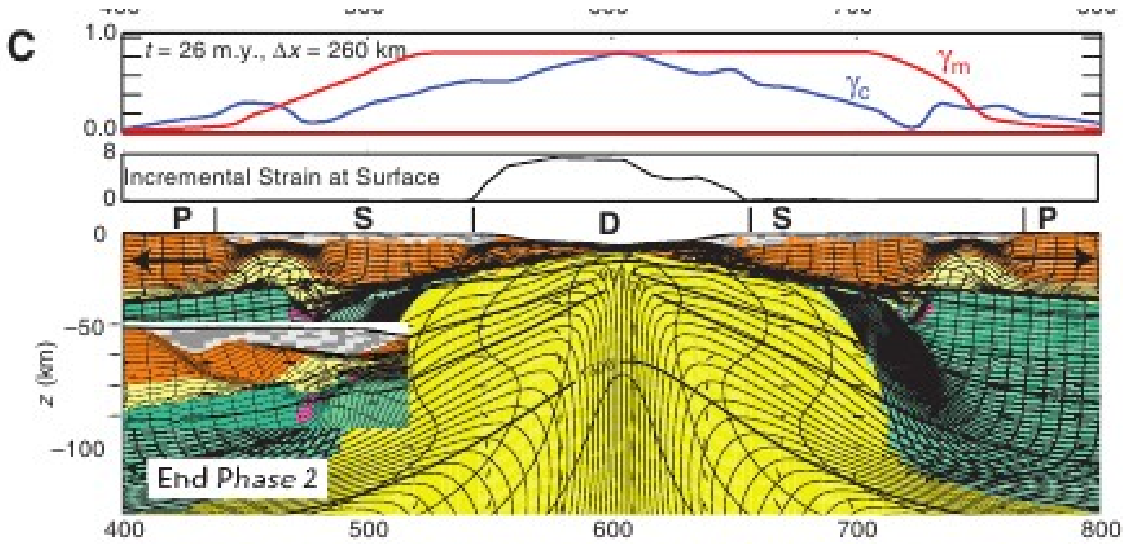

Distensão de área ampla do manto e fluxo lateral de manto posteriores.

Complex rifted continental margins explained by dynamical models of depth-dependent lithospheric extension. Ritske S. Huismans and Christopher Beaumont GEOLOGY, February 2008

Introdução

Origem

Depósitos

Seqüências Deposicionais

Inversão

GEOCIÊNCIAS USP

Characteristic properties of type I and type II margins.

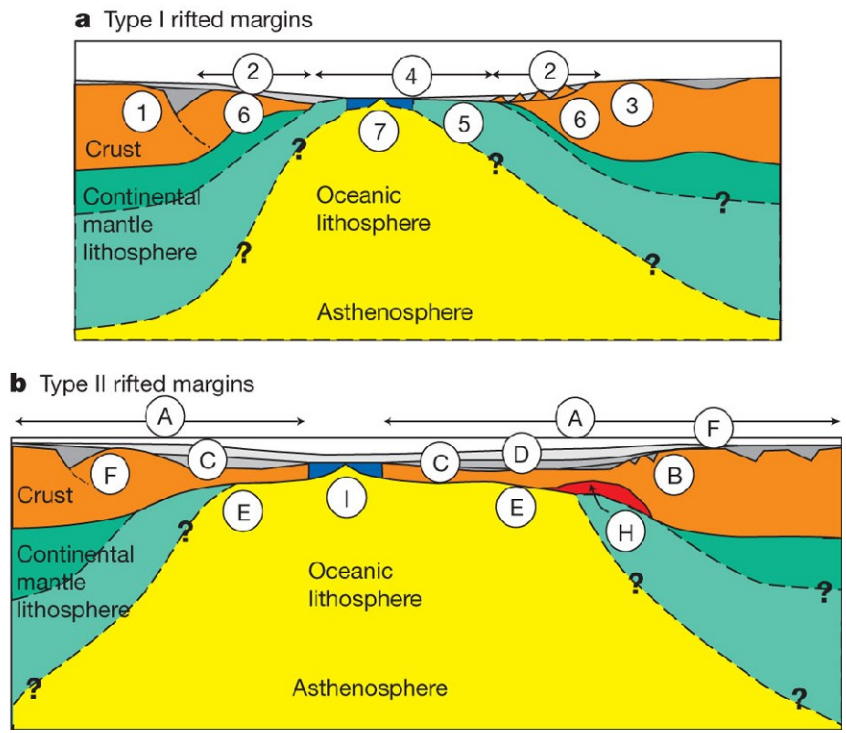

R Huismans & C Beaumont *Nature* **473**, 74-78 (2011) doi:10.1038/nature09988

nature

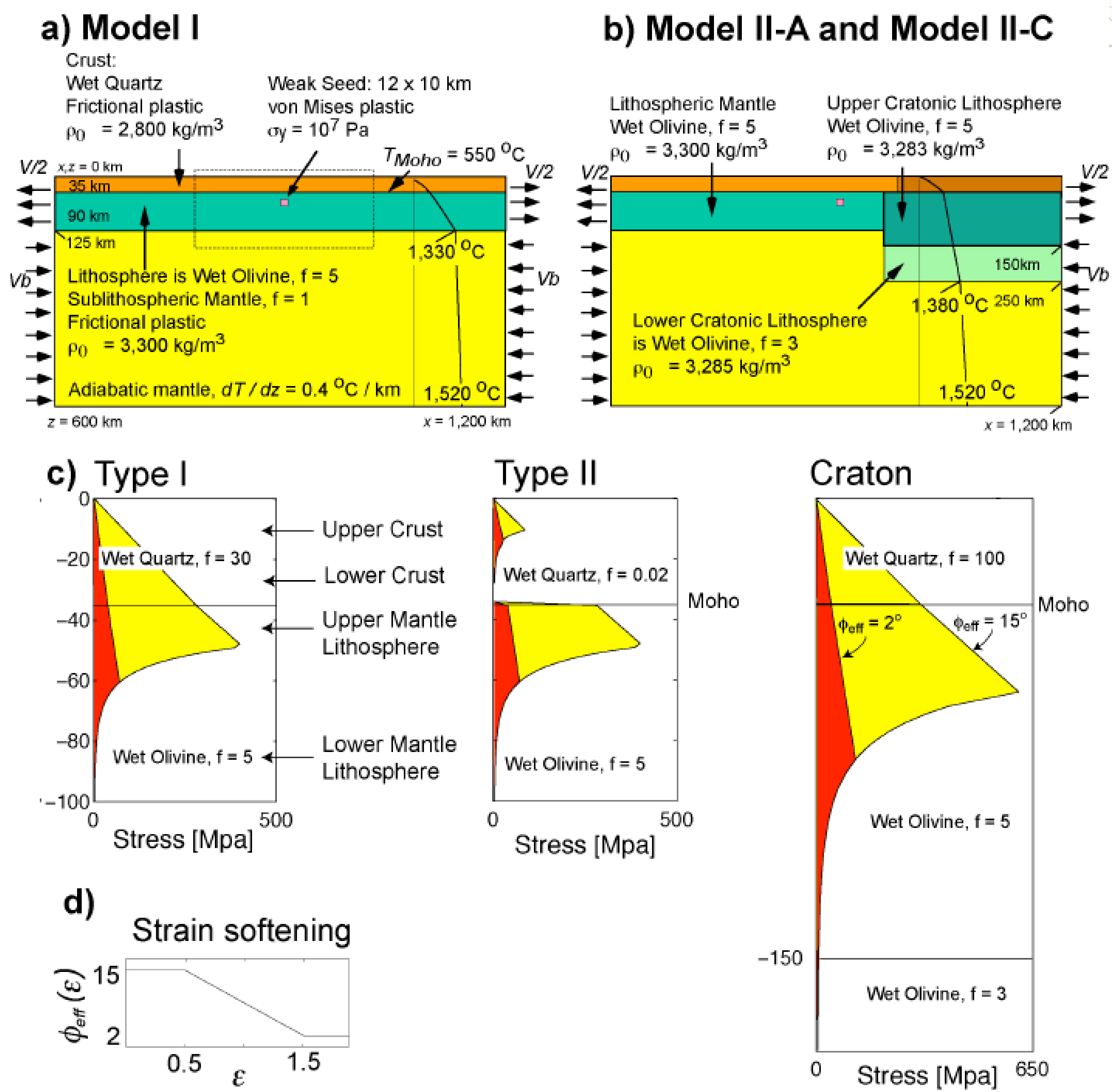
a) Model I
Crust:
Wet Quartz
Frictional plastic
ρ0 = 2,800 kg/m3
Weak Seed: 12 x 10 km
von Mises plastic
σy = 10^7 Pa
TMoho = 550 °C
V/2
x,z = 0 km
35 km
90 km
125 km
1,330 °C
Vb
Lithosphere is Wet Olivine, f = 5
Sublithospheric Mantle, f = 1
Frictional plastic
ρ0 = 3,300 kg/m3
Adiabatic mantle, dT / dz = 0.4 °C / km
1,520 °C
z = 600 km
x = 1,200 km
b) Model II-A and Model II-C
Lithospheric Mantle
Wet Olivine, f = 5
ρ0 = 3,300 kg/m3
Upper Cratonic Lithosphere
Wet Olivine, f = 5
ρ0 = 3,283 kg/m3
150km
1,380 °C
250 km
Lower Cratonic Lithosphere
is Wet Olivine, f = 3
ρ0 = 3,285 kg/m3
1,520 °C
x = 1,200 km
c) Type I
Wet Quartz, f = 30
Wet Olivine, f = 5
Upper Crust
Lower Crust
Upper Mantle
Lithosphere
Lower Mantle
Lithosphere
Stress [Mpa]
Type II
Wet Quartz, f = 0.02
Moho
Wet Olivine, f = 5
Stress [Mpa]
Craton
Wet Quartz, f = 100
Moho
φeff = 2°
φeff = 15°
Wet Olivine, f = 5
−150
Wet Olivine, f = 3
Stress [Mpa]
650
d)
Strain softening
φeff (ε)
15
2
0.5
1.5
ε

Dois tipos de margens pobres em magma: rigidez original da crosta

Tipo I: Ibéria – Newfoundland

- Crosta originalmente muito resistente
- Ruptura crustal localizada e anterior à ruptura mantélica
- Rifts fundos e exumação de manto

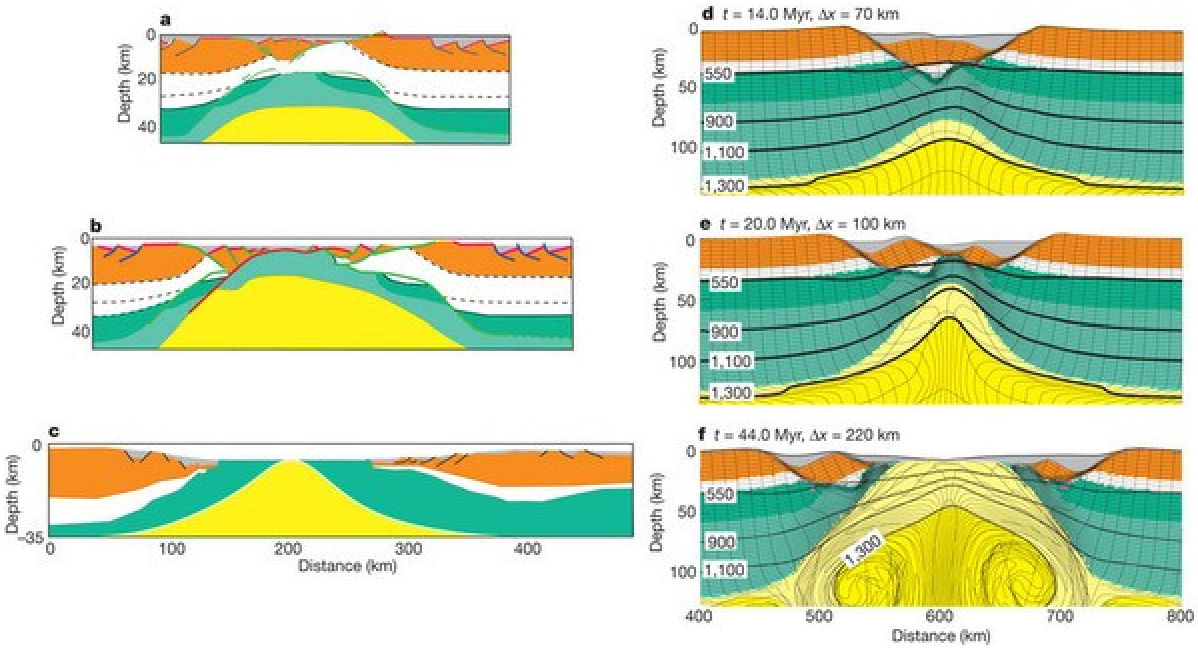

R Huismans & C Beaumont *Nature* **473**, 74-78 (2011) doi:10.1038/nature09988

a, b, Conceptual reconstructions9, 10 of the Iberia–Newfoundland conjugate margins (see Supplementary Information). c, Interpreted observations7, 8, 9 restored to late Aptian. Compare with model I results. d–f, Model I results (shown for a subregion of the model domain; see Supplementary Movie 1). Myr, millions of years; t, time since the onset of extension; Δx, extension at uniform velocity 0.5 cm yr−1. Contours are isotherms in degrees Celsius. Shown are sediments (grey), upper and mid-crust (orange), lower crust (white), frictional-plastic (dark green) and viscous (green) continental mantle lithosphere, oceanic lithosphere (pale yellow) and asthenosphere (yellow).

Dois tipos de margens pobres em magma: rigidez original da crosta

Tipo II: Atlântico Sul

- Crosta originalmente pouco resistente
- Bacias rasas – distensão dúctil de crosta inferior
- Ruptura mantélica antes da ruptura crustal
- Possível fluxo lateral de manto litosférico cratônico (modelo IIc)

Legenda do slide seguinte:

a, b and e, Model II-A. c, d and f, Model II-C. g, Interpreted observations from central South Atlantic margins5, 6, 16, 17, 21, 22, 23. Model style and colouring as in Fig. 2. Also shown are salt (magenta), early (dark grey) and late (medium grey) syn-rift sediments, possible magmatic underplate (red), craton lower-mantle lithosphere (light green) and craton crust (brown). See Supplementary Information for model II-C explanation and Supplementary movies 2 and 3).

a

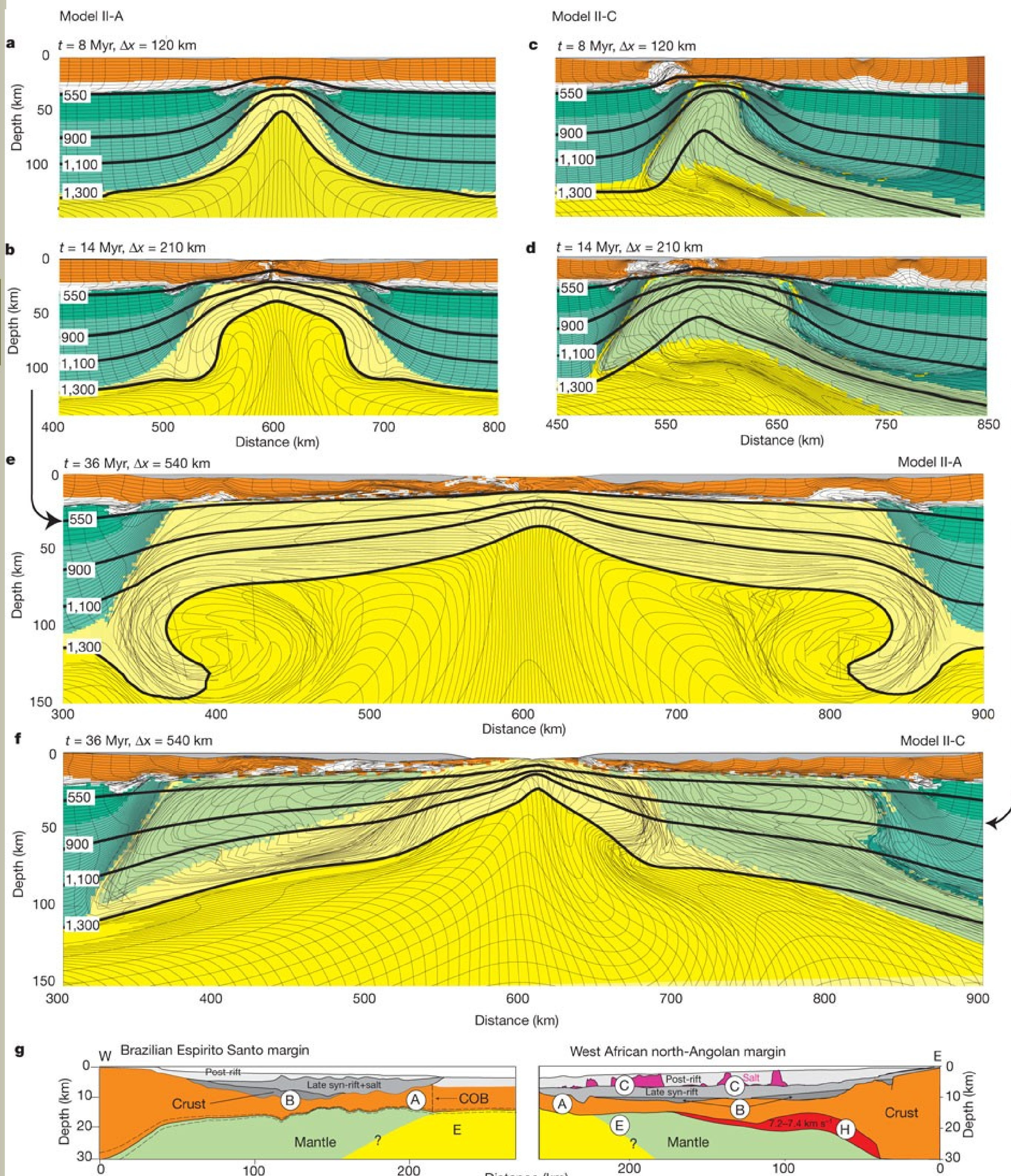

R Huismans & C Beaumont *Nature* **473**, 74-78 (2011) doi:10.1038/nature09988

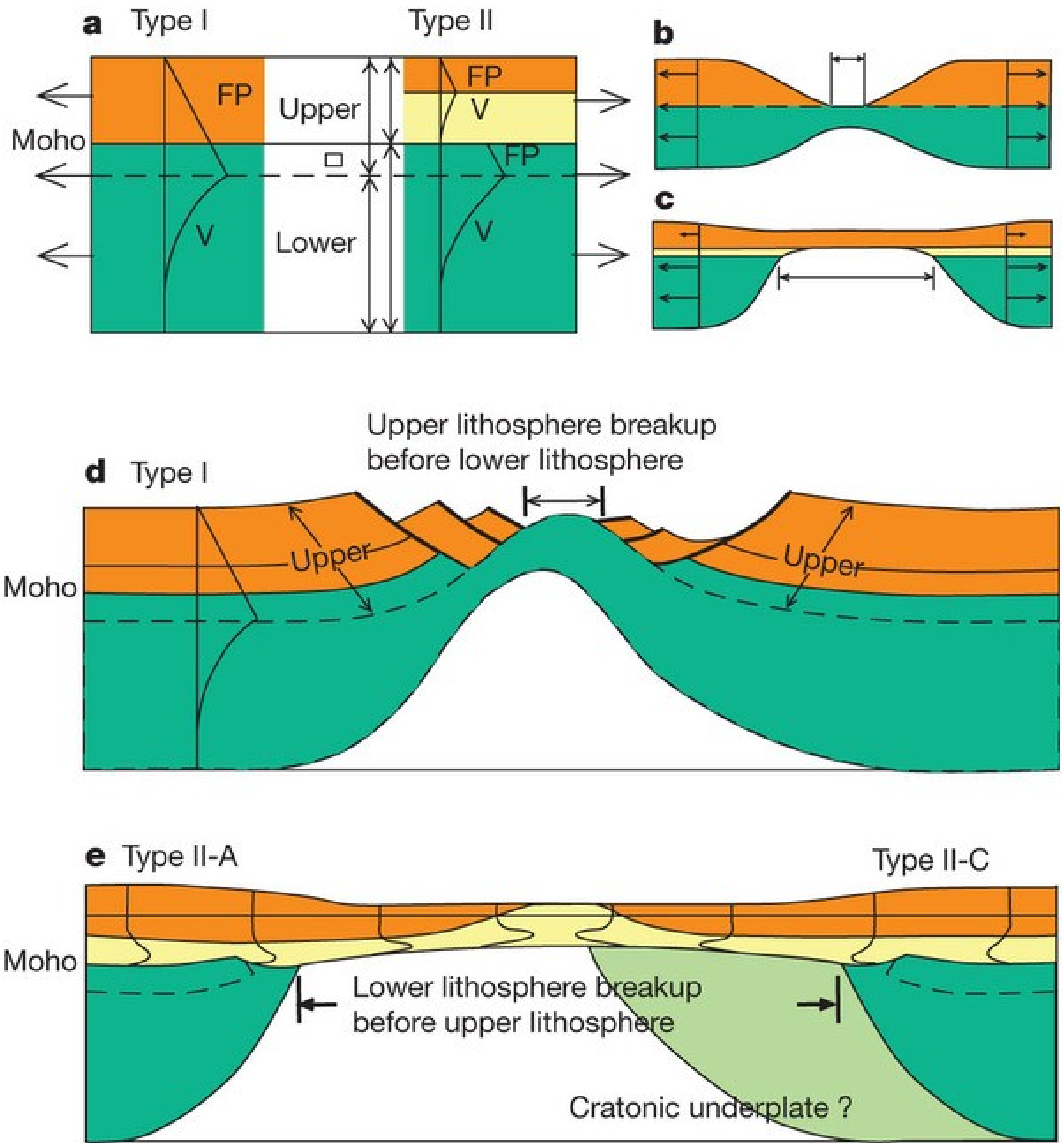

R Huismans & C Beaumont *Nature* **473**, 74-78 (2011) doi:10.1038/nature09988

a, Properties of the two types. FP, frictional–plastic; V, viscous; pale yellow, low-viscosity crust. b, c, Conceptual laminate necking styles showing respective early breakup of crust and mantle lithosphere. Adding isostasy gives: d, Type I. e, Type II-A and type II-C, with asthenospheric (left) and cratonic (right) underplate. We note that the region of the embedded cratonic lithosphere is to the right of panel e. Shown are strong FP crust (orange), low-viscosity crust (pale yellow), mantle lithosphere (green) and cratonic underplate (light green).

Margens transformes

Exemplo Gana-Costa do Marfim e Margem Equatorial Brasileira

- Pobres em Magma, mas...

- COT abrupto

- Zona de alta alta velocidade muito restrita (sem *underplating* claro)

- Distensão original em bacias trasncorrentes (controverso)

11. GEODYNAMIC EVOLUTION OF THE CÔTE D'IVOIRE-GHANA TRANSFORM MARGIN: AN OVERVIEW OF LEG 159 RESULTS1

Christophe Basile,2 Jean Mascle,3 Jean Benkhelil,4 and Jean-Pierre Bouillin2

In

Mascle, J., Lohmann, G.P., and Moullade, M. (Eds.), 1998
Proceedings of the Ocean Drilling Program, Scientific Results, Vol. 159

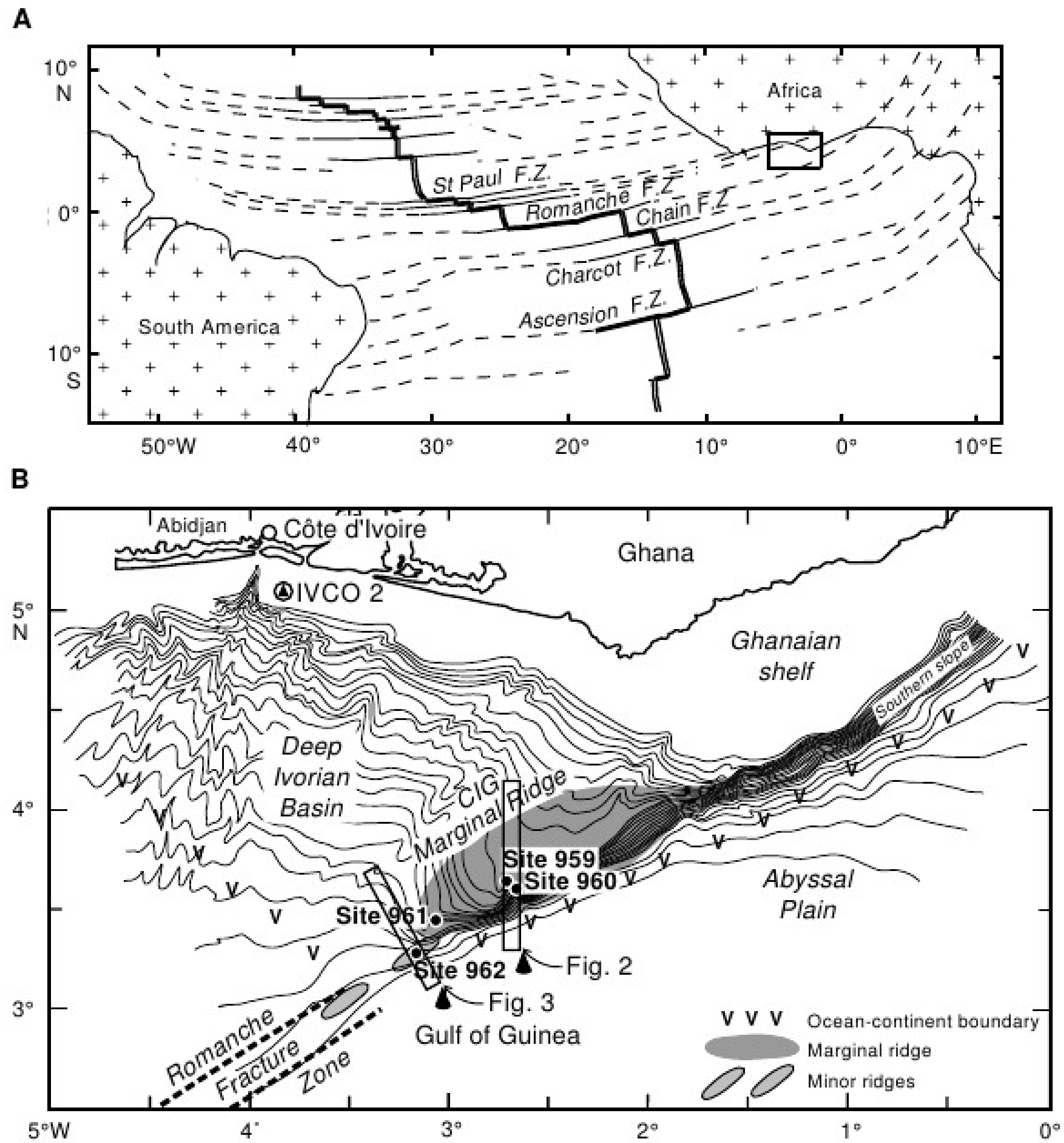

Figure 1. Geodynamic (**A**) and bathymetric (**B**) framework of the Côte d'Ivoire-Ghana transform margin. Boxed area in (A) is shown in detail in (B). The solid circles indicate the location of Leg 159 sites. The rectangles show the location of the multichannel seismic reflection lines shown in Figures 2 and 3.

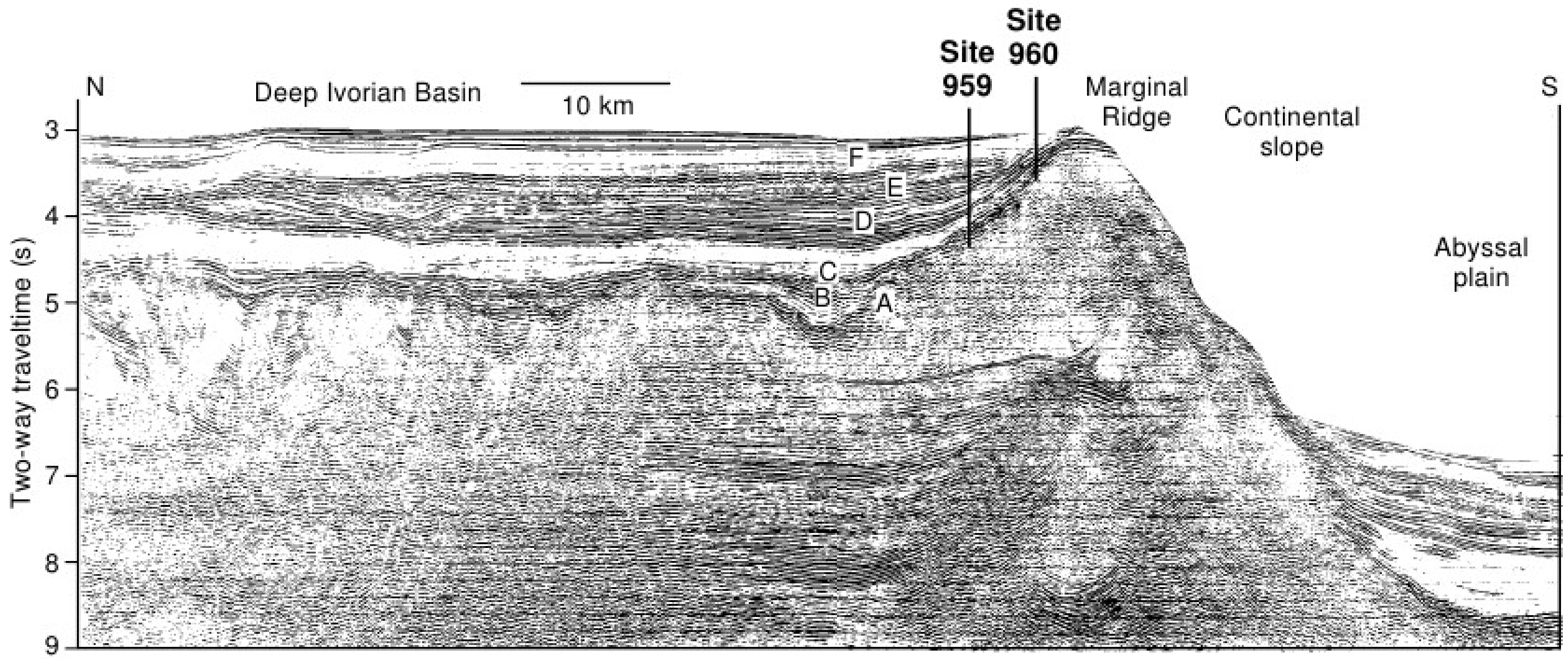

Figure 2. Migrated seismic line MT02 across (from north to south) the deep Côte d'Ivoire-Ghana divergent basin, the marginal ridge, the continental slope, and the Gulf of Guinea abyssal plain. The marginal ridge and the oceanic crust of the Gulf of Guinea are overlain by thick undeformed sedimentary sequences. Main seismic units are shown according to Basile et al. (1996).

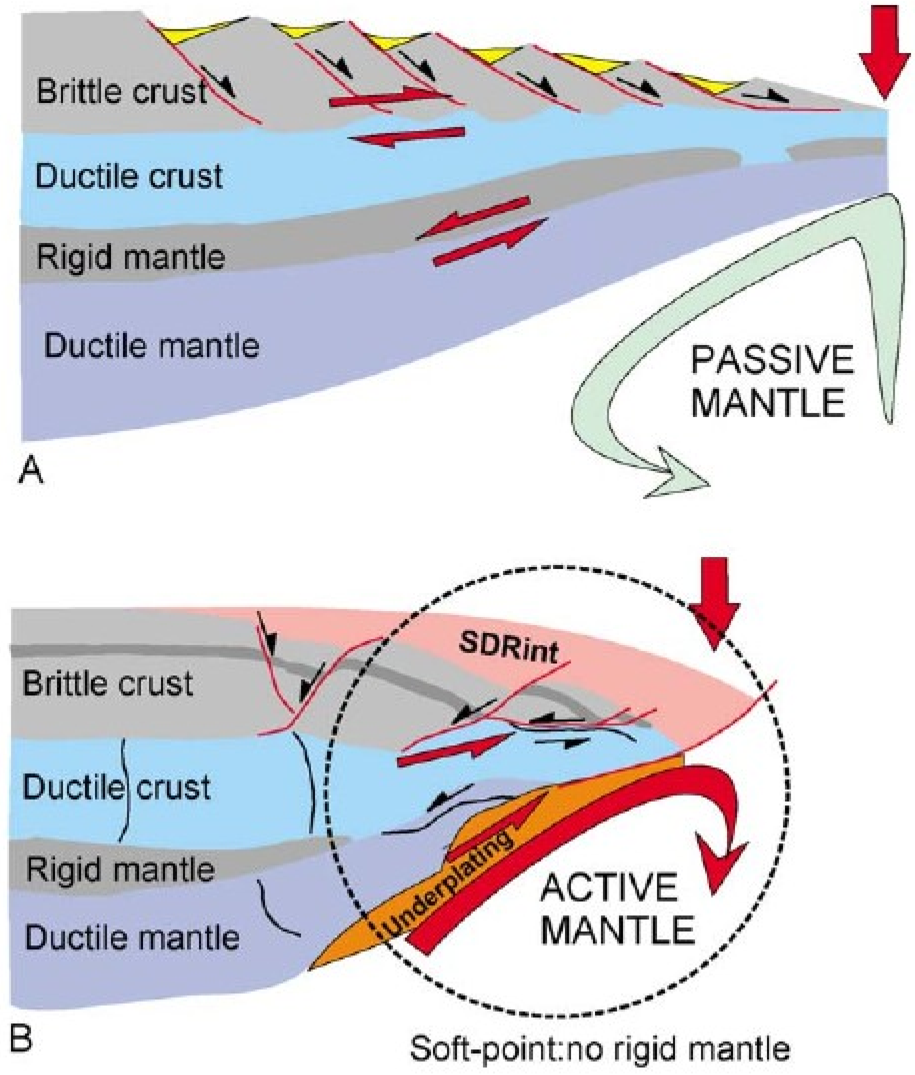

Fig. 10. Proposed relationships between mantle dynamics (**A**: passive, SPM; **B**: active, VPM) and lithosphere extension. These figures are inspired from published [11–13,28] and unpublished analogical and numerical experiments. **A**: Sedimentary passive margin, **B**: volcanic passive margin. Further explanations in the text. Vertical red arrow: break-up area and first oceanic crust.

Topografia dinâmica e estratigrafia de sequências: “small-scale convection”

Journal of the Geological Society, London, Vol. **167**, 2010, pp. 637–648. doi: 10.1144/0016-76492009-127.

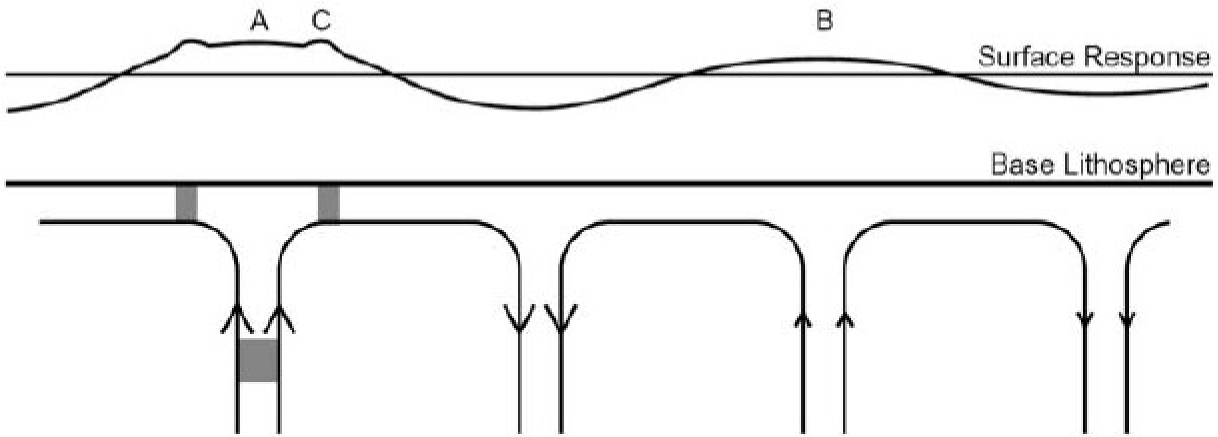

Fig. 2. Sketch to illustrate how mantle convection controls relative sea level. The upper mantle beneath the lithosphere is everywhere stirred by convection cells. The Earth’s surface is deflected upwards above hotter, upwelling limbs and downwards above cooler, downwelling limbs to form a tessellating pattern of swells and depressions. The cells vary in their thermal anomaly, and the amplitude of the response at the Earth’s surface varies in consequence (A and B). These cells control second-order cycles of sea level. The Rayleigh number of the Earth’s mantle is 10 to the power of 6–8, depending on whether convection occurs in one or two layers; we thus expect the convection flow to be time dependent. This is illustrated here by blobs of hotter mantle (grey patches) and cooler mantle, carried round the convection cells. These blobs cause a surface response that is superimposed on the swell pattern (C), here referred to as pulsing. This pulsing controls the higher-frequency third-order cycles of sea level. Figure by S. Jones.

Small-Scale Mantle Convection Produces Stratigraphic Sequences in Sedimentary Basins K. D. Petersen et al. Science 329, 827 (2010); DOI: 10.1126/science.1190115

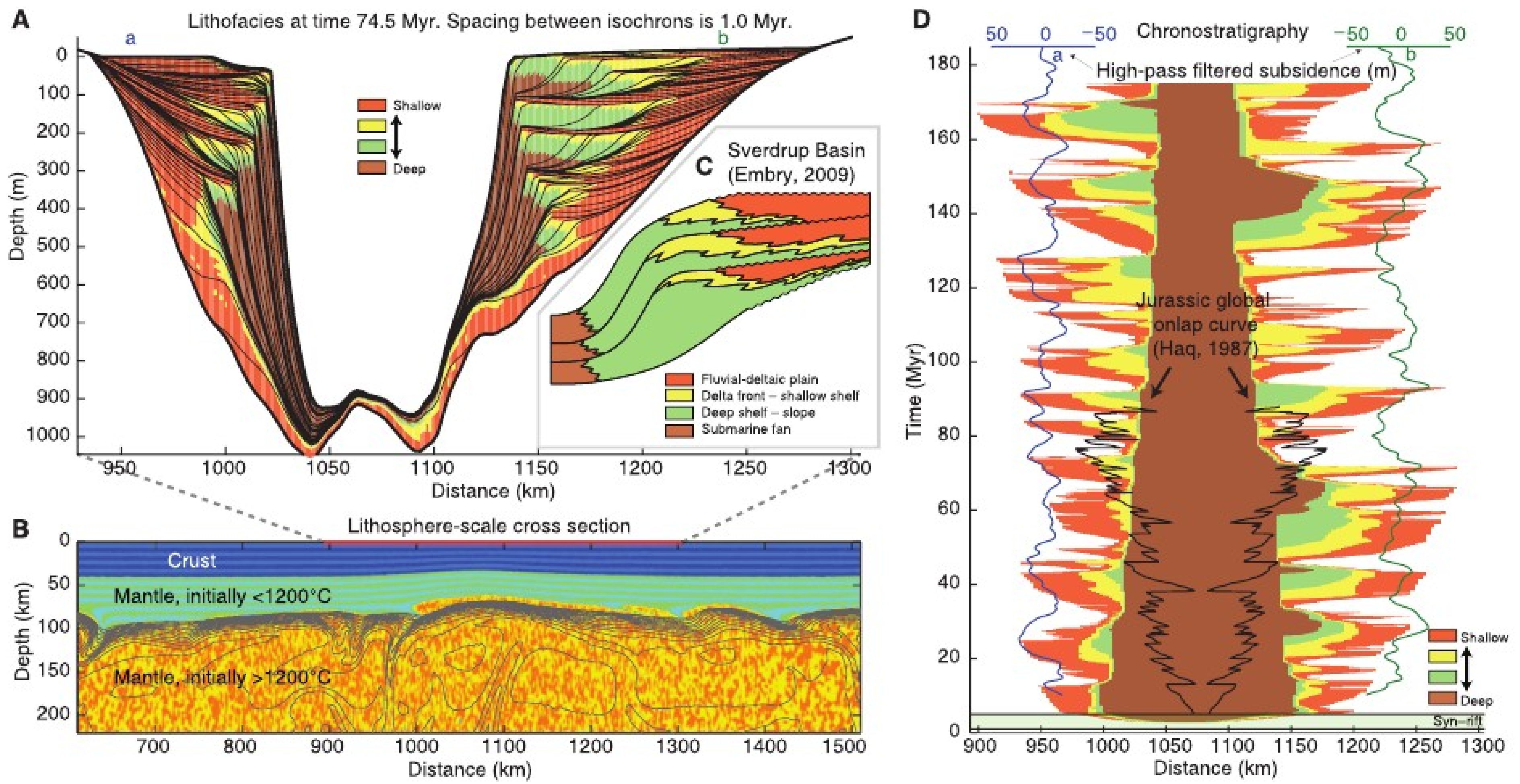

Fig. 3. Rift model with small-scale convection and constant sediment input and eustatic sea level. (**A**) Lithofacies (indicated by paleo water depth). Cyclic deposition is evident from unconformities and lateral migration of lithofacies; subsidence curves for locations a and b appear in (D). (**B**) Lithospheric cross-section showing gently thinned crust and mantle lithosphere and isotherms from 1200° to 1440°C (solid lines). (**C**) Cross section of the Sverdrup Basin, Canada (*29*). (**D**) Chronostratigraphic diagram and short-term vertical basement displacements at locations a and b. The inferred Jurassic global onlap curve (*2*) is shown in black for comparison. Differences in local vertical movements cause the two opposite basin margins to exhibit asymmetric stratigraphic evolution with different onlap patterns. In both cases, the time scale of cyclicity resembles that of the global Jurassic onlap curve.